KANSAS GEOLOGICAL SURVEY
OPEN-FILE REPORT 83-20

A Groundwater Flow Model for the Great Bend Aquifer,
South-central Kansas

by

Patrick M. Cobb
Susan J. Colarullo
Manoutchehr Heidari

KANSAS GEOLOGICAL SURVEY
1930 Constant Avenue
University of Kansas
Lawrence, KS 66047

A GROUNDWATER FLOW MODEL FOR THE GREAT BEND AQUIFER, SOUTH-CENTRAL KANSAS

Patrick M. Cobb
Susan J. Colarullo
Manoutchehr Heidari

1982

A study completed by the Kansas Geological Survey's Geohydrology Section, Under Contract No. 14-08-0001-17943 for the Water Resources Division, United States Geological Survey

Table of Contents

LIST OF TABLES

LIST OF TABLES (con't)

LIST OF FIGURES

LIST OF FIGURES (con't)

LIST OF FIGURES (con't)

LIST OF FIGURES (con't)

SUMMARY

The unconsolidated Quaternary aquifer which underlies the Great Bend Prairie in south-central Kansas has undergone a significant increase in irrigation development during the past several decades. In 1974, about 1,160 irrigation wells withdrew roughly 270,000 acre-feet of groundwater from the unconfined aquifer. Optimal allocation of irrigation withdrawals over the long term will require a fundamental understanding of the dynamics of the groundwater aquifer. With this goal in mind, the Geohydrology Section of the Kansas Geological Survey contracted with the Water Resources Division of the U.S. Geological Survey to simulate flow in the aquifer using finite difference algorithms developed from continuity principles.

All data used in the modeling effort were provided by the USGS. After considerable effort involving modification of the data base and adjustment of boundary locations, a finite-difference predictive model of the alluvial aquifer was designed for purposes of identifying aquifer parameters and recharge rates using a forward approach. The USGS two-dimensional flow model and the Texas Tech two-dimensional calibration model were used to calibrate for hydraulic conductivity K, specific yield S_y, net natural recharge rate R, and an irrigation consumptive-use correction factor α.

In the first phase of the study, a steady-state calibration for K and R was performed using the USGS finite-difference model and 1950 pre-development head levels. A specific yield of zero was chosen in order to force convergence of simulated head to a unique steady-state head distribution using constant-head river and permeable boundary nodes. Natural recharge R was varied on a node-by-node basis using trial-and-error techniques by assuming a uniform hydraulic conductivity K of 100 ft/day until calibration errors of less than ±20 feet were observed. R was not permitted to exceed 6 in/yr in order to minimize the adverse influence of such a large number of degrees of freedom implied by the node-by-node adjustment.

When the calibration error at each node was reduced to ±20 feet by varying R, hydraulic conductivity K was uniformly varied between 75 ft/day and 120 ft/day. A minimum sum of squared error of roughly 21,000 ft^2 was obtained at a uniform hydraulic conductivity of 85 ft/day. The resulting simulated head represented the steady-state water table upon which all transient influences were imposed during simulation of the subsequent groundwater development period.

The effects of groundwater development on boundary and river contributions to the aquifer were introduced using a constant-gradient, variable-flux algorithm initialized by the fluxes which occurred under constant-head conditions. Transient calibration involved variation of a consumptive-use correction factor α against fixed K and R estimates from the final steady-state calibration model and a uniform specific yield of 0.15. The correction factor was necessitated by the fact that reported pumpages, when applied to the flow model, induced much more drawdown than had been observed during the development period. Using modified versions of the 1955, 1960, 1965, 1970, and 1975 water tables, an α of 0.6 was found to produce the closest overall match between simulated and modified head distributions.

In the second phase of this study, a steepest-descent optimization procedure was used to refine the natural recharge distribution obtained from the USGS steady-state calibration and to identify a distributed set of hydraulic conductivity estimates under steady-state conditions. Problems

associated with assigning zero-valued specific yields to force steady-state convergence were ultimately related to the properties of the unrelaxed Gauss-Seidel iterative scheme used to solve the governing flow equations. Introduction of non-zero specific yield values resulted in a final calibrated head distribution which was not in steady state. Steady-state conditions were simulated after three 1-year time steps using the final calibrated head and refined recharge and conductivity parameter sets to initialize the simulation. The final sum of squared calibration error relative to the pre-development water table was equal to 5,100 ft^2, which amounted to nearly a four-fold reduction in the sum of 21,000 ft^2 obtained from the steady-state calibration performed using the USGS model and a trial-and-error approach. Average calibration error was reduced from 0.5 feet to 0.2 feet, while the error variance was decreased from 30.3 ft^2 to 7.8 ft^2.

The steepest-descent procedure was also used to perform several transient calibrations with respect to modified versions of the 1955, 1960, and 1965 observed water tables. Temporal and spatial averages of natural recharge, hydraulic conductivity, and specific yield were obtained from these calibrations. In addition, a linear relation between the consumptive-use correction factor α and reported annual pumpage was developed on the basis of adjustments in input pumpages during operation of the steepest-descent optimization model. This relation offered a means of indirectly validating the model during the 1970 and 1975 pumping periods.

Results of the validation process were not satisfactory. The poor agreement between simulated and observed head levels throughout the 1950-1975 development period was primarily attributed to the small transient effects occurring in the aquifer during this time and to the associated large standard errors of estimate for specific yield values. It is believed that transient head measurement errors in the aquifer were of the same order of magnitude as the small drawdowns observed during the development period, and that successful validation will have to be postponed until the transient effects of increasing groundwater withdrawals begin to dominate the error influences.

INTRODUCTION

The Great Bend Prairie encompasses an area in south-cenral Kansas of approximately 5,400 square miles south of the Arkansas River (see Fig. 1). The major portion of the prairie has been incorporated into Groundwater Management District #5. It is currently being converted to cropland for purposes of providing feed crops to an expanding cattle industry within the area. Irrigated agricultural development within the prairie was not significant until the late 1960s, when center-pivot sprinkling systems facilitated conversion of the sandy prairie grasslands to more economically-productive croplands. District managers expect that future development of the grasslands will proceed quite rapidly, and that a comprehensive groundwater-management scheme will be required within the next several years to ensure economically-optimal allocation of limited groundwater supplies.

As of 1978, 45 million acre-feet of groundwater was estimated to be stored in the areally-extensive deposits which underlie the prairie (Fader and Stullken, 1978). Recognition of the availability of such a large water supply has encouraged recent agricultural development of the prairie grasslands, but the extent of this development had not been significant enough to result in noticable depletion of the groundwater supply. Between 1950 and 1974, the number of irrigation wells rose from 50 to 1,160, with total annual municipal, industrial, and agricultural withdrawals increasing from 50,000 acre-feet to 270,000 acre-feet (Stullken, personal communication, 1982). It is believed that the effects of this increased rate of withdrawal have not differed significantly from normal, long-term effects of climatic changes, and the system may therefore be considered to be governed by steady-state conditions for most practical purposes. However, if this trend in irrigation development

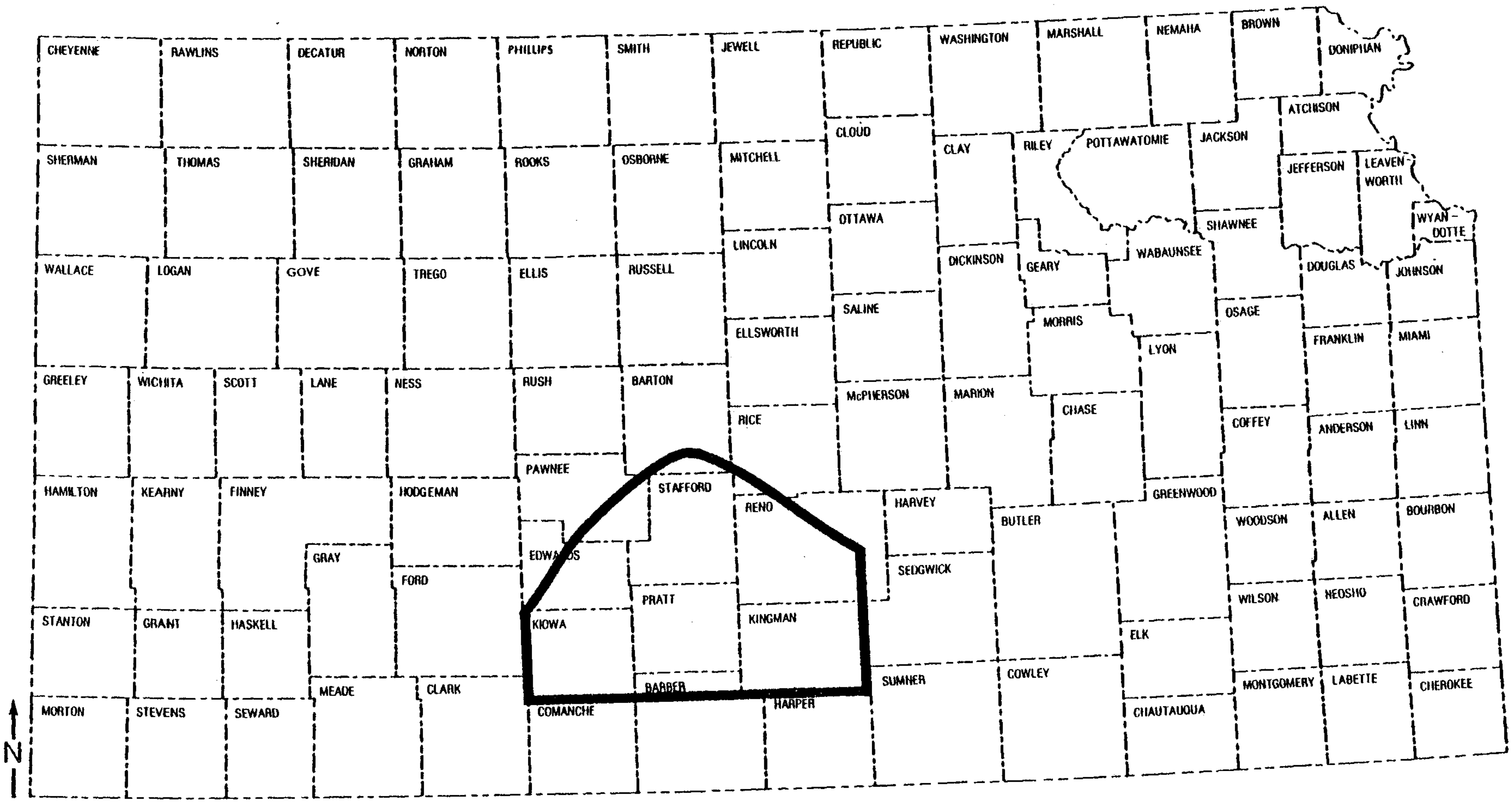

Figure 1. Location of study area.

continues, the increased rate of well withdrawals will impose a perturbation on the steady-state head distribution and the system will become characterized by transient conditions. At some point in the future, these increased withdrawals may cause depletion of the alluvial aquifer.

Future decisions regarding the allocation of groundwater supplies in the Great Bend Prairie will greatly depend on the physical properties and flow dynamics of the prairie alluvial aquifer. Identification of aquifer properties and the prevailing flow regime will allow these decisions to be made in the context of quantified storage, transmission, recharge, and advective solute-transport characteristics of the groundwater reservoir. This report describes the development and calibration of a finite-difference model of the Great Bend alluvial aquifer. Calibration was first performed on the basis of the 1950 pre-development water table and five water table configurations observed during the 1950 to 1975 development period using trial-and-error methods, with the intent of obtaining estimates of aquifer parameters and regional flow properties. A second, least-squared-error calibration (see Appendix C) was performed using water tables from 1950,1955, 1960, and 1965, with the 1970 and 1975 water tables used in an attempt to verify parameter estimates. The model may ultimately be used to predict the physical and economic impact of future irrigation development on the Great Bend Prairie groundwater supply if it enters into a more pronounced transient stage. The modeling efforts which have been documented in this report were oriented towards identification of the behavior of the alluvial aquifer flow system, with the intent of deriving meaningful physical constraints for future decision-making processes regarding management of groundwater supplies in the context of both quantity and quality.

STUDY AREA

The Great Bend Prairie is located in the south-central part of Kansas, extending across all of Pratt and Stafford counties and parts of Barton, Rice, Reno, Kingman, Harper, Barber, Commanche, Kiowa, Clark, Ford, Edwards, and Pawnee counties (see Fig. 2). The general land surface of the prairie is characterized by low relief. Surficial deposits range from sand dunes formed by wind deposition to finer eolian deposits in the southern highlands. To the south, the topography becomes dominated by deep, eroded valleys and the water table becomes characterized by steep, local hydraulic gradients.

Average annual precipitation over the prairie has been estimated by U.S. Department of Commerce sources to range from 22.5 inches along the western border to 31.5 inches along the eastern boundary of the grasslands. The 1941-1970 average annual precipitation over the entire prairie is roughly 25 inches per year (Fader and Stullken, 1978). Storage of groundwater supplies in the Great Bend alluvial aquifer changes quite rapidly in response to changes in precipitation from year to year due to the high recharge capacity of surficial deposits and to the large conductivity and porosity of the underlying alluvial aquifer. The slight transience of the flow regime during the 1950 to 1975 development period tended to be dominated by these climatic effects, and made accurate identification of the specific yield aquifer parameter subject to large estimation errors during attempts to perform transient calibration.

The prairie is drained by several major stream channels which are generally in hydraulic connection with the allvuial aquifer. Principal stream channels include the Arkansas River, Cow Creek, Wild Horse Creek, Rattlesnake Creek, Peace Creek, North and South Fork Ninnescah Rivers and tributaries, and Silver Creek. The major streams have frequently been reported to flow

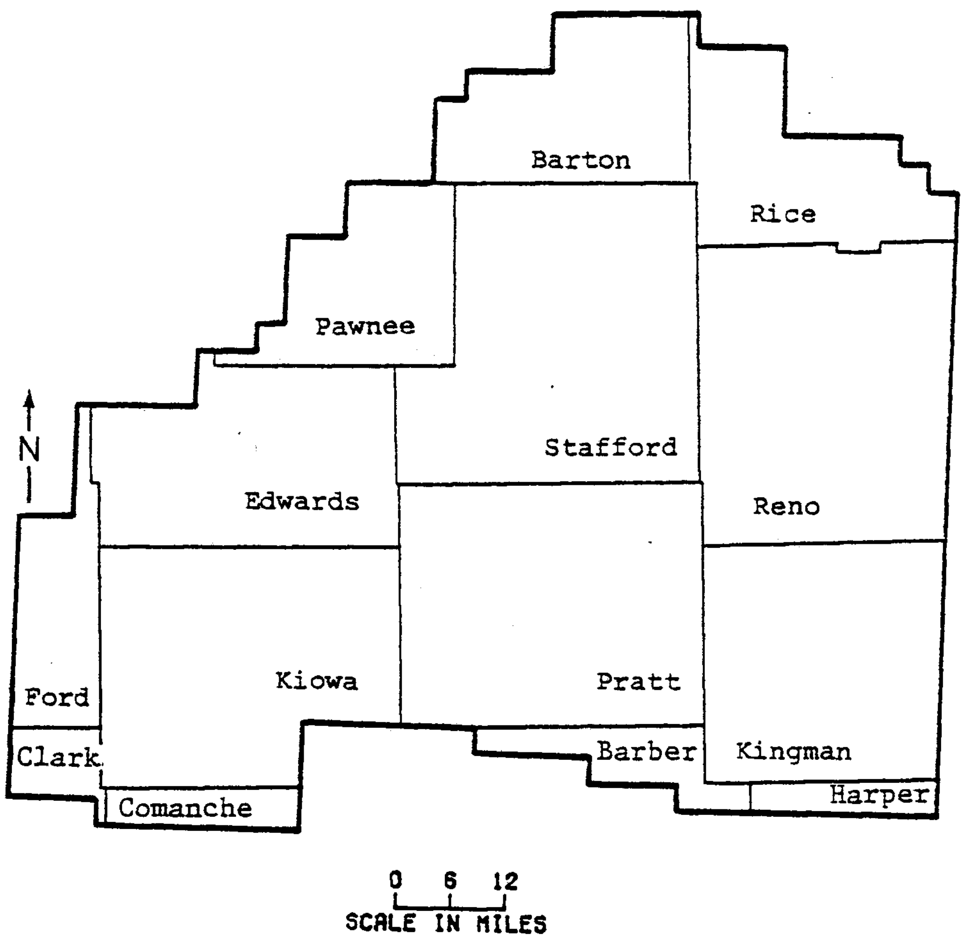

Figure 2. Counties located in the Great Bend Prairie model area.

perennially, but field observations by KGS staff members have suggested that flow is probably somewhat ephemeral in nature in some parts of the prairie at the present time, especially in late summer. The ephemeral characteristics of these streams are a reflection of storm-term transience in the aquifer system. The streams flow eastward in the general direction of the topographic gradient.

THE GENERALIZED GEOHYDROLOGY OF THE GREAT BEND STUDY AREA

Description of the Stratigraphic Units

The geologic and hydrologic properties of the stratigraphic units occurring in the Great Bend Aquifer Study area have been extensively reviewed by previous investigators (Waite, 1942; Latta, 1948; McLaughlin, 1949; Fent, 1950; Latta, 1950; Bayne, 1956; Bayne, 1960; Lane, 1960; Bayne, Franks, and Ives, 1971; Layton and Berry, 1973; Bayne and Ward, 1974; Fader and Stullken, 1978). This discussion constitutes only a brief and general outline of the material cited above. The purpose of this section is to establish the geohydrologic setting for the reader and to lend clarification to the relationship between the physical properties of the aquifer and the model characteristics.

Most simply stated, the geology of the area consists of a veneer of unconsolidated to semi-consolidated sands, gravels, clays, and silts of Quaternary and Tertiary age overlying the consolidated sandstones, siltstones, and shales of Cretaceous and Permian age (see Fig. 3). The focus of interest in this model study is the large aquifer formed by the first group of units

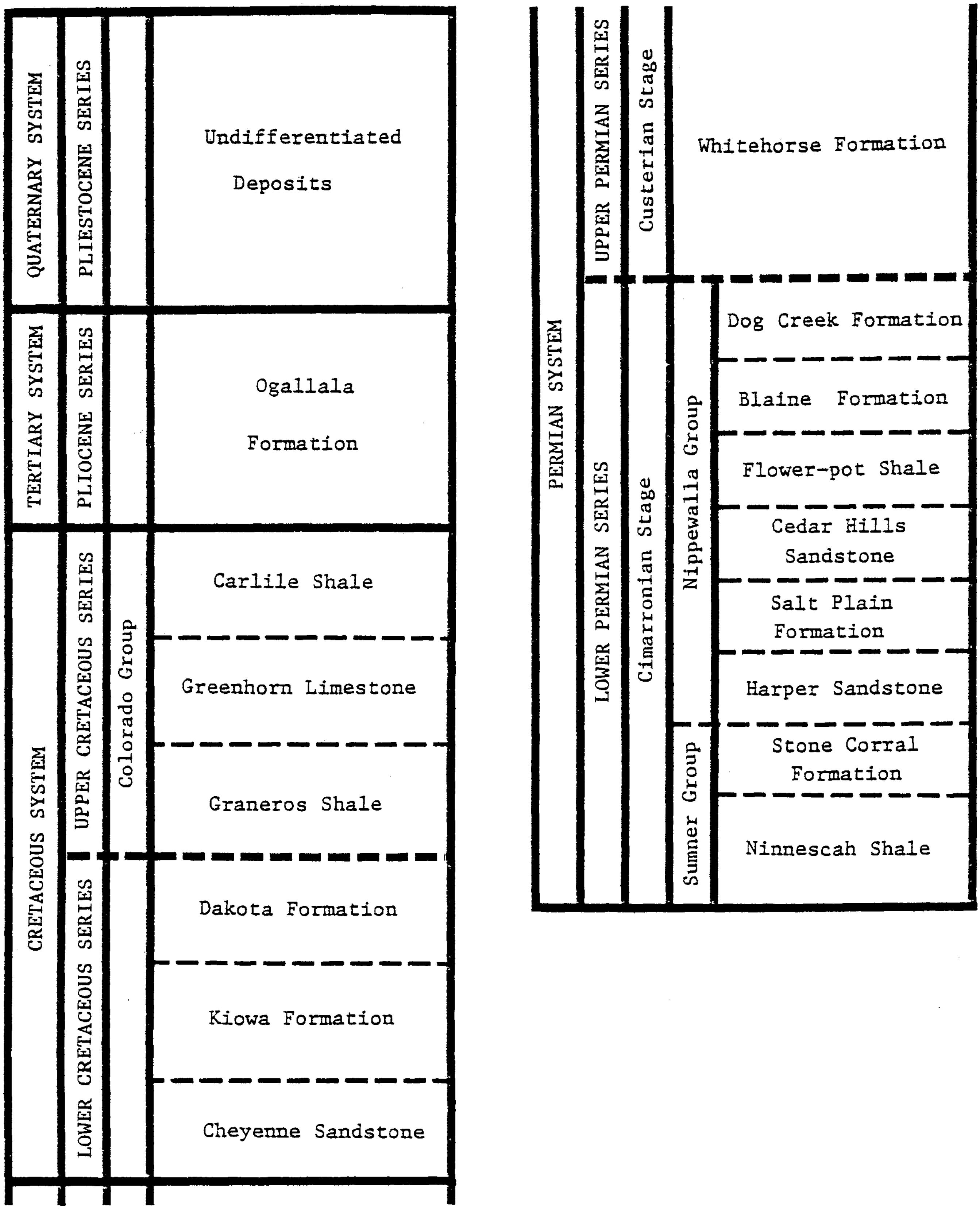

Figure 3. Stratigraphic column of the study area (nomenclature adopted from Zeller, 1968).

and bounded by the second. There are several units, such as the Cedar Hills Sandstone of Permian age and the Cheyenne Sandstone and Dakota Formation of Cretaceous age, which also constitute aquifers and are apparently in hydraulic connection with the unconsolidated aquifer. Evaluation of these interactions will be deferred until the structure of the model is discussed in the context of the prevailing geohydrologic conditions which govern flow in the principal Cenozoic alluvial aquifer.

Graneros Shale, Greenhorn Limestone, and Carlile Shale

These units occur in the uplands of Ellsworth, Barton, Pawnee, and Ford counties, generally on the margins of the unconsolidated aquifer and usually in association with the underlying Dakota Formation. They typically yield only small quantities of water to domestic wells and are not a part of the High Plains aquifer. Their water-yielding capacity is probably a reflection of the degree to which they are fractured or weathered. These units act as an impermeable boundary in some peripheral parts of the study area.

Dakota Formation

Extensive outcrops of the Dakota Formation occur from Ellsworth County westward to Ford County and southward into Kiowa and Comanche counties. The Dakota Formation in Kansas consists of alternate beds or lenses of claystone, siltstones, and sandstone. As much as 70% of the formation is estimated to consist of lenticular beds of claystone and siltstone. Sandstone occurs in erratically distributed lenses that differ in thickness and extent of interconnection. Some lenses may have wide areal extent (Keene and Bayne, 1977). Results of aquifer pumping tests conducted in the Dakota are not widely available, but one test conducted in Ford County and one test conducted in Hodgeman County resulted in hydraulic conductivity estimates of 41 ft/day and 16 ft/day, respectively (Lobmeyer and Weakly, 1979). Wells that penetrate the thicker coarser-textured sandstone lenses have yields ranging from a few gallons per minute to a few hundred gallons per minute (Latta, 1950). It has been reported that the total dissolved solids in Dakota Formation water ranges from 300 to 1,475 parts per million (McLaughlin, 1949). Thus, the Dakota Formation appears to be capable of supplying relatively large quantities of slightly saline water to the fresh-water alluvial aquifer.

Groundwater movement in the Dakota Formation in south-central Kansas appears to be toward the northeast and east (Keene and Bayne, 1977; Kume and Spinazola, 1983). Keene and Bayne identified a potentiometric ridge which trends northeast through Ford, Edwards, and Pawnee counties. This may indicate recharge from overlying unconsolidated units. Recharge from or leakage into the overlying alluvium was considered to comprise part of the areal recharge component. In the northern part of the model area, the Dakota is apparently recharged by the unconsolidated aquifer (Keene and Bayne, 1977).

Kiowa Shale

The Kiowa Shale occurs as a belt of outcrops and subcrops extending from Rice and Ellsworth counties, westward through Barton and Rush counties and southward through Pawnee, Ford, Edwards, Kiowa, Comanche, and Barber counties. The Kiowa is principally a dark marine shale containing some thin limestone beds and sandstone lenses. Although not generally regarded as an aquifer, some occurrences of naturally-pressurized low quality water are reported. These reservoirs are apparently confined, but drilling activities may inadvertently vent them into more porous formations and hence, into the unconsolidated aquifer. In general, however, this unit is not suspected of contributing large quantities of water to the Cenozoic aquifer under investigation, and should be considered as part of the impermeable base upon which this aquifer has been deposited.

Cheyenne Sandstone

The Cheyenne Sandstone outcrops in Clark, Comanche, Kiowa, and Barber counties, and occurs as subcropping units in Rice, Ellsworth, Barton, Stafford, Pawnee, Edwards, Kiowa, Barber, and Ford counties. The principal constituents of this unit are fine- to medium-grained sand with some shale and siltstone. Where the Cheyenne outcrops or subcrops, it is capable of discharging or receiving water, depending upon the hydraulic-head gradients in the vicinity. In Kiowa County, fresh water apparently enters the Cheyenne Sandstone, while in Barton County, brackish water has been found under artesian pressure in the Cheyenne. Much of the water in the Cheyenne seems to be of unacceptable quality for human needs.

Undifferentiated Permian Units

For the purposes of this report, several formations of Permian age are grouped together for discussion. These include the Whitehorse Formation, the Dog Creek Formation, the Blaine Formation, and the Flowerpot Shale. The principal reasons for this grouping are 1) the limited occurrence of these units as subcrops in the study area, with most of these occurrences being in Stafford, Pratt, Edwards, and Kiowa counties, and 2) the lack of documentation of the hydrologic characteristics of these units. These units consist almost exclusively of redbeds and evaporites. The Flowerpot Shale consists mostly of shale, with some thin siltstone and sandstone beds. Some anhydrite and halite may also be associated with the shale. The Blaine Formation is the principal evaporite unit of the Nippewalla Group (see Fig. 3). Depending upon the location at which the unit is encountered, it may exist as either an anhydrite or a gypsum. Some shale and salt also occur. The Dog Creek Formation consists of silty shale, siltstone and a minor amount of fine-grained sandstone. The Whitehorse Formation is principally a sandstone unit with minor occurrences of shale, siltstone, and dolomite. The sandstone ranges from resistant to soft, depending upon quantity of cementation. None of these formations are known to supply large quantities of water to wells. Only the Whitehorse Formation is known to supply potable water. For the purposes of this model, these units are considered impermeable.

Cedar Hills Sandstone

Although a considerable amount of work has been done on the geology of the Cedar Hills Sandstone, comparatively little published knowledge exists about its hydrology. Here, only the published knowledge will be referenced, but in Appendix A some unpublished data are cited concerning "slug" tests in the lower Nippewalla Group. This formation consists chiefly of very fine-grained sandstones, sandy siltstones and siltstones. Some silty shale is also known to exist. Disposal of oil field brine under atmospheric pressure into this formation occurs in some counties. This would indicate that the formation, or at least some parts of it, have a small but significant transmissivity. To date, salt water discharge from this unit has not been quantified. However, available studies indicate that salt water encroachment into the Quaternary deposits starts in the vicinity of the subcrop of this unit in northern Stafford County and proceeds to the east. Similar encroachments are known in southern Stafford County and in parts of Pratt

County. It is clear that this unit is in hydraulic connection with the unconsolidated aquifer, but its contribution to the system is not documented. This unit should be considered as a source of recharge to the system, but at present it is not possible to accurately verify its hydraulic parameters. For the purpose of this study, its contribution to the alluvial aquifer will be considered as an implicit part of the recharge component.

Harper Sandstone - Salt Plain Formation

These units are difficult to separate stratigraphically and hydrologically. For the purpose of this discussion, they are considered as a continuous unit. These units are mostly siltstone, silty shale and shale, with only a small amount of sandstone. Researchers at the Kansas Geological Survey obtained cores from these units while doing field work in Reno and Pratt counties. These cores were generally red in color. The soft siltstone was frequently washed out, leaving behind the more resistant sandy siltstone and silty shales. Occasionally, a thin gypsum bed has been encountered. These observations correspond to the descriptions in the literature. The cores have never been tested for laboratory conductivities, but the holes from which some of them were cut have been "slug" tested. These slug tests involved measuring the rate of head recovery in a well which has been subjected to an instantaneous input of a known quantity of water. Results of these slug tests are presented in Appendix A. These units are exposed in Reno, Kingman, Harper and Barber counties. They also occur as subcropping units in Barton, Stafford, Rice, Reno, Kingman and Pratt counties. They form a portion of the eroded surface upon which the unconsolidated material constituting the principal aquifer was deposited. Some significant leakage out of these units may occur where gypsum stringers are present, but in general the material appears to be relatively impermeable. Most of the water obtained from these units in subcropping areas is of low quality.

Stone Corral Formation

The Stone Corral consists of dolomite, anhydrite, and gypsum. Solution of the gypsum and anhydrite in the vicinity of the outcrop has caused thinning of the formation. This has probably created a collapse zone which could act as a local aquifer. Subcrops and outcrops of this unit occur in Harper, Kingman, and Reno counties. This unit is not a significant aquifer, and where subcropping, is considered to form part of the eroded Permian surface on which the unconsolidated material was deposited.

Ninnescah Shale

The Ninnescah Shale is composed primarily of red and light-gray shale, silty shale, and siltstone. Some thin veins of gypsum are also known to occur. Where the formation is weathered or fractured, or has localized sandstone units, it is capable of yielding water to wells. This water is typically of low quality, but suitable for stock and domestic wells in outcrop areas. It is not clear from the literature whether formation water is under artesian pressure. If such a pressure differential exists, leakage could occur into the fresh-water unconsolidated aquifer. Due to lack of information regarding this point, it was conservatively assumed that the formation is essentially impermeable in its unweathered portion. Where it subcrops, the formation defines the bedrock surface upon which the alluvial aquifer material has been deposited.

Post-Cretaceous Deposits

All sedimentary units composing the aquifer referred to in this study as the Great Bend Aquifer were deposited in post-Cretaceous time. These units include Pliocene, Pleistocene, and Recent deposits. Hydrologically, they behave as a single unit, although they by no means constitute an isotropic and homogeneous medium. The principal aquifer materials are sands and gravels, some of which are cemented. Associated materials include clay and silt, which usually occur in conjunction with the sands and gravels in the poorly-sorted bedding, although some relatively clean clay beds occur. In reality, these materials form restrictive beds and lenses in the aquifer and give it a marked degree of anisotropy and heterogeneity, principally in the vertical direction. They are also responsible for locally-confined conditions throughout the sand and gravel deposits.

The principal coarse-grained units of the unconsolidated aquifer include the Holdrege and Grand Island formations of the Nebraskan and Kansan Glacial Stage. Other coarse-grained deposits include the Ogallala Formation of the Pliocene series and the dune sand deposits ranging in age from Pleistocene to Recent. Stream alluvia exist for all the major streams in the region and are deposited in channels cut into the older deposits. Most of these alluvia consist of material very similar to that over which they are deposited. In essence, the newer deposits are simply reworked deposits of older materials. In the stream alluvia, coarser material tends to occur at the bottoms of the depositional sequences. Throughout the modeling procedures, vertically averaged values of hydraulic conductivity were used to describe two-dimensional, depth-uniform flow. Therefore, it was not necessary to differentiate the aquifer material properties with respect to depth, and no further discussion will be directed towards this point.

General Features of Flow in the Great Bend Alluvial Aquifer

Flow in the alluvial aquifer is generally eastward, with most lateral inflow occurring in the vicinity of Ford and Kiowa counties from similar despoits to the west (see Fig. 2). Plate 1, which is a contour representation of the pre-development water levels, illustrates the localized nature of lateral inflow to the aquifer during the pre-development period prior to 1950. Some water appears to have been flowing northward into the Arkansas River during this time. Losses across the southern extent of the prairie are believed to occur through some combination of evapotranspiration from the shallow water table in the area, leakage into Lower Cretaceous and Permian bedrock units which outcrop along the southern boundary of the alluvial deposits when southward-trending hydraulic gradients occur across the bedrock contact, and underflow to alluvial valleys which traverse the outcrop area.

Small-scale upstream potentiometric flexures in the vicinity of the major stream valleys indicate that the streams were gaining along most of their lengths during pre-development time. The orientation of these flexures is substantiated by reports of significant baseflow to the stream channels prior to 1950 by local residents.

The measured bedrock surface slopes eastward, as indicated by the bedrock configuration shown in Plate 2. On a regional scale, the bedrock and water-table configurations show a remarkable similarity, suggesting that flow in the aquifer is greatly influenced by the physical features of the bedrock contact. Pre-development saturated thickness within the study area ranged from a high of about 250 feet in southeastern Edwards County, to saturated thicknesses as small as 10 feet in Reno County (see Plate 3). Local values of up to 200 feet also occurred in the northeastern and northwestern sections of the study area. Most of the 1,160 irrigation wells in operation as of 1973 were located in the high-saturated-thickness west-central area, where predevelopment saturated thicknesses of up to 250 feet occurred and where well yields may once have been as high as 2,000 gallons per minute (gpm) (Fader and Stullken, 1978). Current yields are more frequently in the range of 500 to 1,000 gpm. The occurrence of small saturated thicknesses in western Rice County were attributed to a locally shallow depth to bedrock.

DESCRIPTION OF THE CALIBRATION MODELS

Calibration of the Great Bend alluvial aquifer was based on a forward, or predictive, approach to solving the governing two-dimensional flow equation (Trescott, et al., 1976)

$$\frac{\partial}{\partial x}\left(K_{xx}\, b\, \frac{\partial h}{\partial x}\right) + \frac{\partial}{\partial y}\left(K_{yy}\, b\, \frac{\partial h}{\partial y}\right) + W = S_y \frac{\partial h}{\partial t} \tag{1}$$

for unknown aquifer parameters hydraulic conductivity (K_{xx} and K_{yy}) and specific yield (S_y) as well as for the unknown net recharge variable (W), where

K_{xx} = hydraulic conductivity in the x-direction (L/T)

K_{yy} = hydraulic conductivity in the y-direction (L/T)

b = saturated thickness (L)

h = hydraulic head (L)

W = net distributed and point source-sink rate, positive for net recharge and negative for net discharge (L/T)

S_y = specific yield

Steady-state calibration was initially performed using the 1976 version of the USGS model (Trescott, et al., 1976), while a more refined steady-state calibration and several transient calibrations were attempted using a computerized steepest-descent optimization model which was developed at Texas Tech University (Knowles, et al., 1972). Both algorithms are based on discrete approximations of differential equation 1, although the procedures used to discretize the flow domain in space and time are somewhat different for the two models.

While aquifer parameters K_{xx}, K_{yy} and S_y were assumed to vary only in space, the variables b, h, and W were assumed to vary in both space and time. The values of K_{xx} and K_{yy}, which can formally be viewed as the principal components of the hydraulic conductivity tensor, represent internodal conductivities in the x- and y-directions. These internodal conductivities are obtained by averaging of adjacent nodal conductivity values and are essentially equivalent to K values at the interfaces defined by the cells surrounding each node.

Although the two models are both based on equation (1), the USGS model is block-centered, with each mass-balance cell corner corresponding to a finite-difference node, while the Texas model is mesh-centered. This discrepancy did not present any serious problems within the modeled area, but it did result in different approximations of the boundary conditions on the periphery of the study area. In addition, the averaging procedures used to define internodal conductivity under heterogeneous conditions and the methods of approximating saturated thickness are quite different for the two models, and were ultimately considered responsible for the frequently-encountered differences in model output.

The USGS Model

The USGS finite-difference model was used to simulate two-dimensional, steady-state flow in the Great Bend alluvial aquifer during the first calibration phase. Implicit to the assumption of two-dimensional groundwater flow is that vertical flow in the aquifer is negligible. While this assumption may be justified for the case of the undeveloped water table, vertical flow components may be introduced during the later prediction stage when significant well withdrawal rates are imposed on the aquifer system. Use of a two-dimensional flow model also requires that the rate of flow be uniform over the entire depth of saturation. Given that the Great Bend aquifer does not appear to exhibit significant layered heterogeneity, the assumption of uniform flow can be considered valid for this particular study.

Clearly, the Dupuit-Forchheimer assumptions of horizontal, uniform flow greatly facilitated analysis of the Great Bend aquifer flow regime, but required that water-table movement in the vertical direction be completely ignored and that hydraulic gradients be small. Fortunately, the stresses which were imposed on the regime during the validation procedure were not significant and resulted in very little drawdown relative to saturated thickness and only slight increases in the slope of the water table throughout the groundwater development period.

Hydraulic Conductivity K and Specific Yield S_y

In order to allow extension of the final, calibrated model to the time-variant flow regimes expected to occur during validation and prediction stages of the study, parameters were defined to be time-invariant properties of the aquifer. This involved choosing K, rather than transmissivity T, as an indicator of aquifer-transmission characteristics. The assumption of a constant specific yield S_y was justified on the basis of the regionally-unconfined characteristics of the alluvial aquifer, as well as on the assumption of lack of measurable subsidence of the deposits during the development period.

Delayed-drainage effects were not considered during any part of the calibration process. These effects would have required time-variance of specific yield. Due to the large conductivities associated with the alluvium, specific retention was assumed to be negligible, and drainage of the aquifer in response to pumping was considered to be instantaneous with respect to the one-year time steps used for calibration.

Total Net Recharge Rate W

The net recharge rate W was assumed to be the sum of net natural recharge rate R and the pumping rate Q

$$W = R + Q \tag{2}$$

where Q would be described by negative, or discharging, values. Net natural areal recharge R, although actually a system variable, was taken to be a time-invariant parameter of the aquifer system. Seasonal variations in R were considered to be irrelevant to the study, since a one-year time step was used throughout all model operations. Q was assumed to be constant during the duration of each five-year pumping period used for the validation procedure, but was assumed to vary between pumping periods. Due to the tendency for reported pumpage rates to be overestimated, it became necessary to introduce an additional term of $(\alpha-1)Q$ to equation (2) during the validation stage, where α represented a correction factor for irrigation consumptive use.

Figures 4 to 8 illustrate the transient water tables observed at five-year intervals in the alluvial aquifer during the development period 1950-1975. Clearly, these water tables are virtually identical to the pre-development water table shown in Plate 1. The pumping stresses which had been imposed on the system during the development period were apparently offset by boundary contributions or by increases in natural recharge, at least on a regional scale.

Although the USGS model includes options for explicitly accounting for evapotranspiration and leakage from the underlying Permian-Cretaceous system, no attempt was made to simulate evapotranspiration or leakage effects. The mechanisms and quantities of evapotranspiration and leakage are only poorly known, and inclusion of these mechanisms would have significantly increased the complexity of the model without increasing the amount of information obtained from it. Evapotranspiration and leakage were instead assumed to be incorporated into the natural recharge variable R during calibration.

Since any finite-difference model is only capable of treating W as a distributed source or sink over each cell, well withdrawals described by Q at each node were automatically distributed over the associated cell. This presented no serious problems during model operation, because Q at a given node was estimated as the sum of consumptive use over the associated cell, and could be viewed as essentially distributed in nature.

System Boundaries

The parameters K, S_y, W and α comprise the four-dimensional parameter space used for the USGS steady-state and transient calibration procedures. No attempt was made to calibrate the model for boundary configurations or boundary-flux conditions, since this would have introduced an unacceptable number of degrees of freedom into the parameter-adjustment procedure. Constant-head conditions which were initially assigned to the boundary nodes were essentially equivalent to constant-flux and constant-gradient boundaries under steady-state conditions assumed during the initial calibration stage. Use of constant-head boundaries was considered to be an effective means of overcoming the problems associated with unreliable or unavailable flux data at the boundaries without seriously distorting the actual flow relationships at the boundaries. These constant-head values were obtained by interpolating from observed head data. They represented more reliable aquifer responses than flow data could supply and were used during subsequent model operation in order to better define the uncertain flow relationships at the boundaries. Constant-head nodes located along the rivers also served to approximate conditions at the river-aquifer interfaces without explicit definition of baseflows or river losses. Steady-state stream-aquifer fluxes, along with the fluxes at the model boundaries, were instead specified **a posteriori** on the basis of final steady-state head and K estimates, and then systematically varied during transient validation and prediction stages according to Darcy's law by assuming constant-gradient conditions.

It was expected that problems related to identification of K during the steady-state calibration of the USGS model could arise near the northern boundary of the model area due to negligible flux across this boundary. Examination of the observed steady-state water table (see Plate 1) indicates that the northern boundary of the Great Bend study area is virtually perpendicular to the contours of the equipotential surface along most of its extent. The small amount of flux crossing this boundary can cause K to become undefined, since any conductivity value which is assigned to the near-boundary nodes will produce approximately zero-valued flow across the boundary under conditions of negligible north-south gradients. From figures 4 to 8, it is clear that no-flow conditions prevailed along the northern boundary of the model area throughout the development period, and that values of K obtained from transient calibrations would also be subject to large errors of estimate.

The Steepest-Descent Optimization Calibration Model

The second phase of the parameter-adjustment procedure involved use of the computerized steepest-descent optimization algorithm. Like the USGS model, the Texas model approximates two-dimensional, depth-uniform flow over the study area. Assumptions concerning K, S_y, and W, as well as assumptions concerning boundary conditions, were extended to operation of the Texas model.

Aside from conductivity and saturated-thickness averaging procedures, the two models simulate aquifer response according to a discretized version of equation (1). However, the optimization model incorporates a steepest-descent calibration component which is alternated with the simulation component during model operation. Details of the steepest-descent optimization procedure are outlined in Appendix C.

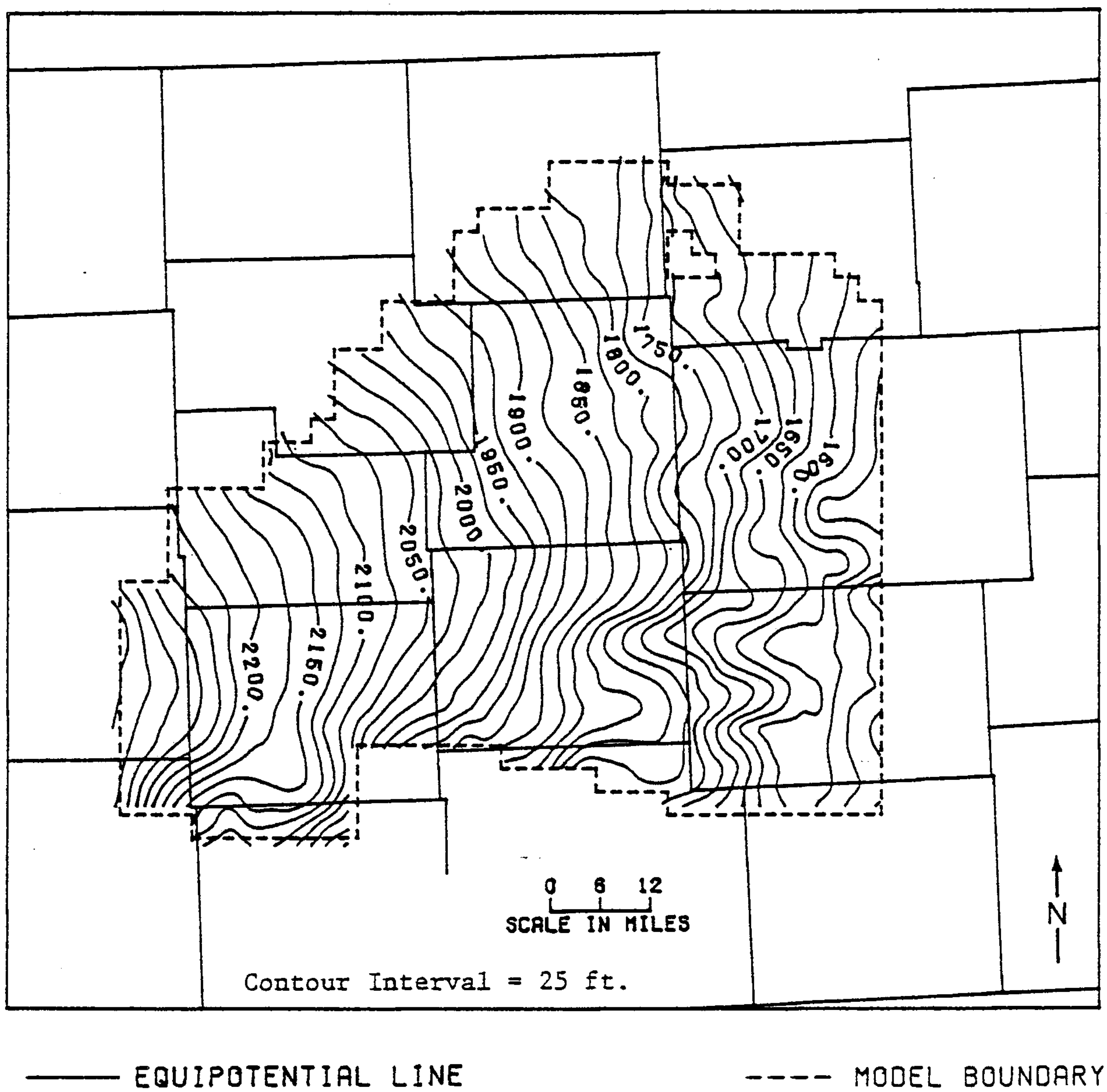

Figure 4. Observed 1955 potentiometric surface (feet).

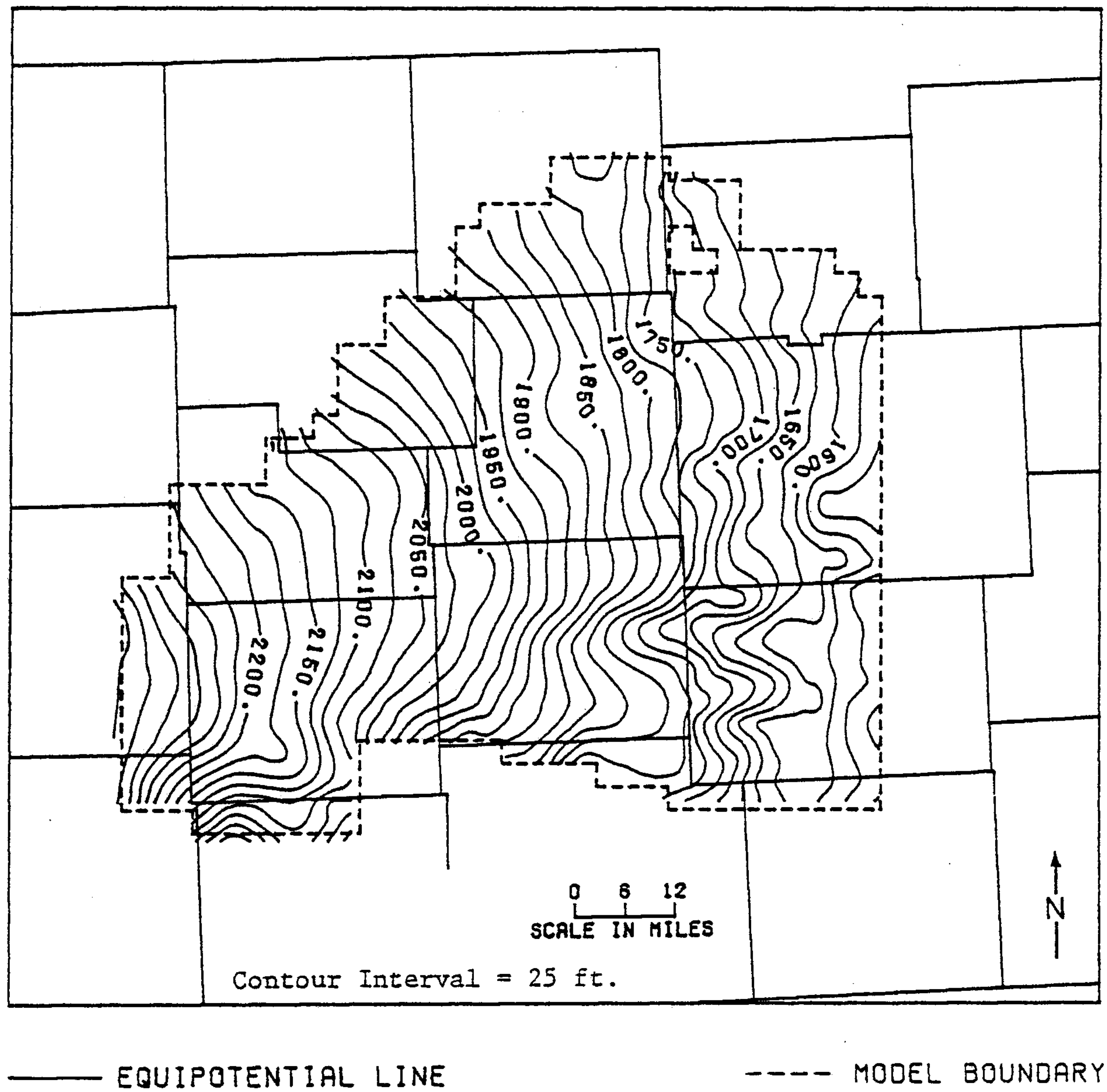

Figure 5. Observed 1960 potentiometric surface (feet).

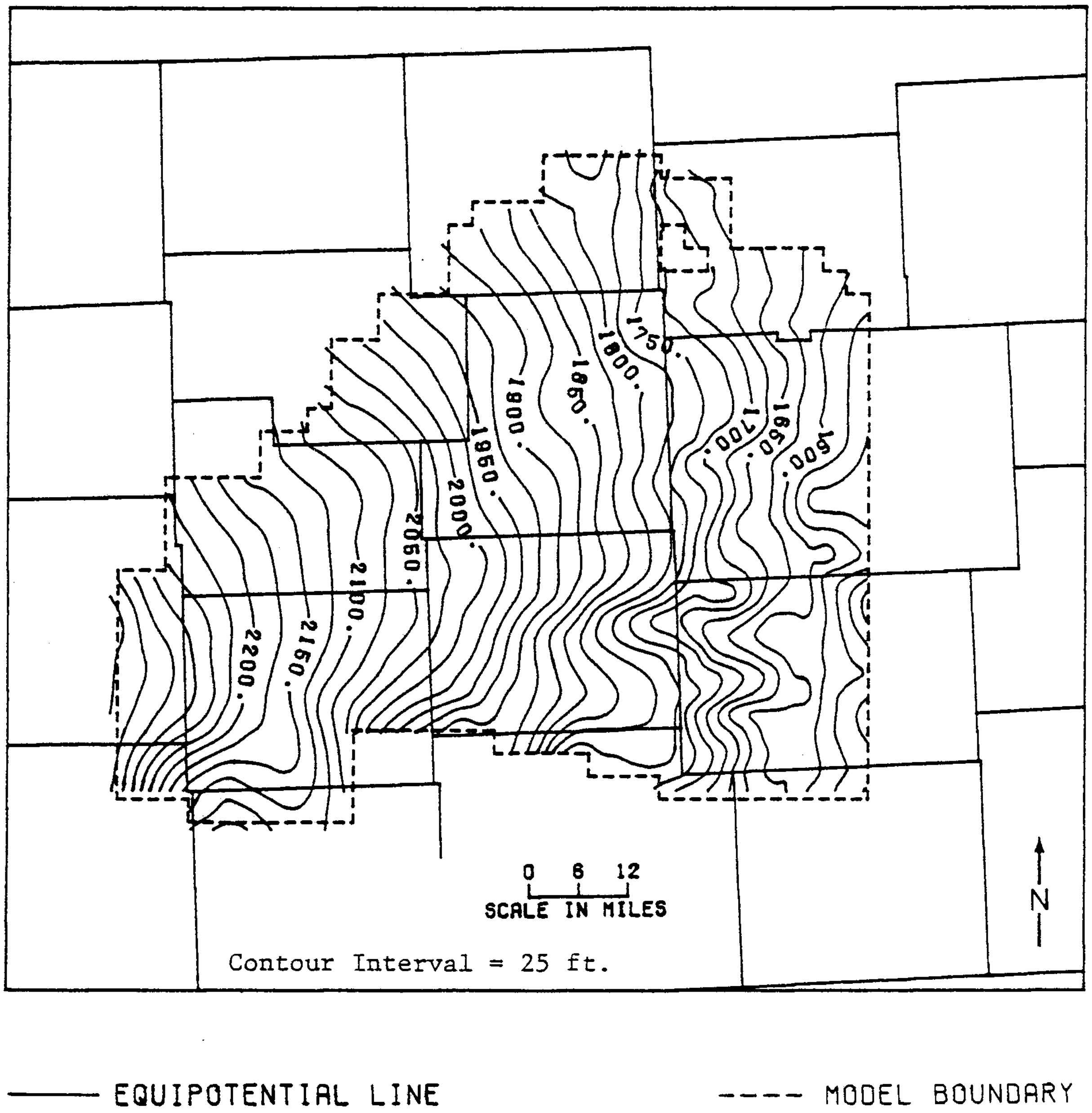

Figure 6. Observed 1965 potentiometric surface (feet).

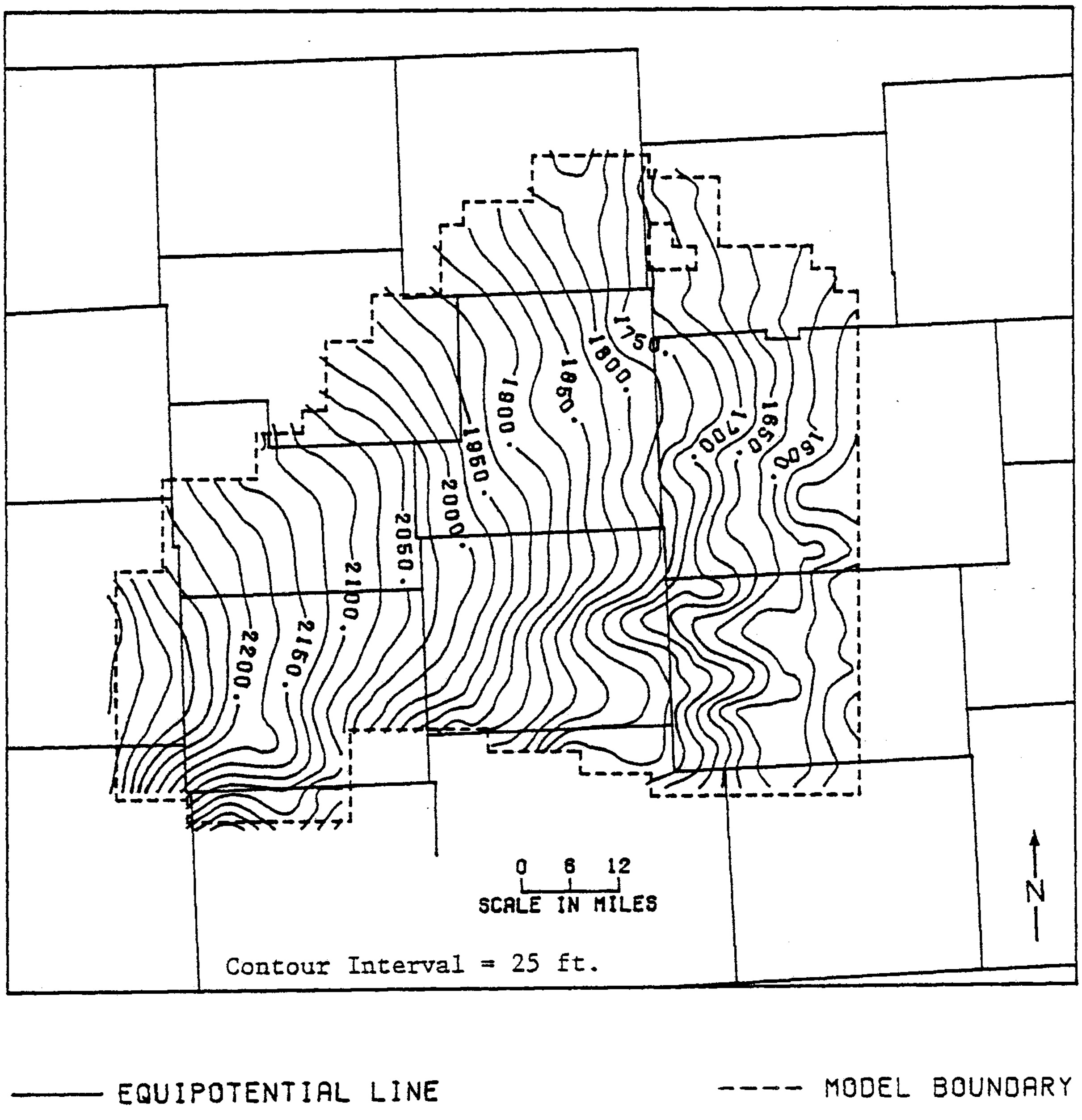

Figure 7. Observed 1970 potentiometric surface (feet).

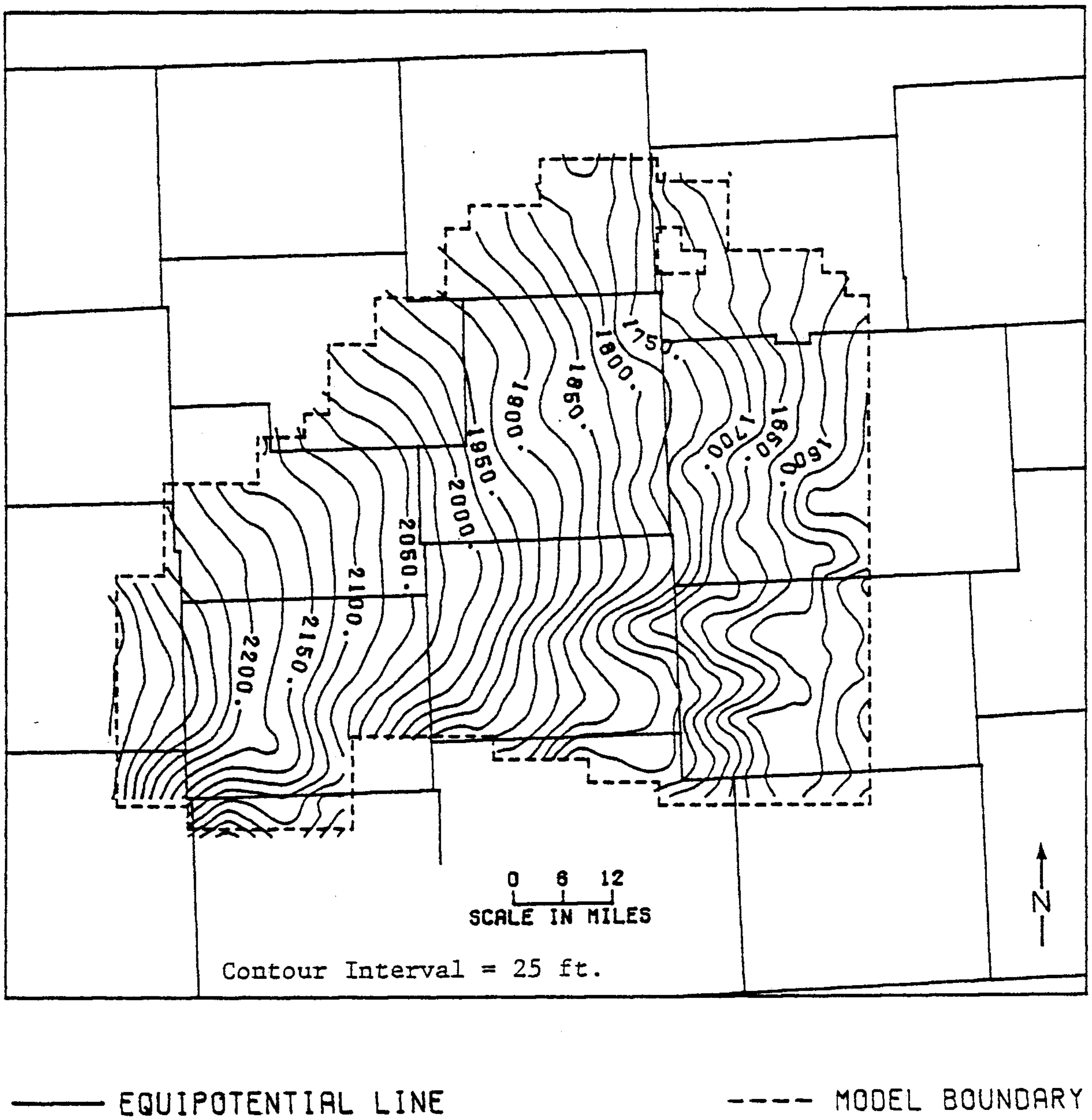

Figure 8. Observed 1975 potentiometric surface (feet).

In addition to potential boundary problems related to K, the possibility of obtaining poor estimates of specific yield due to misplacement of constant-head boundary and river nodes occurred during the steepest-descent transient calibration runs. Misplacement of constant-head river or boundary nodes would presumably become evident during the optimization procedure, when very large sensitivities of head with respect to S_y would occur near the assigned constant-head nodes.

CALIBRATION OF THE GREAT BEND AQUIFER MODEL

Steady-State Calibration for Uniform K and Distributed R Using the USGS Finite-Difference Model

Adjustments of the Original Data Base

The original data base for the Great Bend Aquifer Model Study was supplied by USGS. These data consisted of matrices of potentiometric surface elevations and bedrock elevations. The mesh size of the original base was 5,000 feet. The mesh was isometric in the x and y directions, having 120 rows and 134 columns and was orthogonal with the y axis oriented in the north-south direction. This orientation permitted accurate duplication of regional eastward flow in the aquifer.

The fineness of the model grid at the original spacing was considered to be prohibitive from the standpoint of computational expense and processor time. As a consequence of these objections, and after consultation with USGS researchers, the grid spacing was increased to 15,000 feet. The grid dimensions were correspondingly reduced to 40 rows and 42 columns, and included 1,680 nodes. The extent of this averaged mesh and the active model region is shown in Figure 9. Point A corresponds to node (24,2).

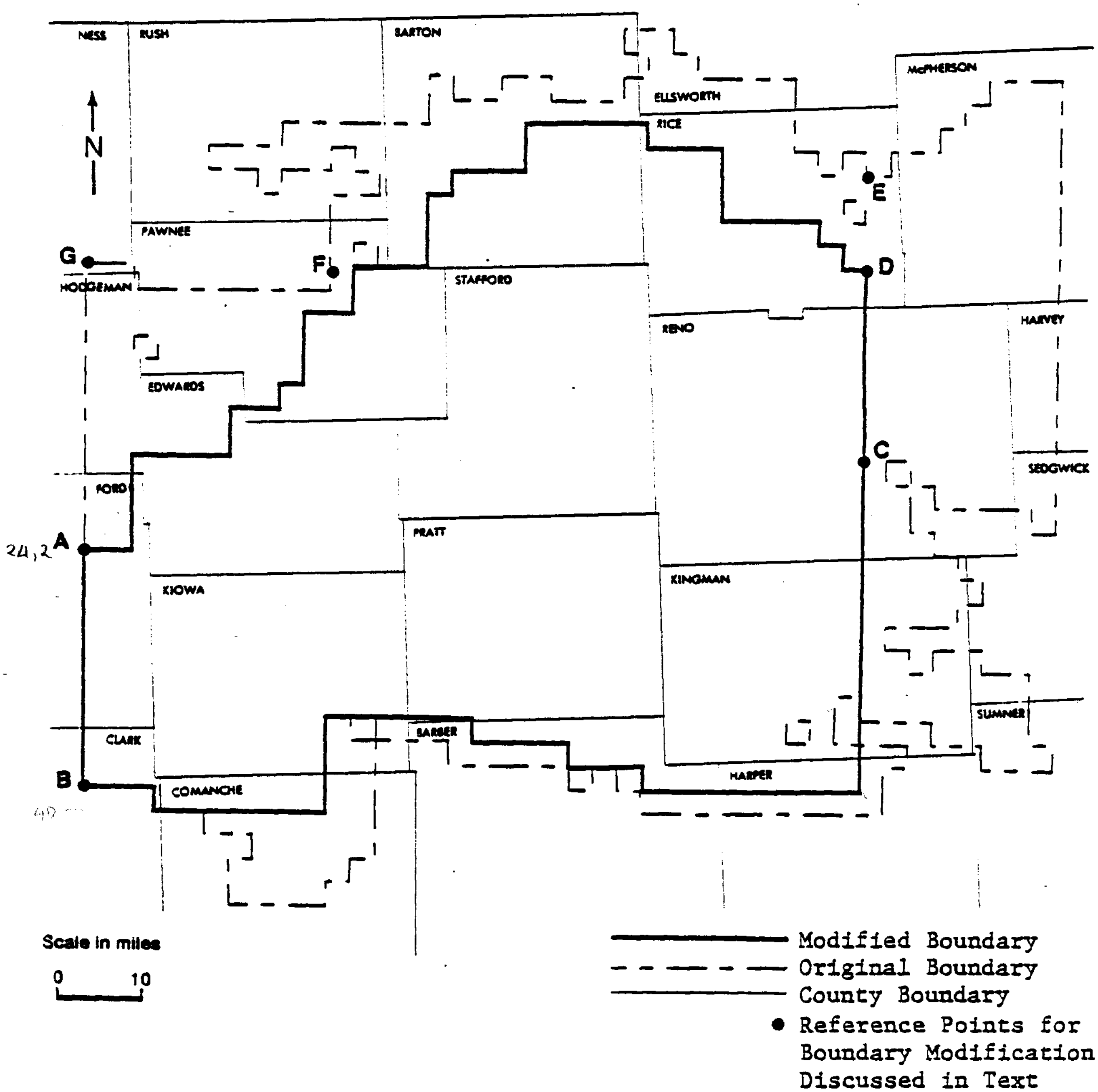

Figure 9. Model boundaries.

The new, coarse mesh was established as an averaged subset of the original mesh. Head levels at the nodes defined by the 15,000-foot mesh were calculated as an average of the head values at each original node and the eight nodes surrounding the original node. Only the non-zero elements of the eight neighbors were included in the average, and no distance-weighting was performed. This process was used to preserve the gradients between the nodes as much as possible. This averaging process actually behaved as a smoothing filter. Its greatest effects were observed in areas of relatively steep hydraulic gradients, such as in regions near gaining streams, while very small perturbations occurred in regions of small gradient. Head levels near the boundaries were not significantly change as a result of the averaging procedure. The averaging process was applied to both the potentiometric surface and the bedrock configuration.

Early in the calibration procedure it was necessary to establish administrative boundaries in the active model domain. These boundaries are those which join directly to models being prepared by other researchers involved in the High Plains Regional Aquifer Systems Analysis. Essentially, they represent loci of nodes along which water is transferred from one model to the next. Refering to Figure 9, the line segment GAB represents the locus of nodes on the original boundary between the Ogallala aquifer and the Great Bend aquifer. The segment CDE represents the boundary between the Great Bend aquifer and the 'Equus Beds' aquifer. The original calibration effort involved all of the region bounded by the original boundary identified in Figure 9, except for the region east of segment CDE, which was incorporated into the Equus Beds model.

Initial Calibration Efforts

No-flow conditions were assigned to the original northern boundary of the model, as well as to the original southern boundary, where flux appeared to be negligible. Variable-flux conditions were assigned to rivers and to the eastern and western boundaries using historical fluxes across boundaries and average rates of gain in streams. All of this information was incorporated into the model, and many trial runs were attempted. The results showed generally erratic changes in the water table, generally with a considerable build-up on the southern boundary and many nodes going dry in the northern margins of the model. An attempt was made to apply a crude "inverse" method to calculate the fluxes necessary to hold the historic water table at a static position. Results of this methodology were less than satisfactory and the procedure was subsequently abandoned. It was decided that a thorough re-evaluation of the model boundaries was in order, especially along the northern and southern extremes.

Based on experiences with the first calibration attempt, further changes were made in the definition of the active nodes of the model. These changes were based upon re-examination of the geohydrology of certain areas and upon consideration of model detail in comparison to the scale of the mesh.

The nodal spacing for the model was 15,000 feet. Consideration of this dimension is critical when physical features being modeled approach the scale of this spacing. It is difficult to reproduce the details of narrow features of the potentiometric surface when their width is on the order of one finite-difference cell. In such cases, attempts to produce meaningful head-contour curvature become difficult. There were several areas where the boundary was totally or partially changed due to the inability of the mesh to adequately simulate the dimensions of the flow features. Cow Creek in southwestern

Ellsworth County, Walnut Creek in west-central Barton and east-central Rush counties, and the Pawnee River in Pawnee and Hodgeman counties are typical examples of this situation. Similar problems were encountered in eastern Kingman County and small portions of Sedgwick and Sumner counties. Many of the details were on the scale of only one or two nodal spacings, and this was believed to have produced extremely anomalous head levels in this area. This problem, as well as other problems, were corrected by modifications of the boundaries as outlined in the next section.

Geohydrological Modifications of the Boundaries

Many of the changes in the model boundary were made due to re-interpretation of the saturated geologic units in a given area. This is not a trivial point. In the area defined by region DEFD (see Fig. 9) a considerable amount of the unconsolidated material is underlain by material of Cretaceous age, particularly the Dakota Formation (Latta, 1950; Fent, 1950; Bayne, Franks, and Ives, 1971; Bayne and Ward, 1974; McNellis, 1973). In many of these areas the measured water table is actually in the Dakota except where modern streams have carved channels into the bedrock and deposited alluvium. These streams are in hydraulic connection with the Dakota. In areas where the water table is above the Dakota, the basic data does not indicate great saturated thicknesses. Some of these upland areas exhibit relatively steep hydraulic gradients. They generally tend to go dry rapidly when simulation began. Inclusion of these areas caused more numerical problems than their apparent contributions to the system justified. In the case of area DEFD, the Dakota was considered to be impermeable and the thin veneer of unconsolidated material was believed to be unsaturated. Rivers and associated alluvia carrying water into the active-model domain from the excluded area were simulated by source-nodes at the boundary, while rivers and alluvia carrying water away from the active domain were simulated by sink-nodes.

The region AGFA presented problems similar to those cited above. The Ford County Bulletin (Waite, 1942) indicates that in northeastern Ford County the Ogallala and Pleistocene deposits are once in hydraulic connection with the underlying Dakota Formation, and are subsequently all water drains to the Dakota. The extent to which this phenomenon is repeated in Edwards, Pawnee and Hodgeman counties is not totally clear from the County Bulletin, but it would not be an unreasonable expectation. The Pawnee-Edwards report indicates the presence of water in the uplands which may be above the top of the Dakota. Much of this area is upland, and these hydraulic heads may only represent localized perched water tables. In the original data, much of this area was shown to be characterized by relatively thin saturated thickness and steep hydraulic gradients. Many nodes went dry soon after simulation began. The only well-documented water table was in the river alluvia of Pawnee River, Buckner Creek and Saw Mill Creek. These narrow alluvia were addressed in a previous section. The same disposition of the thin unconsolidated veneer, the Dakota Formation, and the river alluvia was made as described in the previous paragraph.

As a result of the conclusions regarding geohydrologic influences along the northern extent of the model area, the northern boundary was modified as shown in Figure 9. The thin or absent Cenozoic deposits along the northern extent of the model area were assumed to act as a no-flow boundary and were assigned zero-flux conditions during model operation. This was substantiated by the fact that the hydraulic head contours were perpendicular to the modified northern boundary both before and after development.

The original eastern boundary was redefined as shown in Figure 9 to conform to the previously-mentioned Equus Beds model. Along the western and modified eastern borders of the area, natural hydrologic boundaries do not exist. In the absence of information concerning rates of flow across these borders, constant-head conditions were assigned to corresponding border nodes. These artificial boundaries were later assigned variable-flux conditions using a constant-gradient algorithm to account for potential boundary contributions to irrigation well withdrawals during the development period.

The final areas involved in the modification procedure are located along the southern and southeastern margins of the alluvial aquifer. The dominant feature of this area is the transition from the principally Pleistocene unconsolidated Great Bend aquifer to the deeply incised and eroded consolidated Permian redbed formations, where Pleistocene deposits are confined to narrow stream alluvia. This area is the most poorly documented section of the study area. No county reports exist for Clark, Comanche, and Barber counties. The Harper County Report (Bayne, 1960) contains a significant discrepancy with respect to the Kingman County study (Lane, 1960); researchers reported an interpretational difference of 20 to 40 feet in the water table at their common border. It is fairly clear from the historical data that a considerable volume of water moves out through the southern portion of the study area. There is not, however, a well understood breakdown of this outward flux among the various evapotranspiration, baseflow, underflow, and leakage sink terms. The rather large protrusion of the original boundary into Comanche County would seem to indicate an extensive aquifer system. Field observations made by Kansas Geological Survey personnel left the impression that perhaps several narrow valley alluvia, rather than a single extensive unit, are present in this area. This impression, combined with a less than adequate body of basic data for the area and a consistent inability to get reasonable calibration results from the area motivated the re-establishment of the southern boundary. It might be noted that the lack of basic data in this area demands further investigation.

It was eventually decided to incorporate the modified southern boundary into the model using constant-head conditions to account for aquifer losses. These were subsequently translated into variable-flux conditions during transient phases of model operation. Extensive drainage from the alluvial deposits into the deeply-incised Permian red beds to the extreme southeast was initially described by introducing several artificial pumping wells to the area in order to describe constant-flux conditions which were assumed to govern the drainage rate under steady-state conditions. The configuration of the southern boundary was made to conform approximately to the contact between the alluvial aquifer and the Cretaceous and Permian outcrops occuring along the southern extent of the prairie.

Boundary-Flux Simulation

Simulation of the boundary conditions in the alluvial aquifer was as much an interpretational process as it was a numerical process. Early in the study, a decision was made to apply a variable-flux, constant-gradient algorithm to the eastern and western administrative boundaries of the model (Wilson and Gerhart, 1980) . This was intended to simulate a physical continuity between independent numerical models. As work proceeded, it became apparent that the model was also discharging a considerable volume of water across the southern boundary. Although not specifically broken down in the modeling process, this volume had to represent some combination of underflow, leakage, and evapotranspiration. Since all of these mechanisms are related in some degree to saturated thickness, a decision was made to simulate this boundary, as well as the administrative boundaries, using saturated-thickness-dependent, variable-flux conditions.

Conversion of the constant-head nodes at the model boundaries to constant-gradient nodes was accomplished by performing a nodal mass-balance at each constant-head boundary node after steady-state calibration for hydraulic conductivity and natural recharge, and by subsequently using the calculated nodal fluxes to initialize a constant-gradient, variable-flux algorithm at these nodes. The variable-flux algorithm was then introduced into the model during transient calibration and validation stages, when the effects of irrigation withdrawal were transmitted to the boundaries.

Implicit to the introduction of the constant-gradient algorithm was the assumption that head at interior nodes immediately adjacent to the affected boundary nodes varied by the same magnitude as head at the boundary. While many arguments may be presented in opposition to this assumption, it greatly facilitated the incorporation of time-variant behavior at the boundary nodes. Of course, the problem of specifying values of S_y at these nodes was of considerable concern during model validation and prediction, since the variable-flux nodes had previously been insensitive to specific yield in their constant-head state.

The constant-gradient, variable-flux algorithm was developed according to Darcy's law by equating gradients during two consecutive time periods for each variable-flux boundary node. Using Darcy's law, flux at time 1 and 2 can be expressed as

$$Q_1 = K_1 w_1 b_1 \frac{\Delta h_1}{\Delta x_1}$$

$$Q_2 = K_2 w_2 b_2 \frac{\Delta h_2}{\Delta x_2}$$

where w_1 and w_2 are the widths of the cross-sectional flow area at time 1 and 2. For a time-invariant grid, the two widths will be equal. Hydraulic conductivity, by definition, is also time-invariant. For constant-gradient conditions, the flux algorithm was developed as follows:

$$\frac{\Delta h_1}{\Delta x_1} = \frac{\Delta h_2}{\Delta x_2}$$

Substituting for hydraulic gradients,

$$\frac{Q_1}{K_1 w_1 b_1} = \frac{Q_2}{K_2 w_2 b_2}$$

and assuming constant conductivity and flow widths,

$$Q_2 = Q_1 \frac{b_2}{b_1} \qquad (3)$$

Changes in flux at each variable-flux node during each time step were therefore only a function of changes in the saturated thickness at that node. Use of Darcy's law is strictly valid only for small time steps, within which flow can be viewed as essentially steady-state in nature.

The algorithm described by equation (3) was incorporated into both the USGS and Texas models in anticipation of the usefulness of describing the variable boundary conditions during later model validation and prediction stages, when pumping stresses were expected to result in increasing boundary contributions to the interior flow regime. In order to maintain the validity of the constant-gradient assumption, it was imperative that no pumping wells be placed at or near the variable-flux nodes during transient operation of the models. The occurrence of wells near the variable-flux nodes would have introduced transient effects into the node cells, effectively invalidating the assumption of approximate steady-state flow within each time step implied by equation (3).

Simulation of Stream-Aquifer Interaction

In order to reduce the number of parameters in the calibration process, a decision was made to utilize the variable-flux node configuration to simulate the gains or losses along simulated stream channels. The USGS model has an option for simulating variable-flux stream nodes which is based on the assumption of a leaky confining bed. This option adds an additional set of unknowns to the calibration process. A set of values for the river stage need to be assembled, and estimates for the streambed thickness and hydraulic conductivity are also required. All of these parameters would then need to be adjusted as part of the calibration process. Instead of the leaky bed option, the constant-gradient, variable-flux algorithm was used to simulate baseflows and river losses. However, it was not possible to simulate both losses and gains at the river nodes, because once a river node was identified as a gaining node, it was not possible for it to become a losing node as a result of irrigation development according to equation (3). Fortunately, the pumping stresses which the aquifer experienced during development were not significant, and no flow reversals occurred at the river nodes. The modeler must keep this limitation in mind, however, if the model is to be used to predict the future effects of major agricultural development in the prairie.

Steady-State Calibration Using Constant-Head River & Permeable Boundary Nodes

Assumptions:

With the boundaries adjusted as previously described, and as shown in Figure 9, efforts were again directed to steady-state calibration of the numerical model using constant-head conditions to initially describe the rivers and permeable boundaries. Several operating assumptions were made after consultation with the USGS staff. These assumptions were:

1) The hydraulic conductivity K was assumed to be uniformly distributed and initially estimated to be 100 ft/day.

2) A specific yield of $S_y = 0.0$ would force convergence to a unique, steady-state head solution as long as at least one constant-head node was specified in the grid and either the general magnitude of K or R was known.

3) All boundary nodes were initially no-flow or constant-head types and stream nodes were assigned constant-head conditions.

4) Initial precipitation recharge R was assumed to be 0.5 inches per year at all nodes except constant-head boundary and river nodes.

5) Calibration would be initially performed with respect to recharge against a fixed hydraulic conductivity, since the magnitude of K was better known than the range of R.

6) Head-closure error was originally set at 1.0 feet, in order to prevent an excessive number of iterations which would result from poorly-conditioned data or boundaries.

7) The sum of squared calibration error was used to indicate goodness of fit between the measured and simulated surface, since minimization of the sum of squared error was equivalent to minimization of the error variance; calibration error was defined to be equal to the difference between simulated head and observed head.

The Calibration Procedure:

Natural recharge R was adjusted by means of an algorithm which corrected the current recharge estimate on the basis of calibration error:

$$R^{p+1}_{i,j} = R^{p}_{i,j} + \gamma \varepsilon^{p}_{i,j} \quad , \quad \gamma = .001 \text{ (in/yr)/ft} \tag{4}$$

for values $|\varepsilon^{p}_{i,j}| > 20$ ft

where $R^{p}_{i,j}$ was the recharge estimate at node (i,j) for the current trial (p); $\varepsilon^{p}_{i,j}$ was the error at node (i,j) for the current trial (p); and $R^{p+1}_{i,j}$ was the recharge estimate computed for node (i,j) during the next trial (p+1). Twenty feet was chosen as a purely-subjective measure of error tolerance during this stage of the calibration.

Although most of the nodes responded to this procedure in a convergent fashion, a few nodes, mostly in the southwestern and southeastern regions did not. One problem area occurred in the southeastern part of the grid, where the deposits were apparently draining a large amount of water. Reference to the Kingman County Bulletin (Lane, 1960) indicated a break in the continuity of the water table due to the river alluvium being eroded into the Permian units. As mentioned previously, several artificial wells were introduced to this region, and well-discharge rates were assigned so that simulation errors in the area did not exceed ±20 feet.

The steady-state calibration involved variation of precipitation recharge R on a node-by-node basis until the error between observed head and simulated head was reduced to the arbitrarily-defined tolerance limit of ±20 feet. Although node-by-node adjustment of R introduced a large number of degrees of freedom to the calibration procedure, and theoretically permitted a nearly perfect fit between observed and simulated head distributions, recharge was only allowed to vary from 0.0 to 6.0 inches per year. The maximum precipitation recharge rate of 6.0 in/yr was chosen as a subjective measure of the largest possible rate of percolation to the alluvial aquifer. After errors at all nodes were reduced to below the tolerance limit, hydraulic conductivity K was allowed to vary between 75 ft/day and 120 ft/day to determine a minimum of the sum of squared calibration errors. It was assumed that, as long as the final calibration errors over the model region after calibration for K were less than assumed measurement errors of up to 20 feet, the estimation errors of K and R were within tolerable limits. The 15,000-foot square grid used during all model operations was considered to be fine enough to allow differentiation of homogeneous K and R grid cells within the study area, thus preventing undercalibration, or a tendency for the variance of calibration errors to exceed the error variance of the measured steady-state water table.

The final simulated steady-state head distribution was defined uniquely by the inclusion of constant-head nodes at the boundaries and rivers, which can be viewed as a means of 'fixing' the particular solution to the time-invariant version of differential equation (1) for $S_y = 0.0$ when the magnitude of K or R is known. In the absence of specified constant-head or constant-flux nodes within the model and reliable K or R estimates, any number of steady-state distributions, or homogeneous solutions to the forward partial differential equation, could have resulted from the simulation procedure. These distributions would have all been capable of describing the observed head gradients, and would have differed at each node only with respect to an additive factor. When this additive factor was defined by at least one constant-head node anywhere within the model area and by good estimates of K or R, the steady-state distribution likewise became defined and unique.

It may be argued that the Poisson equation, which results from equation (1) for $S_y = 0.0$, is a nonhomogeneous differential equation with forcing function W=R, and that this forcing function guarantees the existence of a particular solution to the partial differential equation. However, it should be noted that R is actually a variable during the calibration, and that the corresponding particular solution is nonunique. Moreover, if the general magnitude of R relative to K is not known, an infinite number of steady-state head solutions is possible. The use of Poisson's equation, in the context of a recharge-adjustment scheme, does not therefore guarantee a unique steady-state head solution unless constant-head or constant-flux nodes are identified within the model area and unless the magnitude of K with respect to R is known.

Specification of a uniform value of K removed conductivity from the derivative terms in the flow equation and made head solution equally sensitive to variation of K and net recharge R. It was not possible to calibrate the USGS model against specific yield during this particular phase of the study, since the USGS model calibration initially involved only adjustment of parameters that govern steady-state flow.

The SIP option of the USGS model was chosen in an effort to prevent the occurrence of potential problems usually associated with iterative solution of the steady-state flow equation. Although the SIP iterative scheme is significantly more complex than either the ADI or LSOR schemes, it can more effectively damp down the instability potentially caused by the large head changes that are usually associated with steady-state head convergence under unconfined conditions because of the additional iteration parameter β'. The SIP option also reduced computer time and storage. An iterative approach was required due to the steady-state nature of the problem, and because the finite-difference equations were nonlinear in head. The optimal iteration parameter β', although problem-dependent, was chosen as 0.5 in accordance with the results of a series of numerical experiments performed by USGS researchers (Trescott, et al., 1976). Selection of a value of β' less than unity can be viewed as an attempt to under-relax the iterative process, a procedure which is especially desirable for an unconfined, nonlinear system that can become characterized by large changes in head from iteration to iteration. The under-relaxation process served to damp down potential instability during solution of the nonlinear flow equations, essentially allowing interpolation of head between two successive iterations and preventing possible overshooting of head values. The exact value of 0.5 has been found to represent the value of β' which results in the fastest rate of convergence for a regional, nonlinear system which is characterized by spatially-variable T or K (Trescott, et al., 1976).

Calibration Results:

Initial results of the steady-state calibration procedure were disappointing. When uniform values of 100 ft/day and 0.5 in/yr were assigned to K and R, respectively, the USGS model did not converge to a time-invariant head distribution, despite the fact that a specific yield of zero was chosen to force convergence to steady-state conditions. It was recognized that the questionable quality of head and bedrock data in the southern part of the grid was partly responsible for divergence of the head distribution from steady-state. Poor bedrock data in this highly-eroded area may also have contributed to the convergence problem by distorting cross-sectional flow areas.

At this particular stage in the steady-state calibration, it was believed that the primary cause of head divergence could be attributed to the coarse nodal spacing of 15,000 feet used to define the finite-difference mesh. The model was apparently not capable of performing accurate nodal mass balances when such widely-spaced nodes were used, especially in the presence of even moderate 'noise' in the head and bedrock distributions for the southern part of the grid. It was assumed that a more continuous set of head and bedrock data in the southern part of the grid would alleviate problems associated with the coarseness of the grid.

In an effort to define more continuous head and bedrock distributions, anomalous values of pre-development head and bedrock in the southwestern and southeastern parts of the grid were identified and manually adjusted. Since the model was to be later used to predict future head levels, it was considered desirable to adjust head and bedrock as little as possible at this particular point in the calibration procedure. The altered, pre-development head distribution and altered bedrock are shown in Figures 10 and 11. The

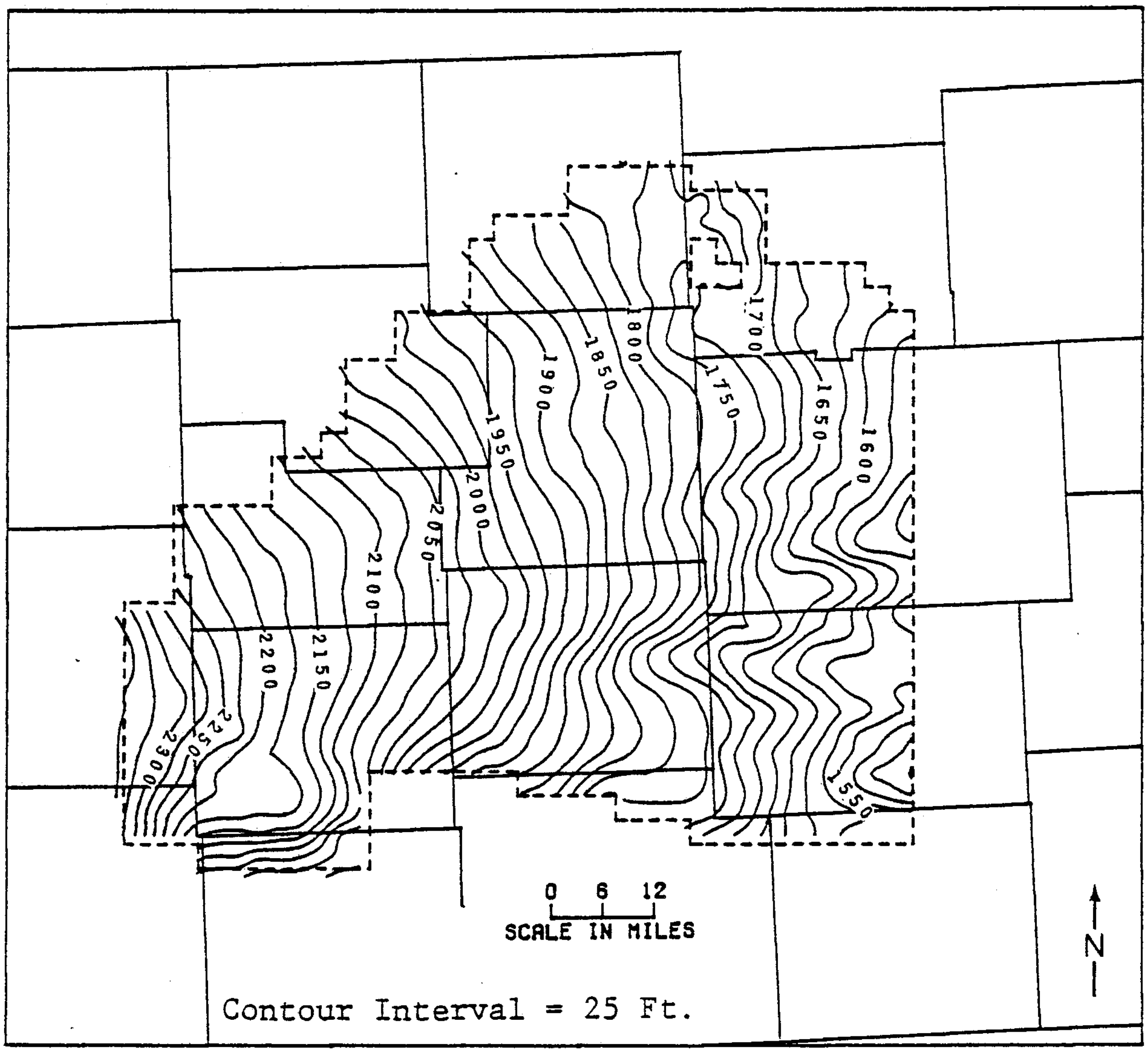

——— EQUIPOTENTIAL LINE ---- MODEL BOUNDARY

Figure 10. Altered pre-development potentiometric surface (feet).

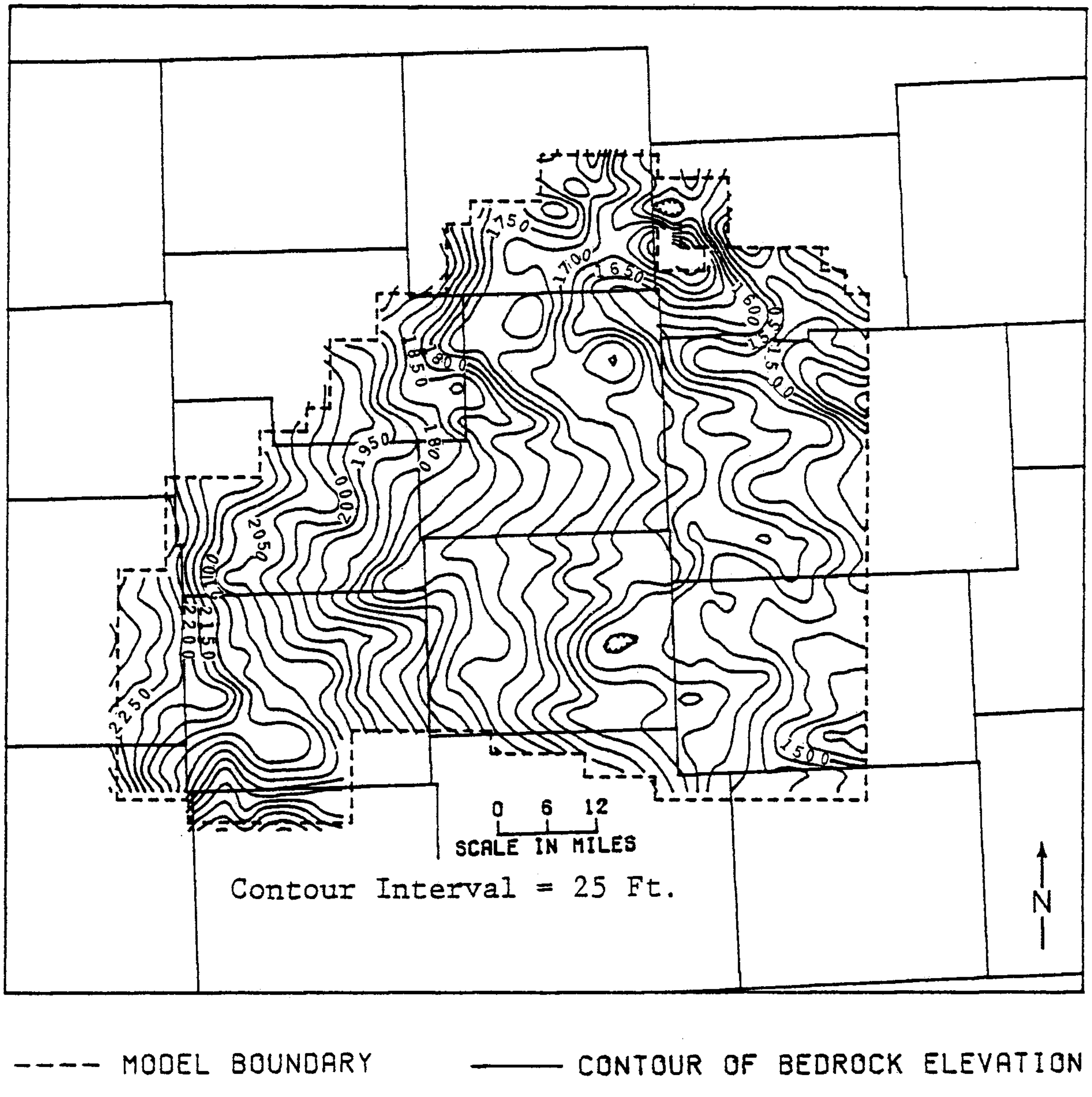

Figure 11. Altered bedrock configuration (feet).

USGS model was again used to attempt to generate a steady-state head distribution. Steady-state conditions were attained after 19 iterations using the modified head and bedrock data.

Using steady-state head generated with 0.01-foot error closure, uniform variation of K against final distributed net recharge resulted in a minimum sum of squared calibration error of 21,000 ft^2 for a uniform hydraulic conductivity value of 85 ft/day. Errors at all 674 active nodes were in the range of ±20 feet, while errors at 88% of these nodes were in the category of ±6.0 feet. The mean calibration error for all active nodes was +0.5 ft, with a standard deviation of 5.5 feet.

Figure 12 shows a histogram of calibration errors for an error interval of 1.0 foot. When an interval of 0.05 feet was used, the histogram showed evidence of an approximately normal distribution. Under the null hypothesis that calibration error was normally-distributed with a mean 0.5 feet and a standard deviation 5.5 feet, a χ^2 -test performed on the refined frequency distribution indicated that the hypothesis should be accepted at the 10% level of significance. Measurement error is generally viewed as the result of a large number of additive influences and, by the central limit theorem, is theoretically normally-distributed. The calibration error may therefore be an indication of the magnitude of measurement error which still pervades the modified pre-development water table.

Figure 13 illustrates the spatial distribution of calibration error obtained from the steady-state calibration. Errors in excess of 5 feet occurred much more frequently in the southeastern and southwestern portions of the model, presumably because the coarse grid still could not accurately describe the steep gradients which characterize these areas, despite head modifications.

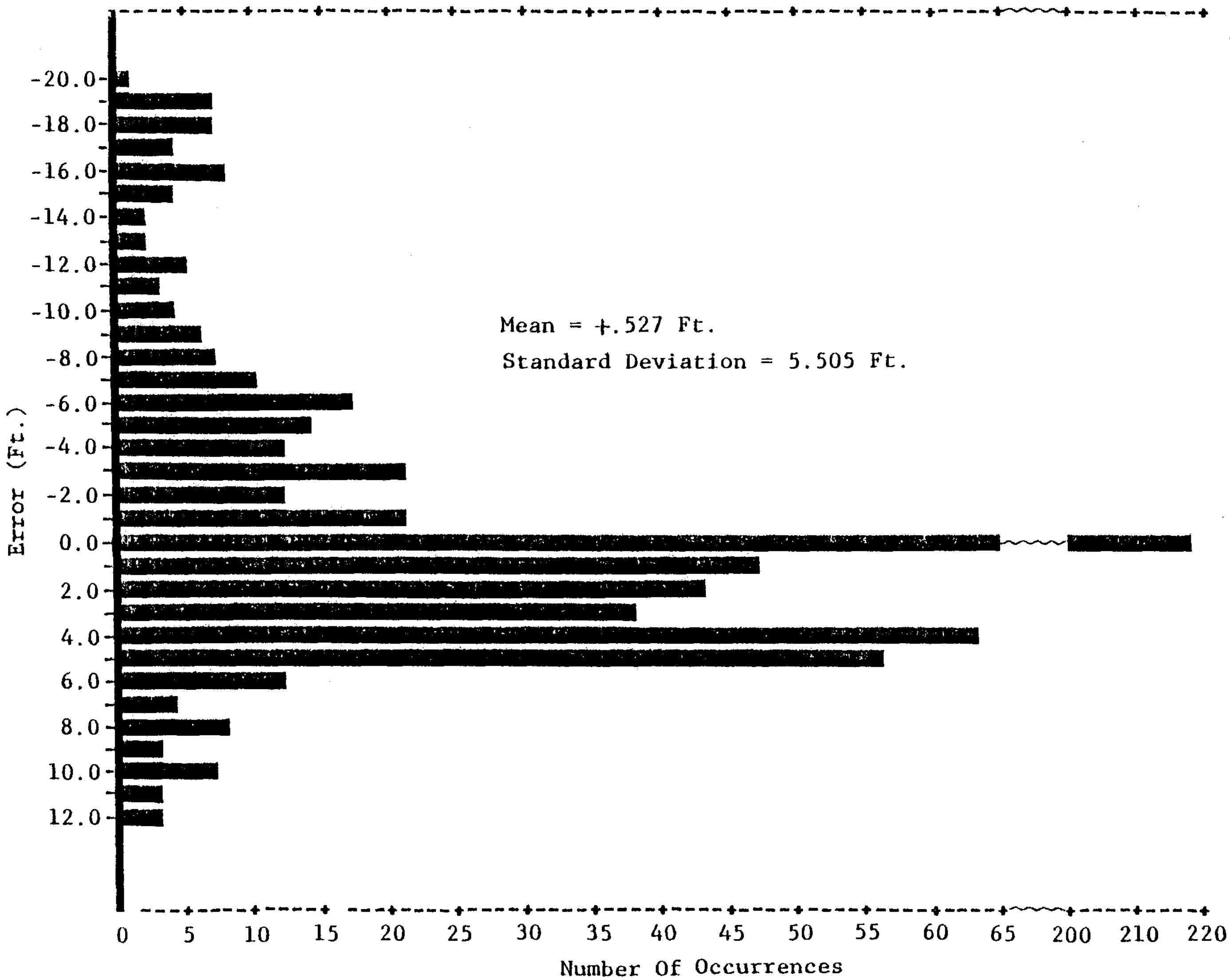

Figure 12. Frequency histogram of calibration error from constant-head USGS steady-state calibration.

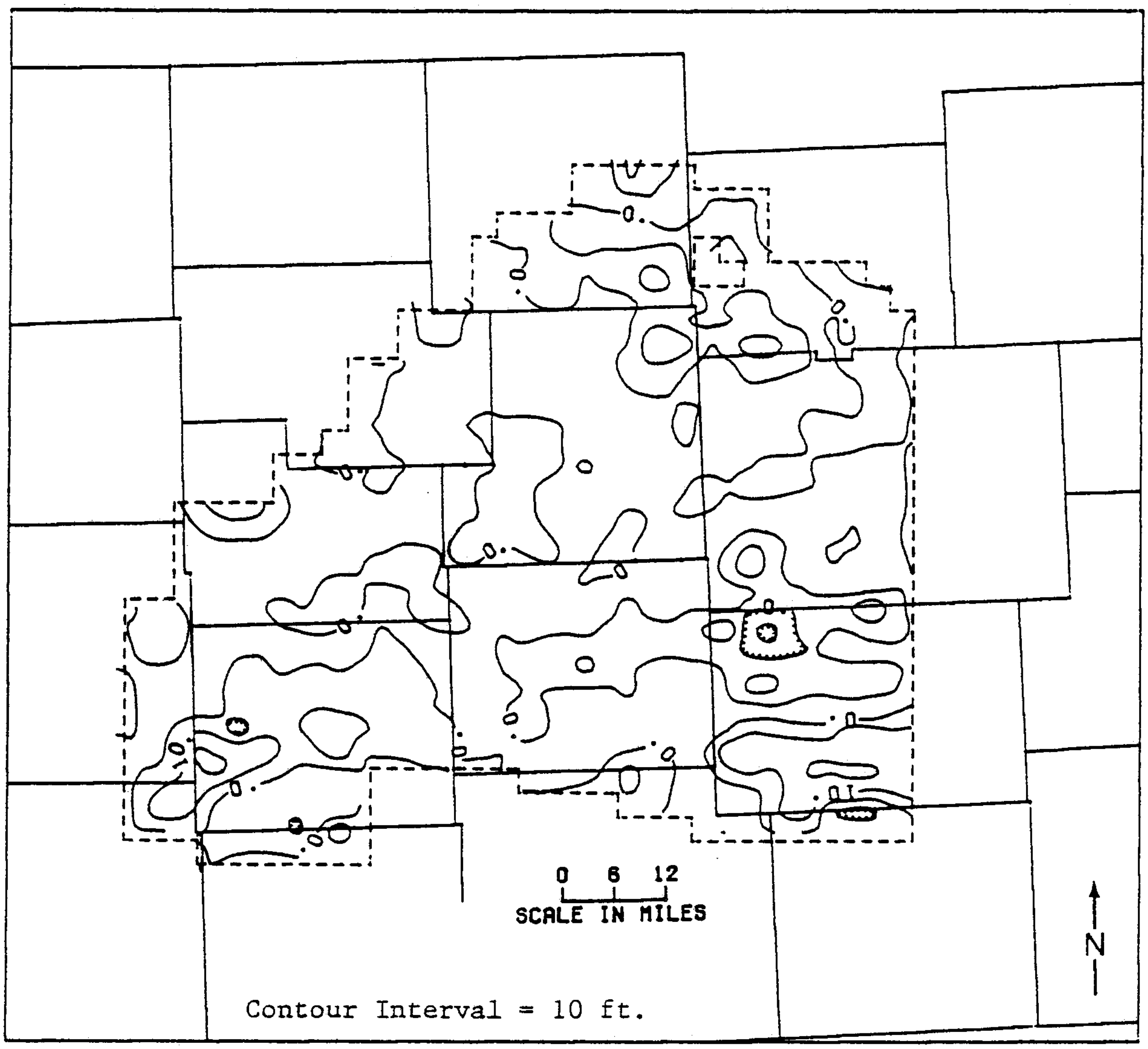

——— CONTOUR OF EQUAL ERROR VALUE ---- MODEL BOUNDARY

Figure 13. Spatial distribution of calibration error for constant-head steady-state calibration (feet).

A detailed regression analysis of the simulated steady-state head distribution was performed in order to determine whether the simulated values differed excessively from the modified pre-development head values. Since it was considered desirable to obtain a strong linear relationship between modified pre-development head and simulated steady-state output head values, the analysis was oriented toward both describing any potential linear relationship and obtaining a measure of the strength of this relationship. A strong linear relationship between modified input head levels and corresponding steady-state output head levels would imply that the shape of the water table configuration was retained during the regeneration procedure, although head levels might have been shifted upward or downward by a constant magnitude throughout the study area. Using formal regression analysis, it was possible to estimate the magnitude of this shift, as well as the degree of linearity or shape retention.

In order to determine the extent of any potential linear relationship between the data sets, the Statistical Package for the Social Sciences (SPSS) scattergram routine was used to generate a plot of simulated steady-state head vs. modified pre-development head and associated statistics. The data points were used to define the linear relation shown in Figure 14 using a least-squares regression technique. Although extrapolation of the regression line to zero-valued altered pre-development head has no physical meaning, the intercept of the line is an indication of the general shift in the water table which occurred during steady-state convergence. The intercept of the line was estimated to be +4.56 feet. This value was initially interpreted to be a measure of the overall vertical shift of the water table during steady-state iteration. However, when the mean pre-development input head and mean steady-state output head were compared, the actual average error calculated during

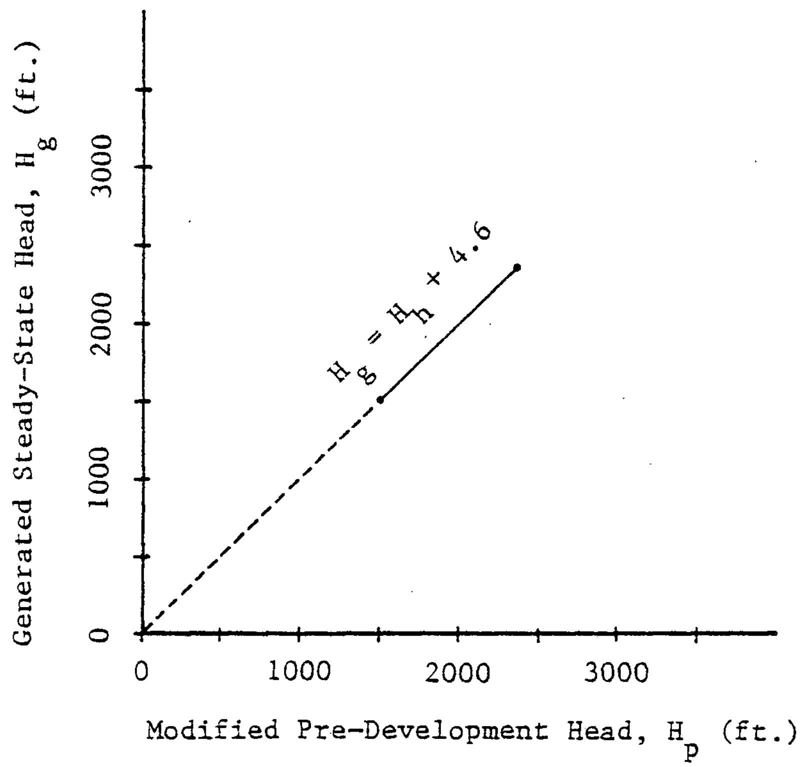

Figure 14. Regression line for steady-state head vs modified pre-develoment head.

model operation was only +0.5 feet. The larger intercept value was presumably caused by a small number of nodes at which head increased by a large magnitude during the iterative procedure. Since the calculation of the intercept value is significantly more sensitive to these large head changes than the calculation of the mean, such large head increases were assumed responsible for the discrepancy between the two measures of water table shift.

Regardless of the extent of overall head shift, the occurrence of any shift at all should not be a cause of great concern. As long as the general shape of the water table was preserved, then one may assume that head gradients were not altered. On the basis of the well-defined linear relationship shown by a scatterplot of the data, it was evident that modified pre-development and generated steady-state heads were systematically related through some additive factor. This impression of linearity was further substantiated by the calculated high correlation coefficient of 0.99. The linearity of the relationship between input and output heads suggested that the water table shape was maintained to a significant degree, and that head gradients had not changed during model operation, despite any overall vertical shift in head that might have occurred over the study area. However, flux relationships, both internal to the model and at permeable boundaries, were undoubtedly altered during model operation because of changes in transmissivity associated with corresponding changes in saturated thickness.

The final recharge matrix was assumed to represent the natural distribution of precipitation recharge for the area. Matrix Listing 1 in Appendix D contains the final precipitation recharge matrix values. A contour map of precipitation recharge values is shown in Figure 15. Values as high as 5 or 6 inches per year occurred in the extreme northeastern region of the model area. These large values may be a reflection of the high recharge

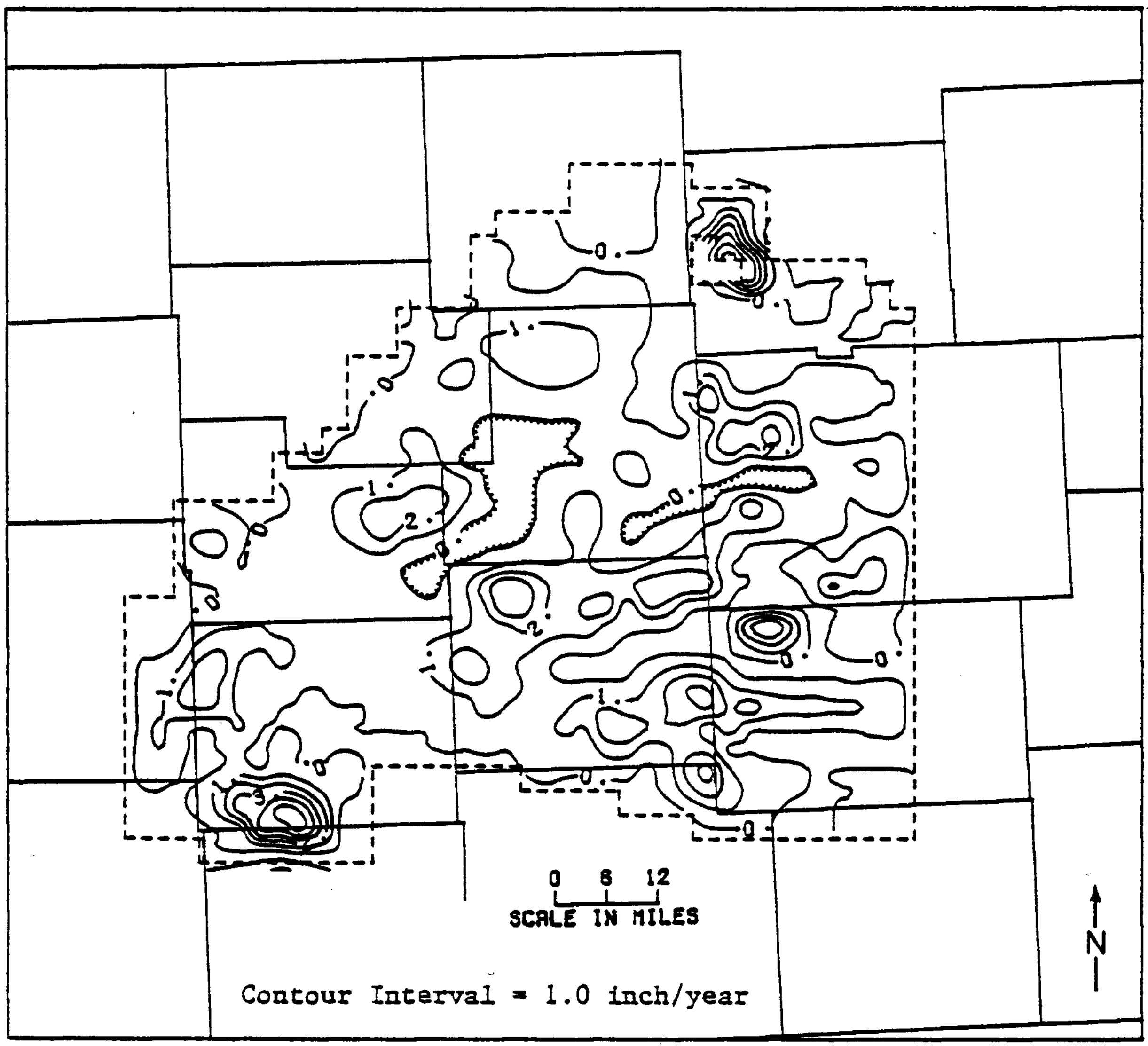

CONTOUR OF EQUAL RECHARGE ---- MODEL BOUNDARY

All values enclosed are = zero

Figure 15. Calibrated natural recharge distribution (inches/year).

capacity of the overlying sand dunes, or may be related to upward leakage from the underlying Permian units, a component which was not explicitly included in the model. The large values of R may also be attributed to overestimated values of hydraulic conductivity. In addition, the small saturated thickness in the L-shaped section to the northeast of the grid may have tended to distort lateral flow in the vicinity of the large recharge estimates. There was no tendency for net recharge to decrease southward as the surficial sand deposits grade into loess. Average recharge at all variable-head nodes was roughly 0.75 inches per year, a value which was less than half the estimate of 2.0 inches per year reported in a previous KGS publication (Fader and Stullken, 1978). 0.75 inches per year represents about 3% of the mean annual precipitation of 25 inches for the area.

The change in the average R:K ratio from 0.005 to 0.009 which occurred during the trial-and-error calibration amounted to nearly 100%, suggesting that the initial estimates for R and K of 0.5 in/yr and 100 ft/day may have been at least partly responsible for initial divergence of steady-state head from observed pre-development head. The initial underestimation of natural recharge or overestimation of hydraulic conductivity would have tended to result in a steady-state distribution which diverged from the pre-development water table.

The final steady-state head distribution obtained from the calibration is shown in Figure 16. The distribution duplicates the regional properties of the modified 1950 pre-development water table.

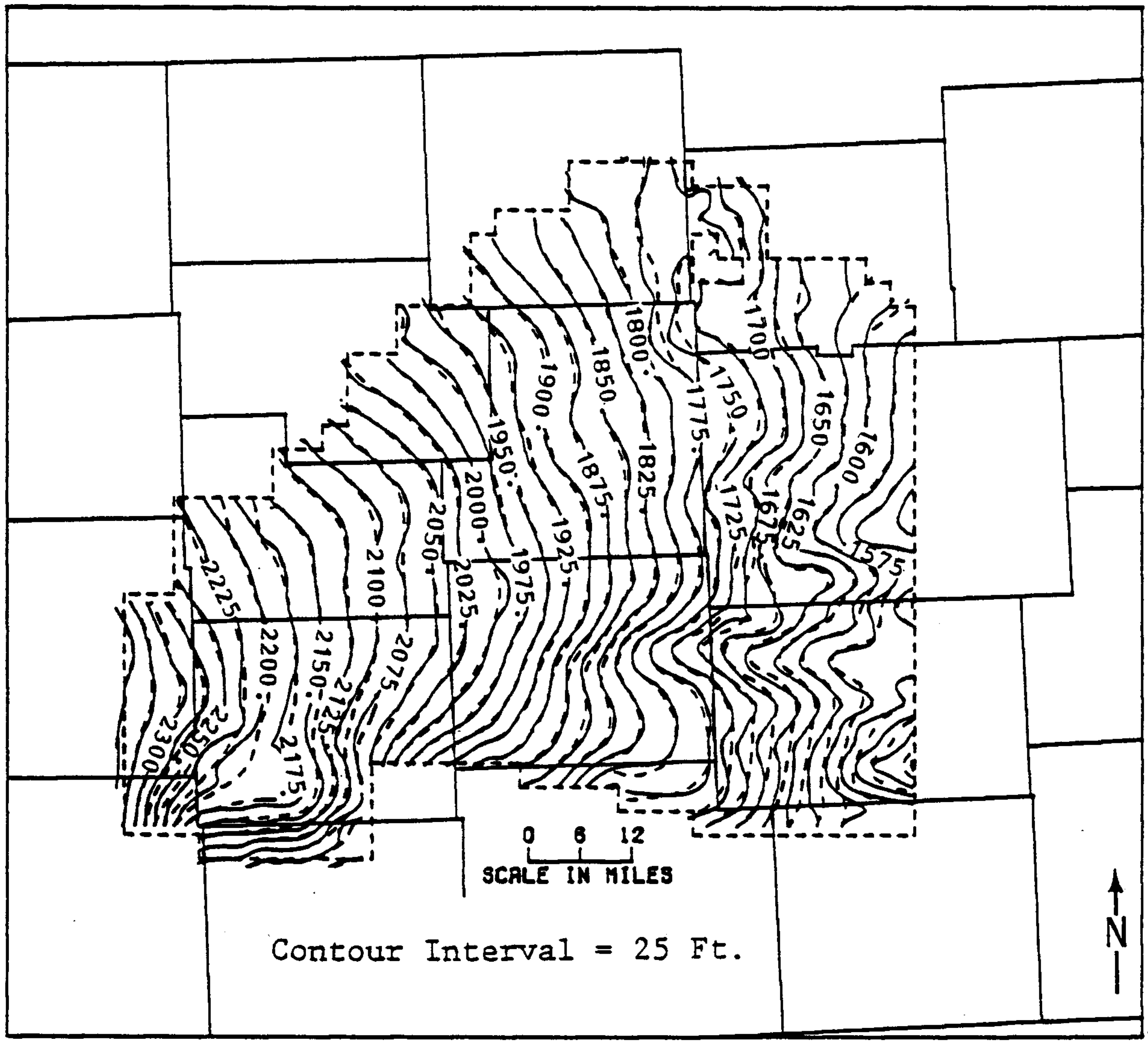

——— OBSERVED EQUIPOTENTIALS

---- CALIBRATED EQUIPOTENTIALS

Figure 16. Distribution of steady-state head obtained from USGS model and modified pre-development head (feet).

Calibration for Variable-Flux River and Permeable Boundary Nodes

As indicated earlier, constant-gradient variable-flux nodes were chosen to simulate the hydraulic behavior of the rivers and the western, southern, and eastern boundaries of the model. Along the boundaries, it was assumed that the gradient across the node was constant and that discharge in the boundary was directly proportional to the average saturated thickness across the cell defined about the node. As water levels declined or increased at the boundaries, the amount of water moving across the boundary correspondingly decreased or increased. The direction of the flux did not reverse in this scheme, but could have approached zero. For the small stresses which have historically been imposed on the aquifer, the problem of flux reversal was not of great concern. However, under conditions of large future pumping stresses, the constant-gradient algorithm could easily be modified to check for gradient reversal between boundary and river nodes and adjacent active nodes.

The previous calibration involved assignment of constant-head conditions at the external boundaries and internal river nodes. For any transient simulation involving imposed stresses, these heads would not be capable of changing in response to these stresses. Due primarily to this consideration, a decision was made to utilize variable-flux boundaries and rivers.

The central concept of the constant-gradient node is that the node is far enough removed from the area of imposed pumpage that gradients at the node do not change over time. Instead, the saturated thickness is assumed to change in response to stress in the aquifer. Wilson and Gerhart (1980) proposed such a modification to the USGS two-dimensional flow simulation model for the strictly-confined situation. There are theoretical objections to the application of a similar concept to an unconfined aquifer, especially when local gradients may be relatively steep. On the other hand, a simple formulation of the variable-flux node does permit approximate simulation of complex processes in the absence of detailed flux data. This argument is especially justifiable along the southern boundary, where it is clear that considerable water is being lost from the system, but not clear how this water is lost or how these losses are distributed in space. The interdependence of baseflow, underflow, evapotranspiration, and leakage is not well documented for this area, but it can be assumed that all three processes are dependent upon saturated thickness in some sense. Use of the constant-gradient algorithm developed from Darcy's law assumes a linear dependence of fluxes on the saturated thickness at a constant-gradient node. Lacking any better information, this approximation was assumed to be satisfactory.

The calibration of the variable-flux boundaries and rivers was initiated by using the flux values obtained by mass-balance calculations at the constant-head nodes. The artificial wells introduced to the southeastern part of the grid to simulate constant-flux conditions were retained. After the variable-flux nodes were initialized to the constant-head flux values, specific yield was assigned a value of 0.15 (Fader and Stullken, 1978). The final hydraulic conductivity from the constant-head calibration was retained at a uniform value of 85 ft/day, and the recharge distribution obtained from this calibration was also retained (see Matrix Listing 1, Appendix D). Flow was simulated with no imposed stresses using equation (3) to simulate boundary and river behavior. The constant-head flux values did not produce a time-invariant water table when used as the initial condition at the variable-flux boundary and river nodes. This was partly attributed to the effects of boundary shifts which resulted when constant-head boundary conditions were translated into variable-flux conditions, a feature which was inherent to the USGS-model flow algorithm. An additional cause of the time-variant behavior may have been the use of a specific yield estimate of 0.15, which could have been somewhat in error. Prior to the variable-flux boundary and river calibration, the constant-head boundary and river nodes and associated lateral fluxes were insensitive to S_y. However, translation of constant-head conditions to variable-flux conditions at the boundary and river nodes caused lateral fluxes at these nodes to become very sensitivie to the value of specific yield chosen. If estimated specific yield was even slightly in error, these lateral fluxes would tend to be greatly distorted. Due to these problems, it was necessary to initiate a calibration effort involving inspection of the simulation results, and recursive correction of the initial fluxes until the corrected initial fluxes satisfactorily maintained the head distribution obtained from the constant-head calibration over a relatively long period of simulation. Since only minor flux modifications were required to maintain steady-state conditions, it was not considered necessary to introduce natural areal recharge to the new variable-flux boundary and river nodes, which had not previously received finite areal recharge in their constant-head state. Moreover, adjustments of recharge at the variable-flux nodes would have entailed a certain degree of re-calibration of the entire model for natural recharge. Calibration error was redefined as the difference between head calculated using variable-flux boundary and river conditions and head obtained from the previous constant-head calibration.

In the process of calibrating the variable-flux nodes, three nodes gave considerable contribution to the sum of the squared calibration error. Errors at these nodes were all negative, indicating the removal of too much water. The nodes were near the simulated Arkansas River within the "L" shaped zone in the northeastern part of Figure 17, and were in a region of a predominate bedrock high in southwestern Rice County, comprised principally of Kiowa Shale

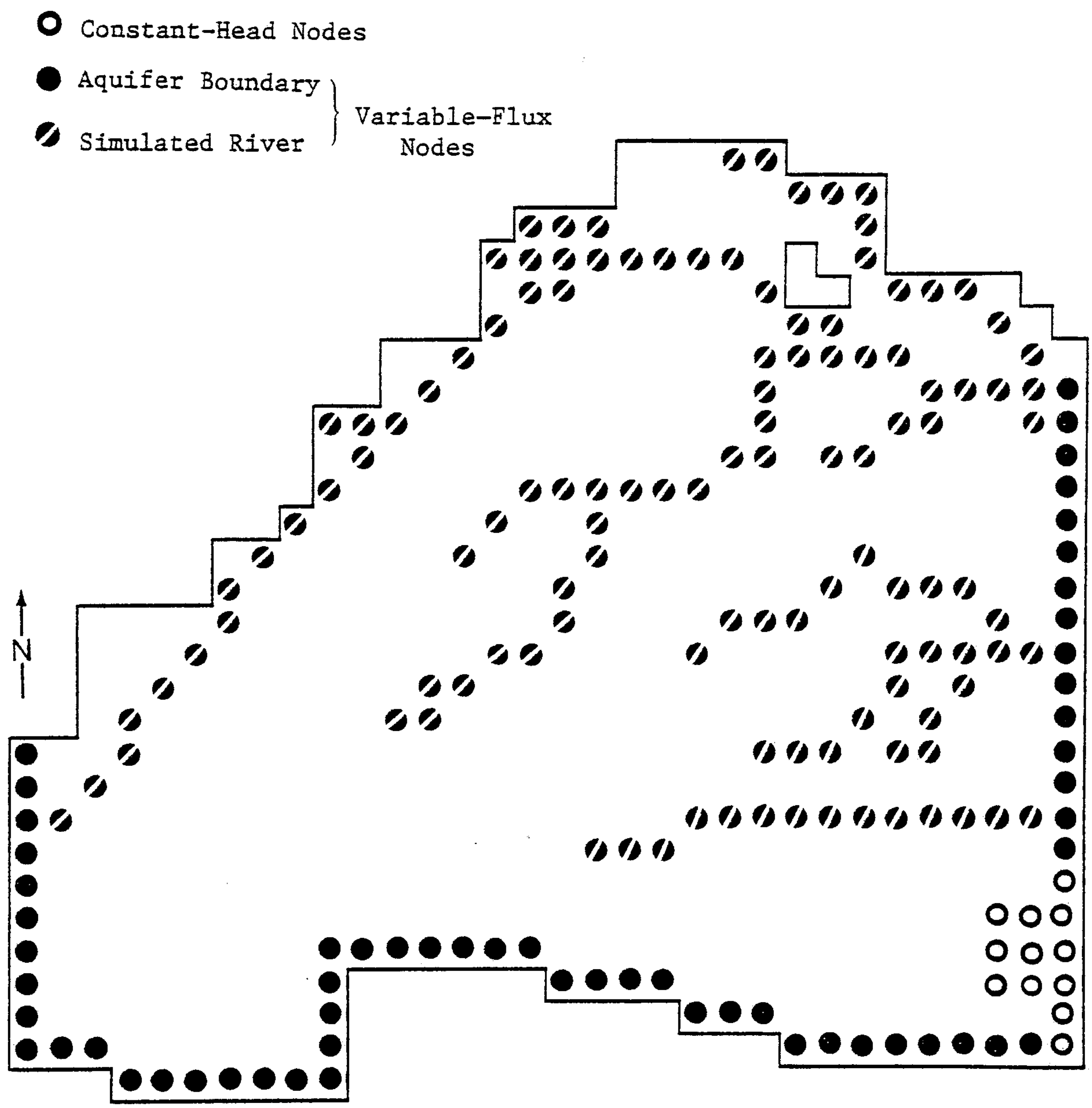

Figure 17. Boundary and river node-type map.

(Bayne and Ward, 1974). This area is more or less coincident with the zero and 20-foot saturated thickness contours and a region of low expected well yield (0-100 gpm). Because of this evidence, it was decided to treat the area as an impermeabale part of the aquifer by setting the value of K to zero at those nodes. In addition, the constant flux nodes used in the extreme southeastern portion of the model were no longer properly maintaining the historical water table as originally intended. These nodes, along with a few adjoining boundary nodes were changed to constant-head nodes (see Fig. 17).

The calibration scheme for the variable-flux nodes was carried out on the basis of 30 years of simulated time, with updating of the fluxes occurring every 1 to 5 years. No pumping stresses were imposed for the duration of the 30-year test. The recursive inspection-adjustment procedure previously discussed was repeated on a trial-and-error basis until simulated head values were within ± 5 feet of the head generated during constant-head calibration. When convergence to 0.01-foot closure occurred after 16 years of simulated time, it was decided that optimum adjustments in steady-state head had been made (see Appendix D, Matrix Listing 2). Table 1 illustrates the roughly steady-state conditions obtained after 16 years of simulation time.

It is clear from Table 1 that the head distribution obtained in the fifth pumping period after 16 years was not a steady-state distribution, as indicated by non-zero values for mass-balance and for the sum of rates. Obviously, more work would have produced a better calibration, but the improvement in squared error would not be great compared to the research effort involved. Head obtained after 16 years of simulation was considered to constitute the 1950 steady-state water table, from which future water levels would be projected. This head distribution maintained the regional properties of the modified pre-development head to approximately the same extent as the head obtained from the constant-head calibration (see Fig. 18). In order to verify this conclusion, comparisons were made between head from the variable-flux calibration and both pre-development head and head generated from the constant-head calibrations.

Table 1. Results of the Variable-Flux Calibration

Period	Simulated Time	Sum of Squared Error (ft^2)	Maximum Error (ft)	Minimum Error (ft)	No. of Active Nodes	Number of CG Nodes	Mass Balance* (%)	Sum of Rates† (cfs)
1	5 yrs	518	-3.90	+3.41	671	179	-0.09	0.36
2	5 yrs	839	-4.36	+3.92	671	179	-0.12	0.45
3	3 yrs	963	-4.45	+3.99	671	179	-0.13	0.59
4	2 yrs	1030	-4.49	+4.04	671	179	-0.13	0.48
5	1 yr	1055	-4.51	+4.06	671	179	-0.13	0.43

*((Outflow Volume - Inflow Volume)/Outflow Volume) x 100
†Inflow Rate - Outflow Rate

A statistical comparison was made between constant-head and variable-flux simulation results. The mean deviation was 0.04 feet with a standard deviation of 1.3 feet. Thus, variable-flux-calibrated head levels were seen to be just slightly higher than corresponding constant-head-calibrated head levels, a result consistent with the mass balance and the rate differential in Table 1, which indicates that model inflow exceeds model outflow. A frequency histogram of deviations indicated that about 90% of the nodes fell in the range of ±2.5 feet (see Fig. 19a). A comparison of variable-flux-calibrated head and modified pre-development head (see Fig. 19b) indicated that all calibration errors were within the range of ±22 feet, the same general error range for the constant-head, steady-state simulation. About 81% of the nodes

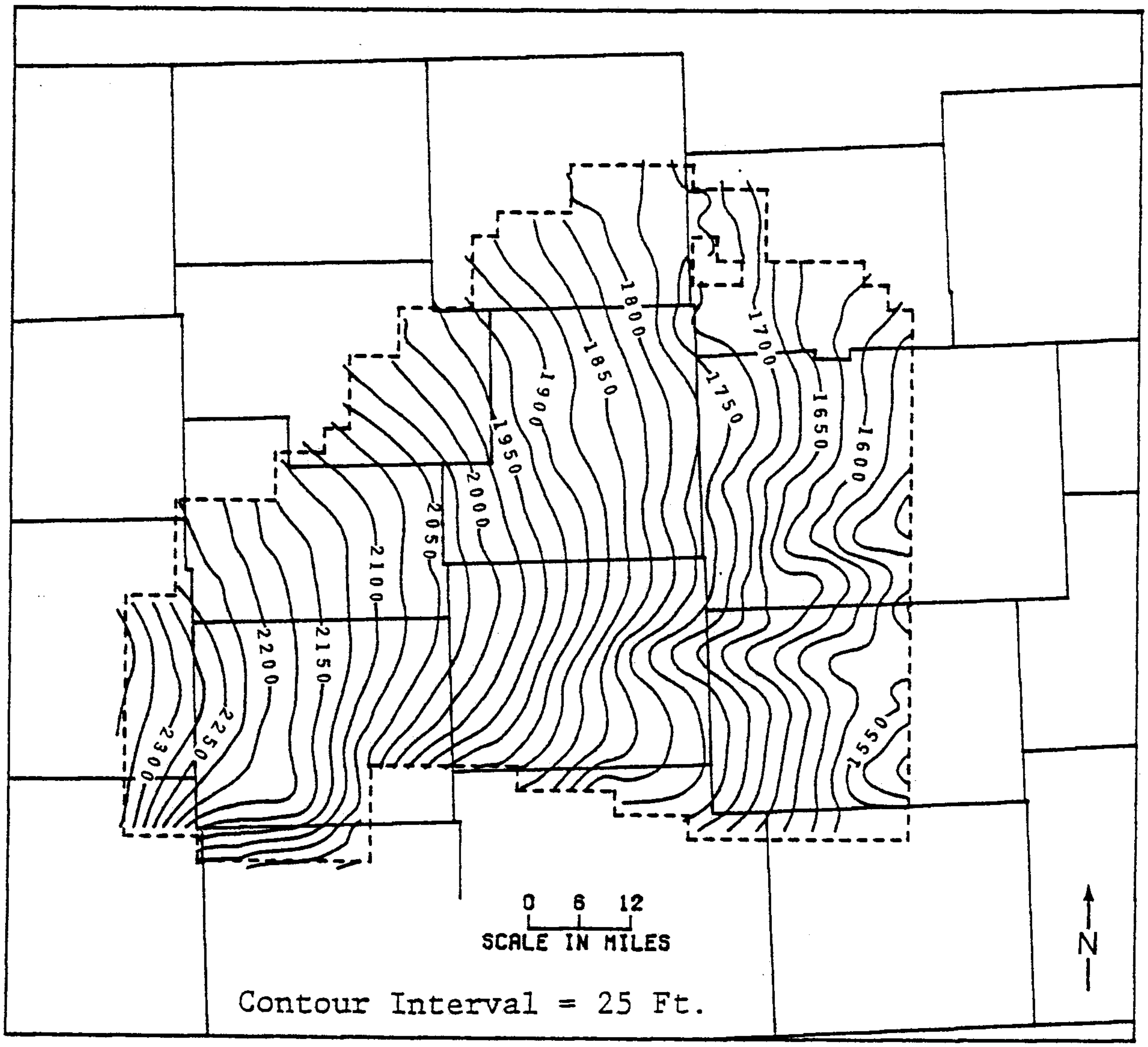

Figure 18. Distribution of head obtained from variable-flux calibration (feet).

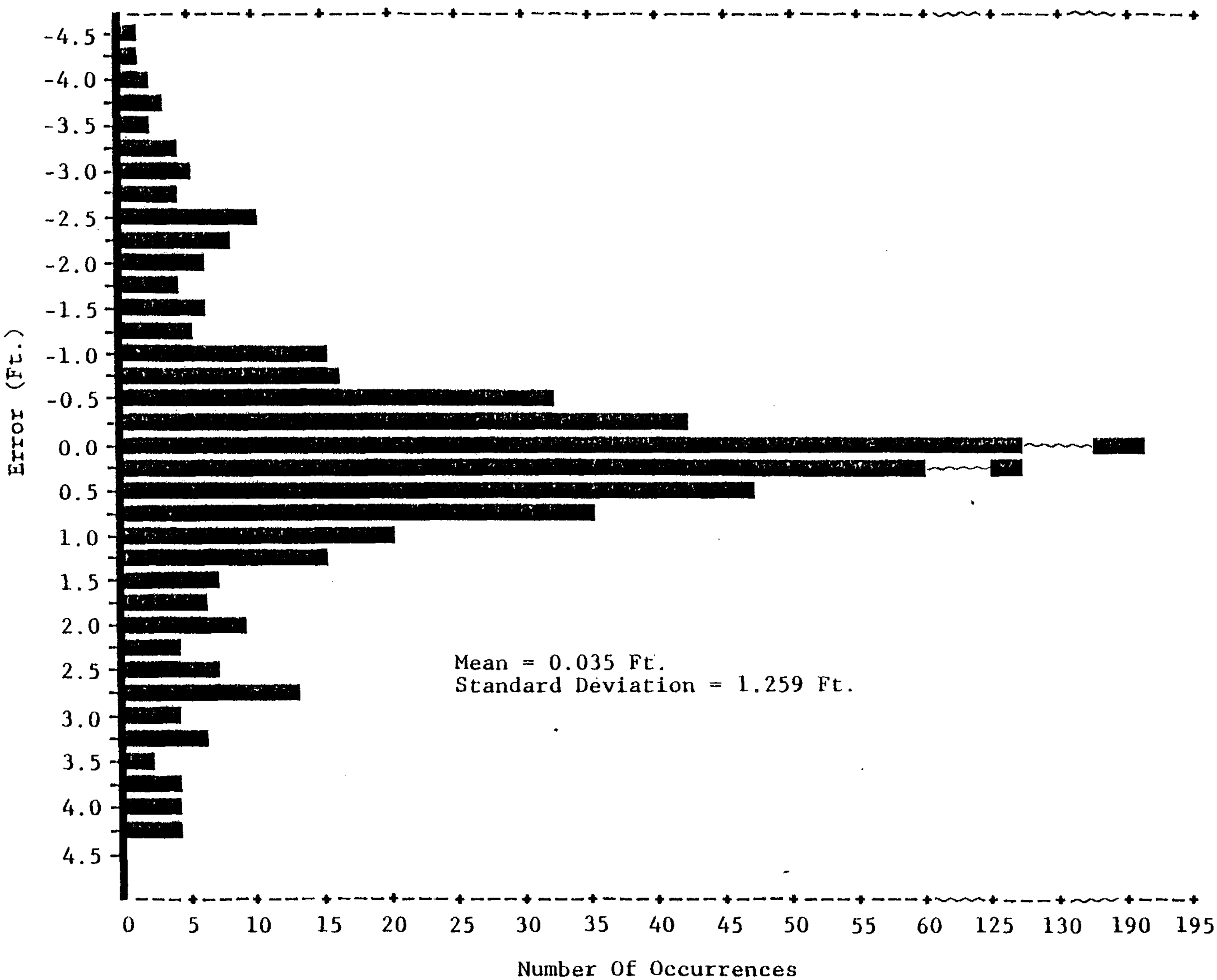

Figure 19a. Frequency histograms of deviations between variable-flux and constant-head calibrated water tables.

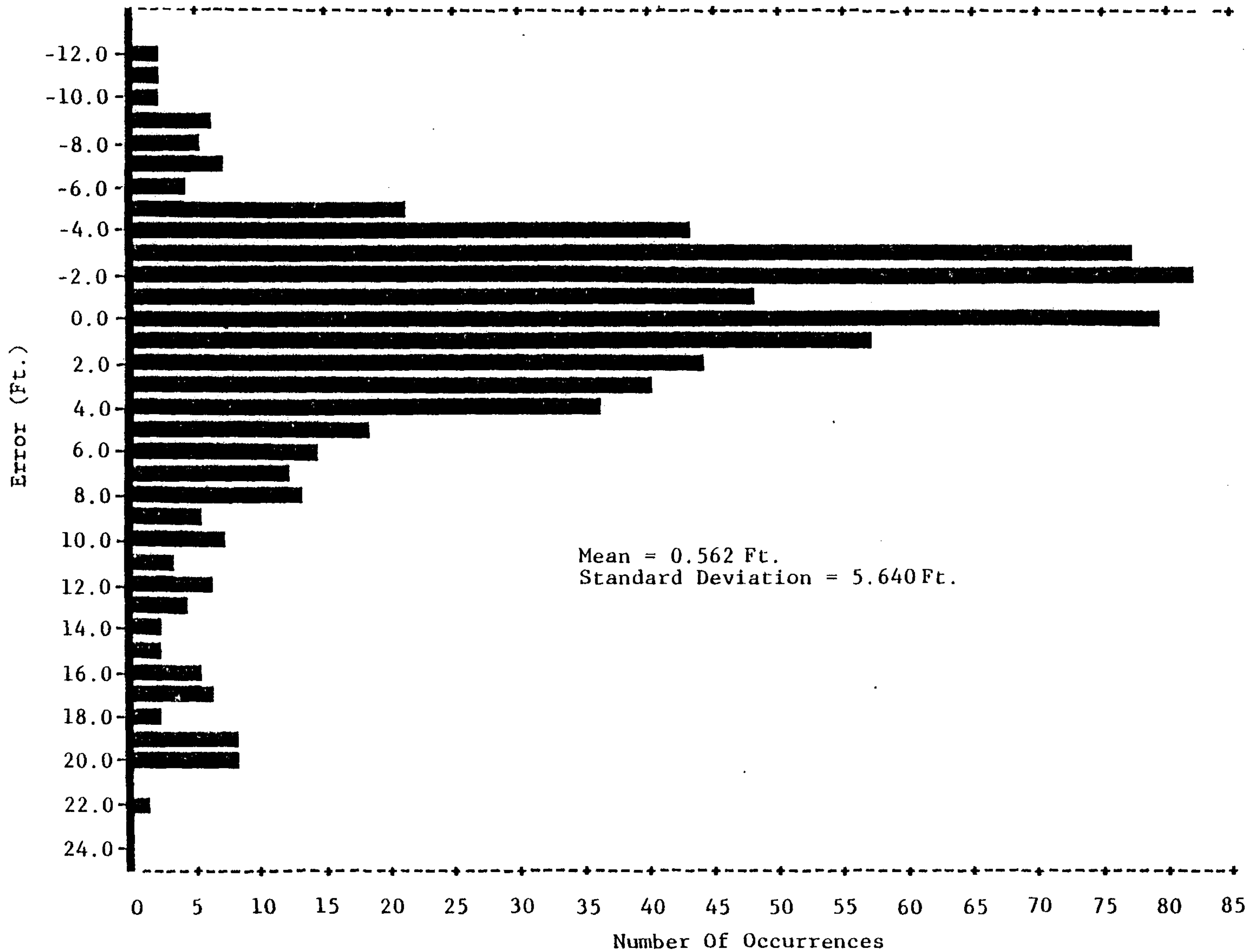

Figure 19b. Frequency histogram of variable-flux calibration error (variable-flux head minus modified pre-development head).

showed residuals within the range of ± 5 feet. The mean calibration error between variable-flux-calibrated head and modified pre-development head was 0.6 feet, with a standard deviation of 5.6 feet. Thus, the simulated surface generated by changing constant-head nodes to constant-gradient nodes and by adjusting the fluxes such that the final residuals after 16 years of transient simulation were in the range of ± 5 feet, yielded a new water table which was essentially equivalent to the starting data. It was therefore decided that projections based on consideration of variable-flux-calibrated head as representative of pre-development conditions in the aquifer could be made with confidence. A map of the associated calibration errors indicated that the nodes with the largest absolute errors tended to occur more frequently near the southern boundary areas where data was considered to be of poorest quality (see Fig. 20). The majority of the small errors occurred in the interior, where data was believed to be more reliable and where most irrigation development was simulated.

Calculated Boundary and River Fluxes:

Pre-development boundary fluxes calculated by the variable-flux model, as expected, were positive along the western boundary and negative along the southern and eastern boundaries. The extremely large negative flux of 62.3 cfs across the southern boundary may be partially attributed to the high evapotranspiration rates from the generally shallow water table believed to be occurring in the vicinity of the boundary and to seepage into underlying Permian units. Although such fluxes would actually be areal rather than lateral, the absence of these flux mechanisms, if these mechanisms are significant, would tend to cause groundwater buildup in the southern part of the grid, larger southward hydraulic gradients, and greater lateral flux

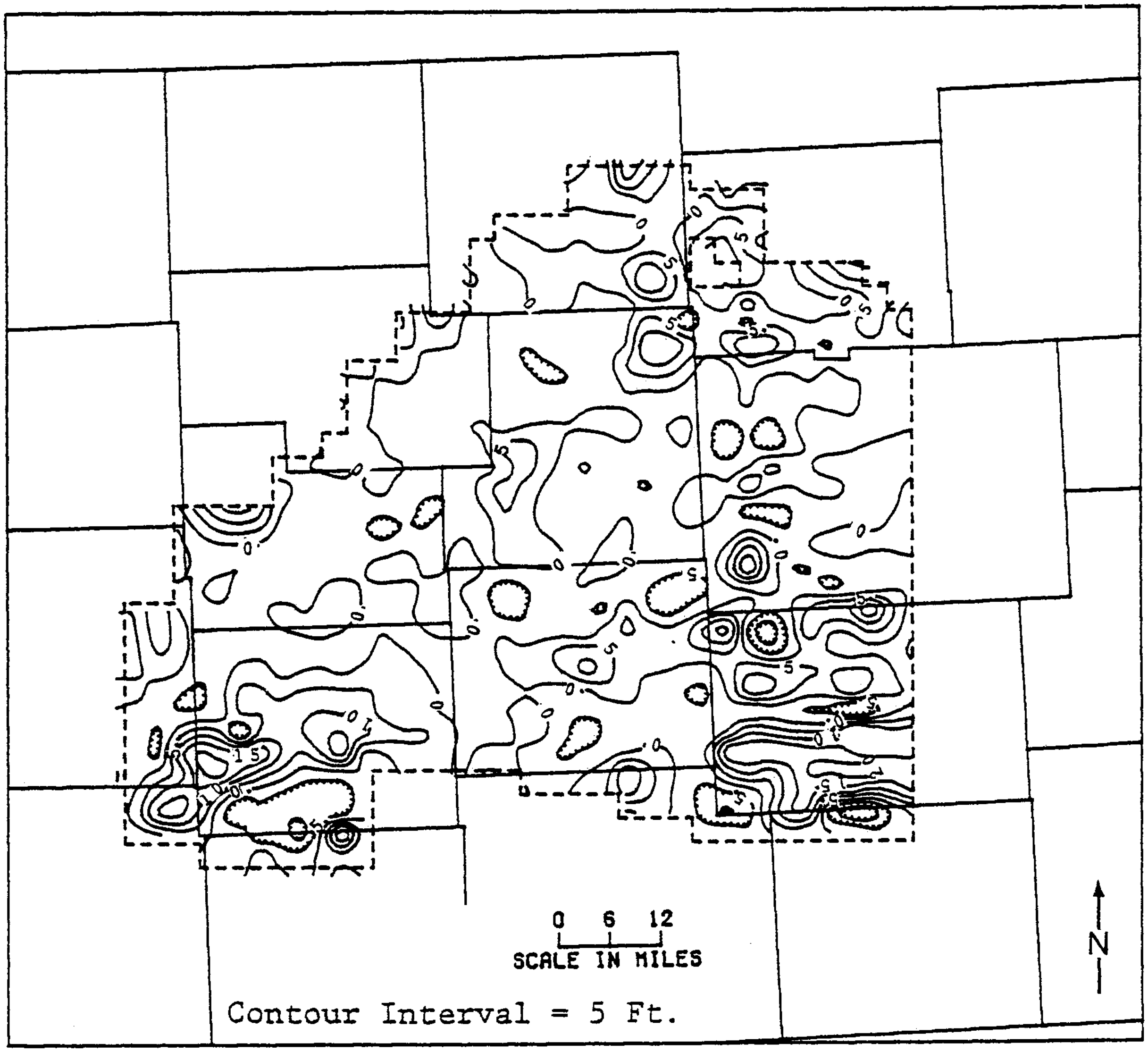

——— CONTOUR OF EQUAL ERROR VALUE ---- MODEL BOUNDARY

Figure 20. Spatial distribution of variable-flux calibration error (feet).

across the southern boundary. The county reports for Kiowa County (Latta, 1948) and Pratt County (Layton and Berry, 1973) indicate a conservative figure of at least 50 cfs moving out across the southern boundaries of these counties under steady-state conditions. A summation of nodal fluxes for the approximate Pratt-Kiowa southern boundary in the model resulted in values of 57.4 cfs for the constant-head boundary and 57.8 cfs for the constant-gradient boundary. These figures match favorably with the rate cited above. It is clear that no great distortion of the total flux occurred in changing from constant-head to constant-gradient boundaries, but examination of the individual nodes indicates a minor redistribution of the fluxes as a result of the change. Simulated flux across the western boundary was calculated to be roughly 16 cfs.

Calculated baseflow rates were generally smaller than reported rates. This was attributed to the coarseness of the finite-difference grid, which was unable to maintain the small-scale upstream-inflections of the potentiometric lines in the vicinity of most major stream valleys. Summation of nodal inflow rates along the total length of the South Fork Ninnescah resulted in an estimate of 67.8 cfs for baseflow contributions to the river, which was in reasonable agreement with the average 1951-1971 value of 94.4 cfs previously estimated by KGS researchers at Murdock, located just outside the model in Kingman County (Fader and Stullken, 1978). It was assumed that the average 1951-1971 baseflow corresponded to pre-development baseflow due to small pumping stresses imposed on the aquifer during this time period, relative to the large volume of water in storage. Estimated baseflow in the North Fork Ninnescah at Arlington, which is just barely inside the eastern model boundary, was 37.0 cfs, compared to a reported 1951-1971 mean baseflow of 38.0 cfs (Fader and Stullken, 1978). Simulated Arkansas River baseflow at the eastern boundary of about 30 cfs was far below the measured 1959-1975 average streamflow of 680 cfs as reported in a USGS Water-Data Report, suggesting that baseflow comprised only 4% of total discharge (USGS, 1975). It was assumed that this 1959-1975 average streamflow represented roughly steady-state discharge from the Arkansas River prior to 1950. The river was actually calculated to be losing water throughout most of its western and central reaches during pre-development time.

In passing, the question might be raised as to why any adjustments had to be made in switching boundary-node types. At steady state, the two boundary conditions should move identical masses of fluid per unit time in the system. A major part of the answer to this question lies in the differences between the ways the boundaries are numerically simulated. This seems especially true for the nodes located at the boundaries of the model. The hypothetical node system shown in Figure 21 suggests several difficulties in converting from constant-head to variable-flux boundaries. Constant-head nodes are indicated by -1's, while variable flux nodes, which are simulated essentially as wells, are shown by circles about the nodes. Note that the model boundary passes through the nodes on the constant-head boundary, but that on the constant-gradient boundary, it is coincident with the cell partition between the constant-gradient node and the grid-margin boundary node. This may have some effect upon the computation of flow perpendicular to the boundary. Perhaps of more importance is the fact that in the USGS two-dimensional code, flow is only computed between constant-head nodes and interior active model nodes (see Fig. 21). No flow is computed between adjacent constant-head nodes and hence, no lateral movement of fluid can occur along a constant-head boundary. On the other hand, any variable-flux node can

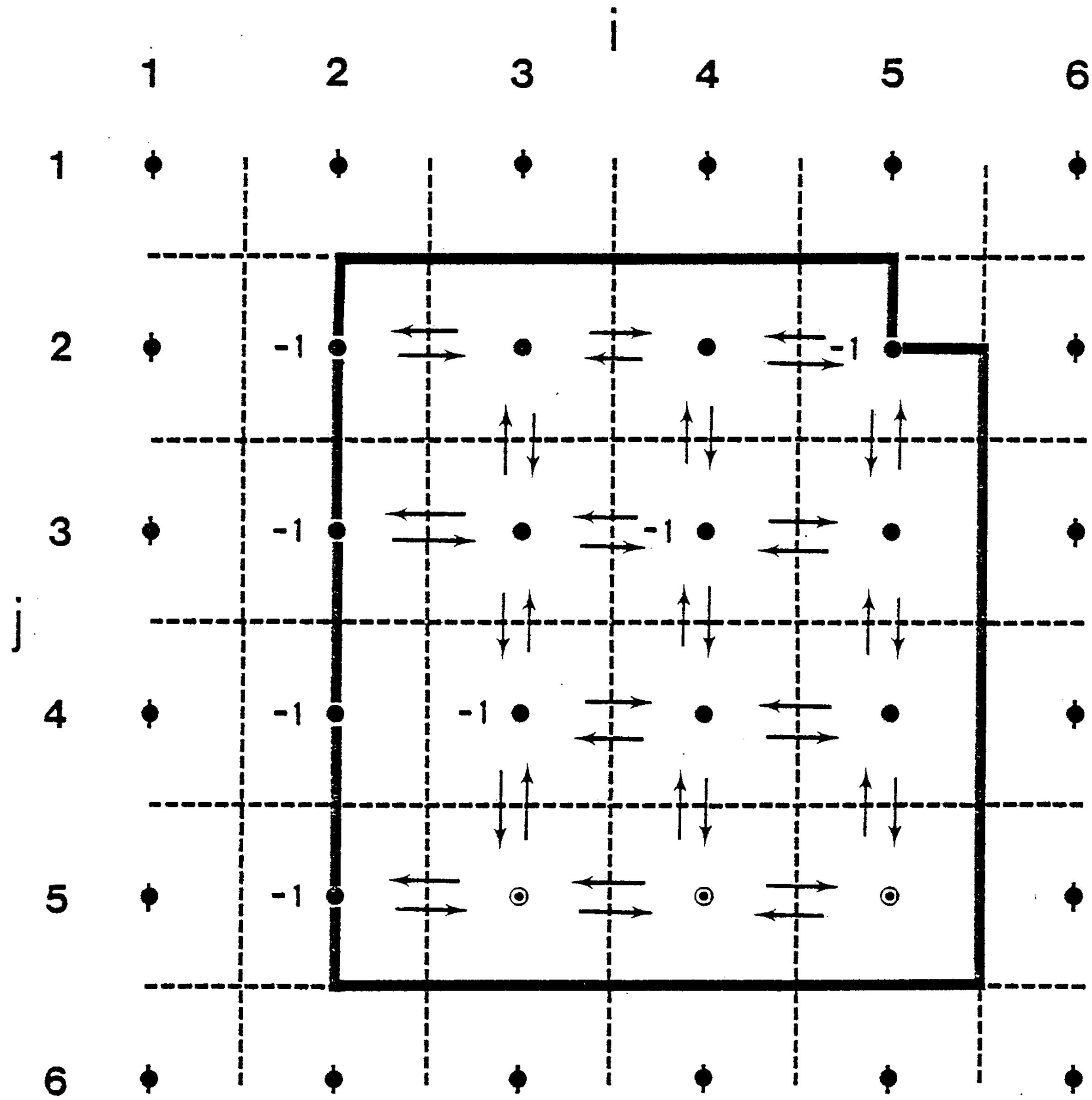

Rows Denoted By Index i
Columns Denoted By Index j

-1 = Constant Head Node
⧫ = Grid Margin Boundary Node (K=0.0)
⊙ = Variable-Flux Node
● = Active Model Node
--- = Cell Boundaries
—— = Model Boundary

Figure 21. Schematic representation of variable-flux nodal mass-balance relations.

exchange flow with any other permeable node. This implies that flow parallel to the boundary can occur through the variable-flux nodes. Consequently, there was be some variation in the flow field at the model boundary when the change was made from constant-head to variable-flux nodes.

Transient Simulation of Irrigation Development

Historical Irrigation Data:

Irrigation pumpages for this modeling study were provided by the U.S. Geological Survey. The original data were tabulated for 10-minute square blocks (Heimes and Luckey, 1982). These data were obtained from U.S. Census records of reported crop acreages and from estimates of consumptive use per acre. Estimated irrigation pumpages for the entire study area were determined by summing pumpages from each 10-minute block. The values listed in Table 2 represent the estimated pumpage rates for the years 1949, 1954, 1959, 1964, 1969, and 1974.

Table 2. Historical Irrigation and Nodal Distribution of Pumping

Year	Irrigation Volume	No. of Pumping Nodes
1949	0 AF	0
1954	50,300 AF	393
1959	127,280 AF	431
1964	110,370 AF	457
1969	161,580 AF	462
1974	272,660 AF	461

In order to perform some initial testing of aquifer sensitivity to pumping stresses over the 25-year development period, pumpage volumes for all benchmark years listed in Table 2 were assigned to each of the four previous years and to the year following the benchmark year. Initial testing involved pumping the annual estimated volume from the aquifer over a six-month period within each year to reflect a realistic discharge schedule. Resulting heads from this simulation were not significantly different than simulated head obtained when estimated pumpage was distributed uniformly over each year, presumably because of the large volume of stored groundwater relative to withdrawn volumes and because of moderate rates of boundary and river replenishment. Given the insensitivity of the aquifer to small pumpage rates, uniformly-distributed annual pumpage was chosen to facilitate model operation. Pumpages were distributed areally by assigning them to the closest nodes in the finite-difference grid.

While conducting these preliminary experiments, some well nodes with thin saturated thicknesses went dry. To circumvent this problem, a redistribution of irrigation pumpage was made from nodes characterized by less than 30 feet of saturated thickness to nodes located in areas of larger saturated thickness.

Historical Water Tables Observed During the Development Period:

The U.S. Geological Survey provided information on the configuration of the water table in the Great Bend Prairie in the form of manually contoured base maps of the data base which had been constructed for the area. These maps were for the years 1955, 1960, 1965, 1970, and 1975 (see Figs. 4 to 8).

Visual inspection of the pre-development water table and the post-development maps indicates a high degree of regional similarity, suggesting negligible system transience.

The development period potentiometric surface maps were machine digitized by the Computer Services Section of the Kansas Geological Survey. These digitized data were then gridded and machine contoured by the SURFACE II graphics system developed at KGS (Sampson, 1978). Visual comparison of the machine-contoured maps with the original manually-contoured base maps indicated that the regional properties of the maps were maintained. Statistical comparisons were carried out between variable-flux-calibrated steady-state head and the 1955 through 1975 surfaces, using the Bio-Medical Computer Programs (BMDP) package (Dixon and Brown, 1979). The results of these comparisons are reported in Table 3.

Table 3. Results of Statistical Analysis for Simulated Transient Head and Steady-State Head.

Comparison Between Steady-State Head and:	Mean Deviation (ft)	Standard Deviation (ft)	Correlation Coefficient
1955	-1.93	10.4	.99
1960	-1.99	11.0	.99
1965	-1.56	11.4	.99
1970	-3.13	11.0	.99
1975	-1.95	11.2	.99

The deviation was defined to be transient head minus the corresponding steady-state head level. From this tabulation, it appears that 1) the average value of the pre-development water table was higher than for any of the development-period water tables, as would be expected, and 2) the water tables have the same general shapes, as indicated by the high correlation coefficients.

It was clear from the small mean deviations that the permanent impact of irrigation was not readily differentiable from shifts in the water table caused by normal climatic variations, which have been reported to cause head changes as high as 20 feet (Fader and Stullken, 1978). Hence, it was concluded that the aquifer was in a state of approximate long-term dynamic equilibrium during the 1950-1975 development period. Mass-balance calculations indicated that the aquifer system had an excess of 3,790,000 acre-feet of water to discharge out of its boundaries over the 25 years of irrigation development being simulated, if steady-state conditions were roughly maintained. The estimated volume of pumped water for irrigation over the development period was 2,883,000 acre-feet. This is approximately 76% of natural losses from the system. Thus, the stresses imposed during aquifer development could be partly offset by reductions in net boundary losses, resulting in a prevailing steady-state flow regime during the development period.

Modifications of the Historical Water Tables:

Initial attempts to reproduce the transient potentiometric surfaces were not successful. It was assumed that the coarseness of the finite-difference mesh was again partly the cause of inaccurate mass balances within the model area. Furthermore, this problem could have been exacerbated by subjective bias possibly introduced by the individual who performed the head contouring. In an effort to alleviate these problems, the five transient water table configurations were smoothed with respect to both space and time. The method used involved a straight-forward time average of each point:

$$\overline{h}_{ij} = (\sum_{t=1}^{N} h_{ij}^{t})/N \qquad , \qquad N = 5$$

The value $\overline{h}_{ij}$ was then subtracted from the corresponding value of steady-state head obtained from the variable-flux calibration, H_{ij}, to yield a residual ε

$$H_{ij} - \overline{h}_{ij} = \varepsilon$$

If $|\varepsilon|$ was greater than 10 feet, an adjustment was calculated to reduce the value of ε to 10 feet, i.e.:

$$|\varepsilon + a| = 10$$

Where h_{ij}^{t} was higher than H_{ij}, a was subtracted from h_{ij}^{t}, and it was added when h_{ij}^{t} was less than H_{ij}. This smoothing did not affect the majority of points in the domain. In fact, its principal effect was on nodes characterized by the greatest fluctuations in head with respect to time. The smoothing operation was considered to be the only means of alleviating mass-balance problems in the absence of information regarding errors in the transient head data. The chief motivation for this process was to smooth out head levels in certain regions of the historical record, principally those areas near the southern and northeastern boundary regions, which showed fairly wide variations in head over time without any substantial stresses.

Modifications of Reported Pumpages:

The values of reported annual pumpages in acre-feet for the 1954, 1959, 1964, 1969, and 1974 benchmark years are repeated in Table 4. In the absence of precise knowledge regarding the trend of irrigation increases between the benchmark years, it was necessary to assume a specific temporal distribution between benchmark years.

Table 4. Reported Annual Pumpage for Benchmark Irrigation Years.

Irrigation Year	Volume (AF)
1949	0
1954	50,300
1959	127,280
1964	110,370
1969	161,580
1974	272,660

Two methods were considered as possible ways of filling in the missing values of the yearly irrigation between the benchmark years to obtain a realistic pumping schedule over the 25-year development period. The first was to assume an increasing linear trend between the benchmark years. The interval from 1949 to 1954 is shown in Figure 22. Total irrigation pumpage for the Great Bend Prairie over the 25-year historical period of development was estimated to be approximately 3,086,200 acre-feet when computed by this method. This volume represents 81% of the aquifer discharge at steady-state. A distinct advantage of this scheme was that the values obtained for the benchmark years were the exact historical values provided in the data

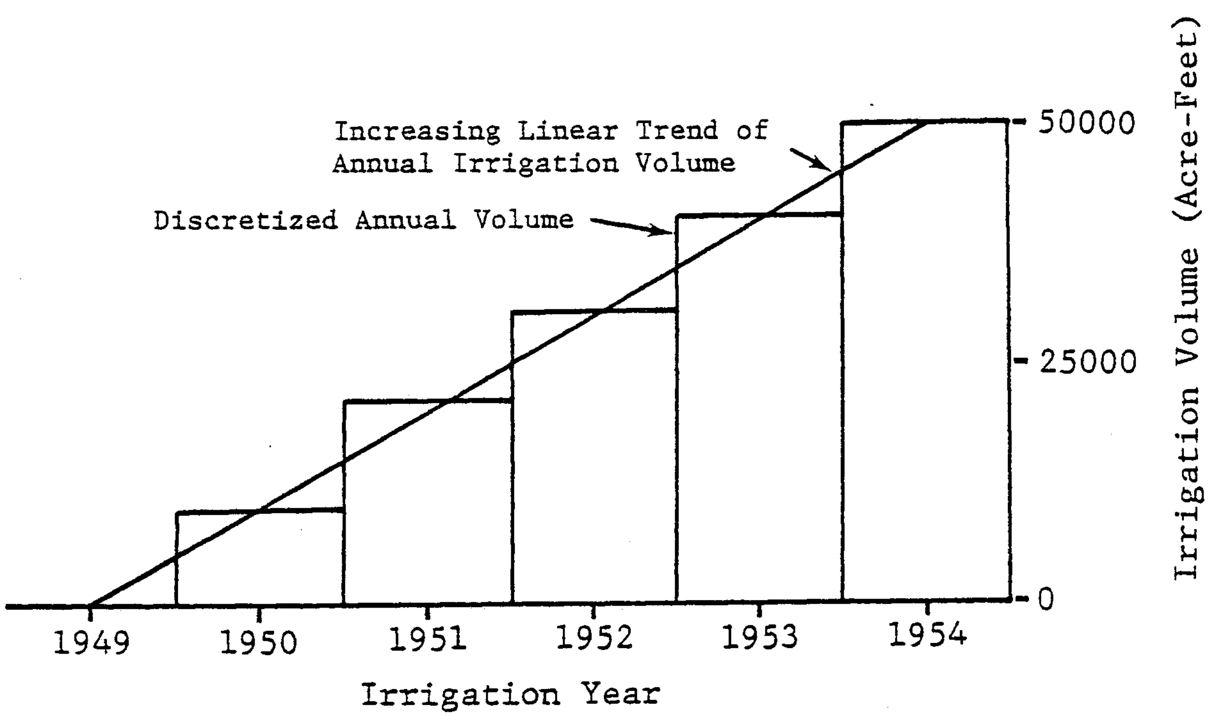

Figure 22. Five-year pumping schedule based on an increasing linear trend.

base. A major disadvantage was the need to construct and store one yearly-irrigation file for each of 25 simulation years. This was considered to involve a prohibitive amount of computer storage space.

The method finally used in the historical simulation was to estimate an average of the linear-trend pumping schedule for 5-year pumping periods, the end points of which were considered to be the initial and final days of the lower and upper bounding benchmark years (see Fig. 23). The average was then uniformly applied to each year in the 5-year pumping period. Calculated pumpage volumes for the modified distributions are shown in Table 5. Calculations indicated that the second method estimated a 25-year irrigation volume of 2,930,000 acre-feet, as compared to 3,086,200 estimated by the first method. The difference of estimation amounts to 5%. The modified pumpage values were used to adjust the nodal pumpage rates by defining a scaling parameter for each benchmark year and multiplying each nodal value by that parameter. The parameter was defined as the ratio of the modified pumpage to the unmodified pumpage for the benchmark years. The modified pumpages were then used to simulate irrigation withdrawals for the transient phase of the study.

Table 5. Values of Modified Annual Pumpage.

Year	Modified Pumpage
1954	25,000 AF
1959	89,000 AF
1964	119,000 AF
1969	136,000 AF
1974	217,000 AF

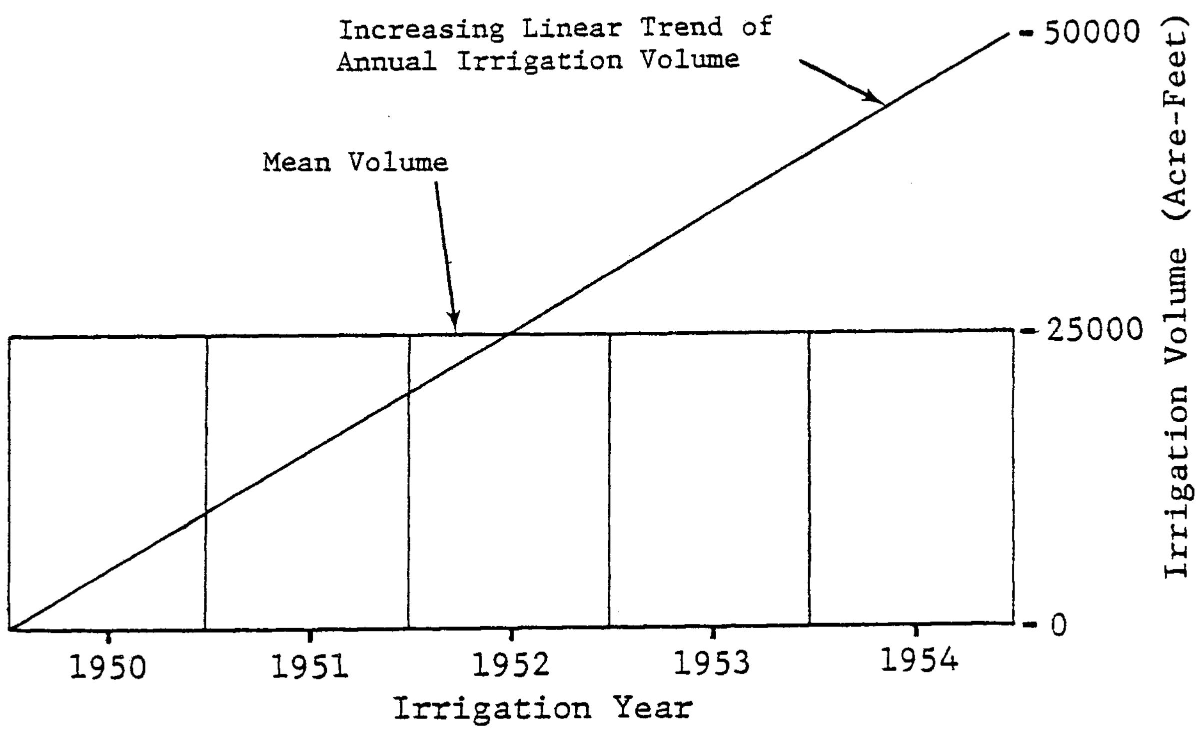

Figure 23. Five-year constant pumping schedule based on the mean value of an increasing linear trend.

In an effort to maintain a certain degree of control over the irrigation pumpage variables during the calibration procedure, an irrigation return factor was incorporated into the model to simulate a recharge mechanism which could account for the fact that some of the water which was pumped and applied to the crop returned to the water table due to seepage and percolation mechanisms. The return parameter was not defined to be physically-based, since it was not derived directly from physical conditions of soil moisture, soil composition, and meteorological factors. It was simply an empirical factor which could be obtained through trial-and-error calibration to simulate the essentially static mass-balance which apparently prevails in the region. The irrigation consumption factor was defined to be a fractional multiplier which could be applied to the irrigation pumping rate at each active node as a means of describing the volume of pumped water which was effectively removed from the aquifer through evapotranspiration processes.

Blaney and Hanson (1965) have suggested that deep percolation losses from irrigation can be as great as 35% for open porous soils. They also have reported that consumptive use fractions for crops similar to those grown in Kansas range from 0.60 to 0.85 in the frost-free period. Thus, an approximate value for the fraction of consumptive-use in the prairie may be expected to be in the 0.60 to 0.85 range, with a percolation return fraction of between 0.15 and 0.40. Layton and Berry (1973) feel that α is approximately 0.90 for Pratt County, although no actual field tests were run.

Strictly speaking, the reported pumpage rates, which were estimated on the basis of crop consumptive use and crop acreages, already incorporated some measure of seepage return into the model study. The consumptive-use factor α that was chosen to obtain a better match between simulated and modified observed head during the development period was therefore actually a correction factor for the pumpages listed in Table 4, and could theoretically take on any positive value. This consumptive-use correction factor α would also tend to be a function of changing climatic conditions.

Prior to attempts to perform a transient calibration for the development period, the historical irrigation pumpage rates were distributed to the nearest finite-difference nodes and scaled to reflect uniformly-distributed pumping volumes during each 5-year pumping period. These irrigation pumpage rates are listed in Appendix D, Matrix Listings 3, 4, 5, 6, and 7. Steady-state head from the variable-flux calibration constituted the initial conditions. Each 5-year pumping period consisted of five 1-year time steps. The variable-flux nodes at the rivers and along permeable boundaries were updated at the end of each pumping period, rather than at the end of each time step. Thus, the impact of the irrigation development was not reflected in the system until the end of each pumping period, and hence was a conservative interpretation of the interaction between the variable-flux rivers and boundaries and the pumping-well nodes.

Results of the Simulations

In an effort to test the sensitivity of the aquifer response to changes in irrigation stresses, α was allowed to vary from 0.6 to 1.0. Table 6 lists the sum of squared simulation errors, where simulation error was equal to the simulated transient head minus the modified post-development head, for each 5-year pumping period.

Table 6. Sum of Squared Simulation Errors (ft^2) for Various Values of α.

Pumping Period Ending January 1 of	Values of α 1.0	0.9	0.8	0.7	0.6
1955	32,830	32,830	32,834	32,793	32,724
1960	31,978	31,371	31,020	30,689	30,418
1965	48,029	46,281	45,013	44,163	43,572
1970	39,473	36,170	33,751	32,398	31,586
1975	71,198	59,108	50,196	44,229	39,589

The results of the numerical experiment indicated that the sensitivity of simulated head to α was slight during early stages of development, but that the simulated head became progressively more sensitive to the choice of α during later develoment stages. This was primarily attributed to errors accumulated over the 25-year simulation period. During the last pumping period, when pumpage increased dramatically (see Table 5), the sum of squared errors increased substantially when large values of α were used. This implied that the reported net pumpage for the 1970-1975 pumping period was greatly overestimated, despite modifications of pumpages which tended to lessen the impact of groundwater withdrawals. In addition, fluctuations in the average simulation error over time suggested that α should not be treated as a monotonic function of time for this particular study. A uniform α-value of 0.60 was chosen for the aquifer because this consumptive-use correction factor produced the smallest sum of squared errors for all pumping periods.

Clearly, it would have been possible to reduce the sum of squared error during any given pumping period by varying net natural recharge R over time.

However, fluctuations in the mean simulation error over time suggested that variations in R would not be systematic and would be of limited use during predictive operation of the model.

Figures 24 to 28 show the simulated water tables obtained with a consumptive-use correction factor α of 0.6. The simulated head configurations reproduced the regional characteristics of the modified historical water tables.

Response of the Variable-Flux Boundaries to Irrigation Development:

Losses from the steady-state pre-development system included outflows due to stream baseflow, evapotranspiration from shallow water tables, and underflow out of the model through boundaries and stream alluvium. It was expected that irrigation withdrawals during the development period would draw upon these losses to some extent. By using variable-flux nodes which were sensitive to saturated thickness, it was possible to quantify this phenomenon. Table 7 is a tabulation of the sum of the rates for modified irrigation pumpage and a consumptive-use correction factor of 0.60.

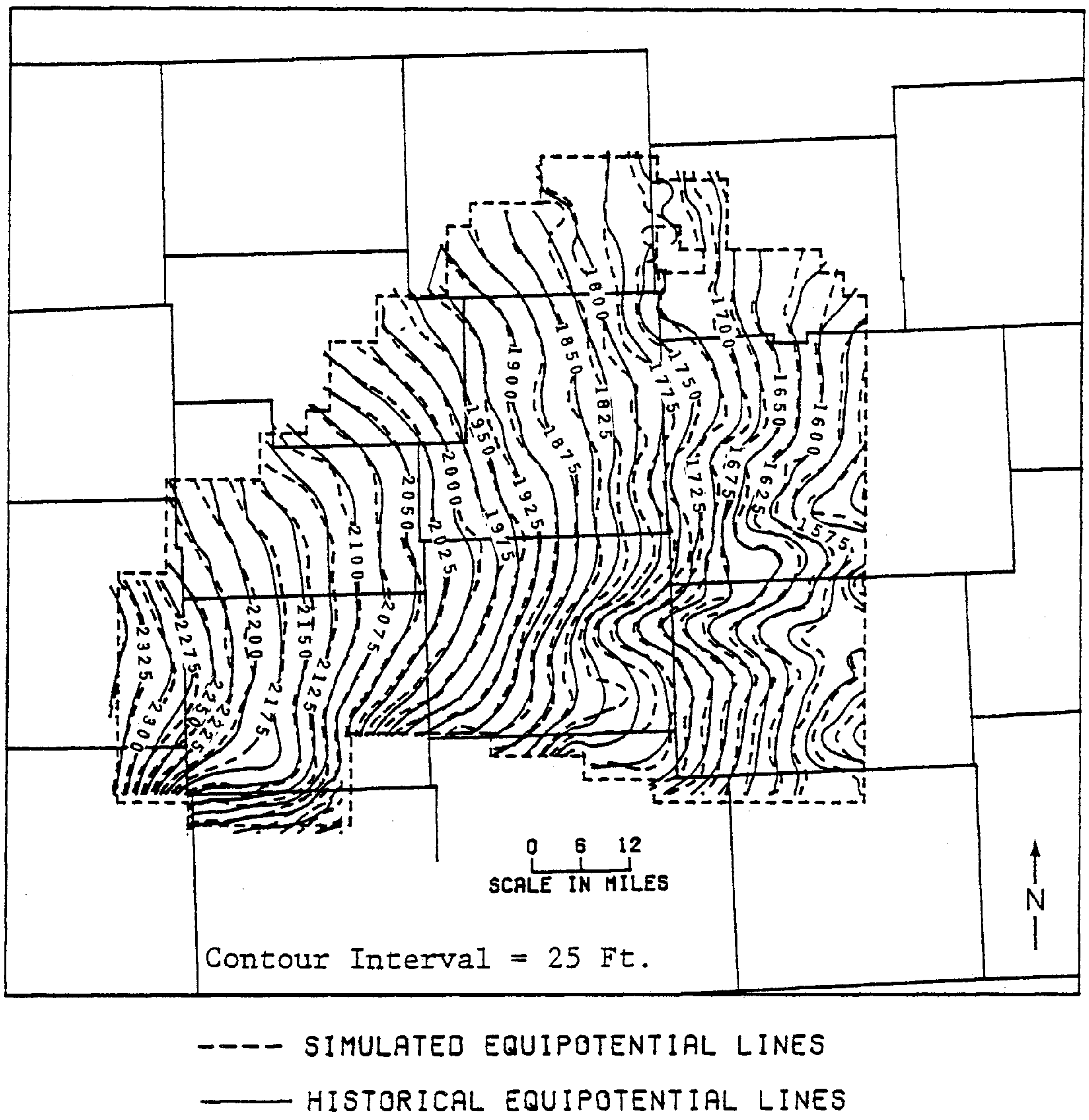

Figure 24. Simulated and altered input potentiometric surface -- 1955 (feet).

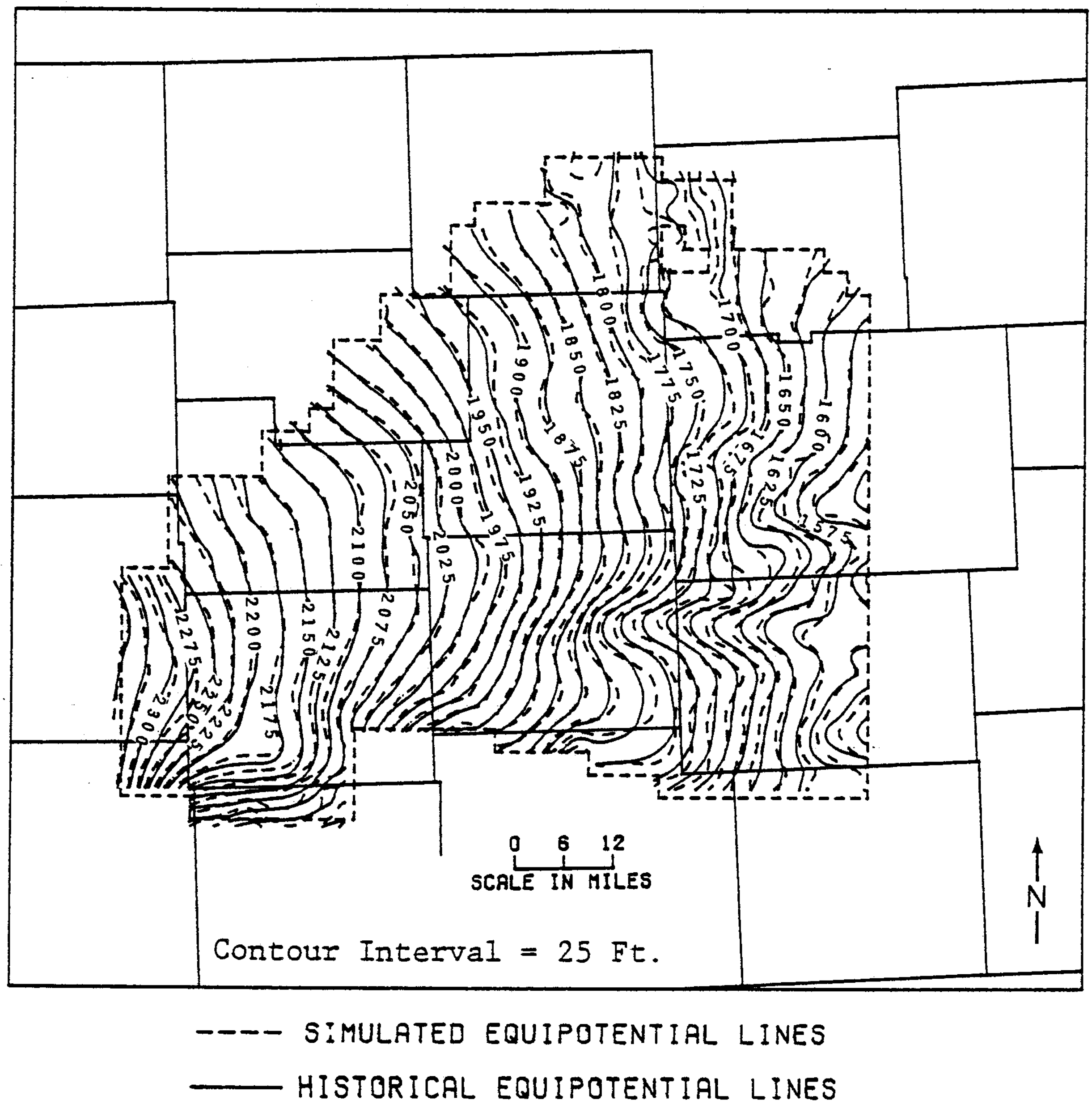

Figure 25. Simulated and altered input potentiometric surface -- 1960 (feet).

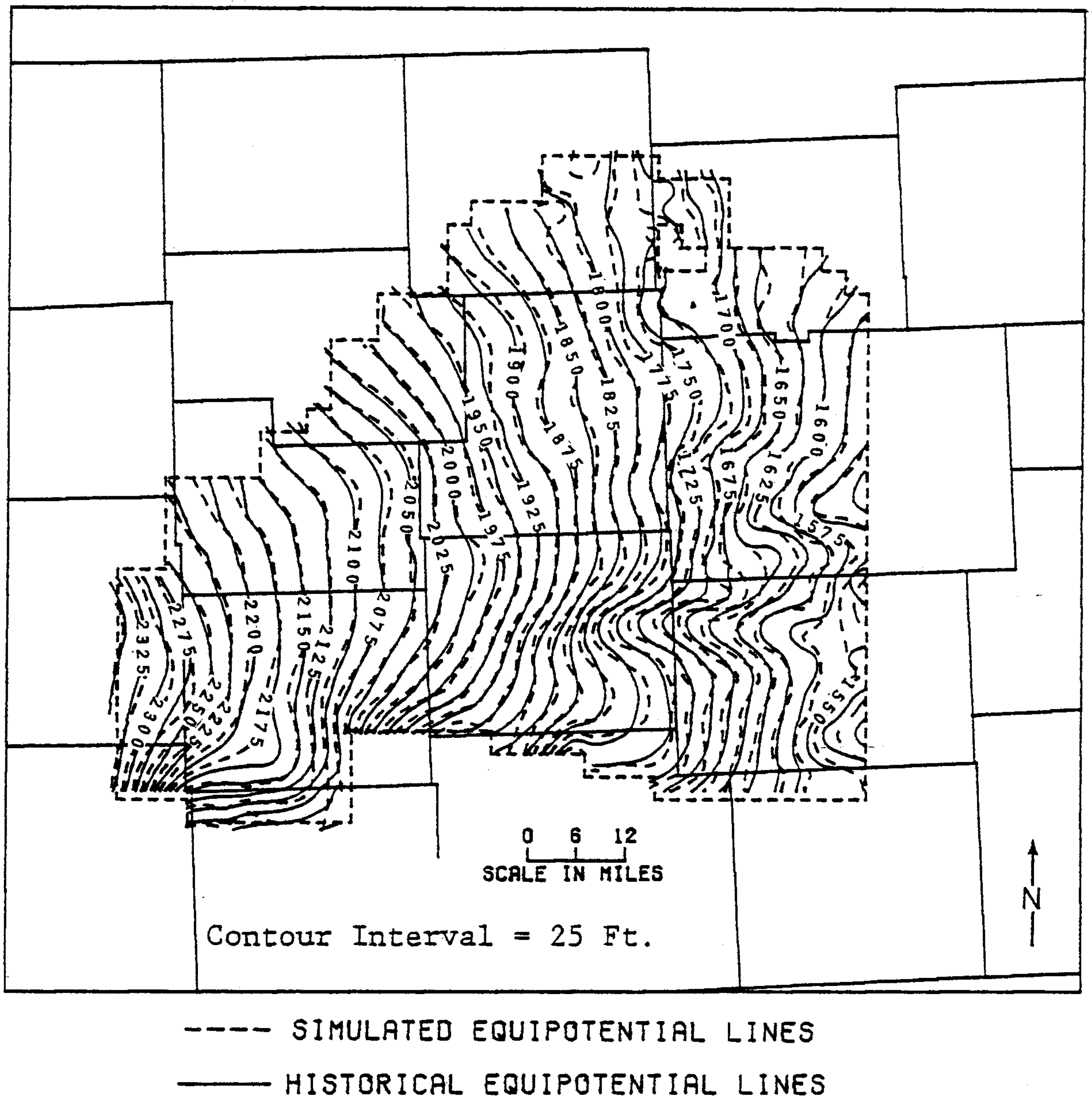

Figure 26. Simulated and altered input potentiometric surface -- 1965 (feet).

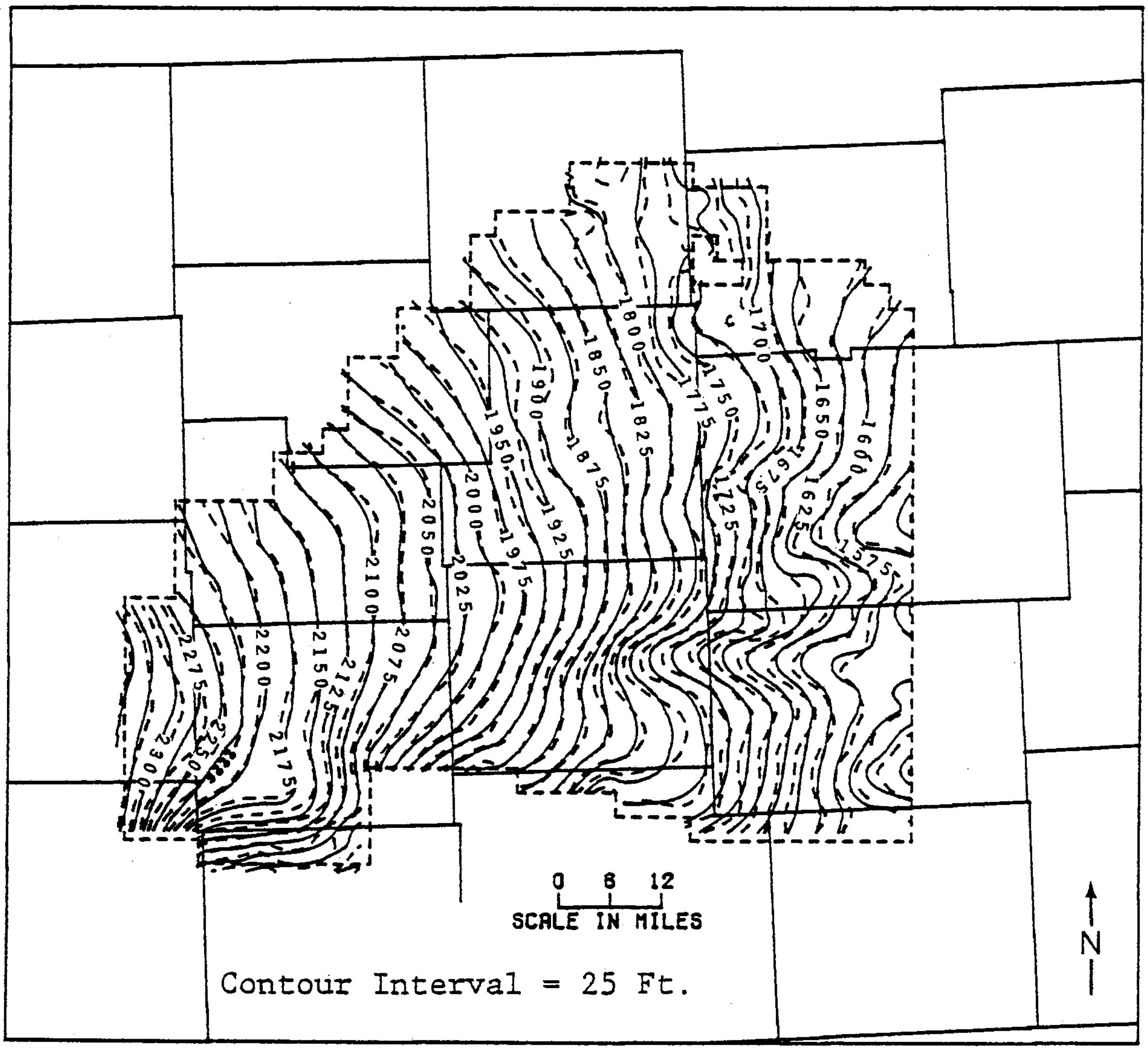

---- SIMULATED EQUIPOTENTIAL LINES

——— HISTORICAL EQUIPOTENTIAL LINES

Figure 27. Simulated and altered input potentiometric surface -- 1970 (feet).

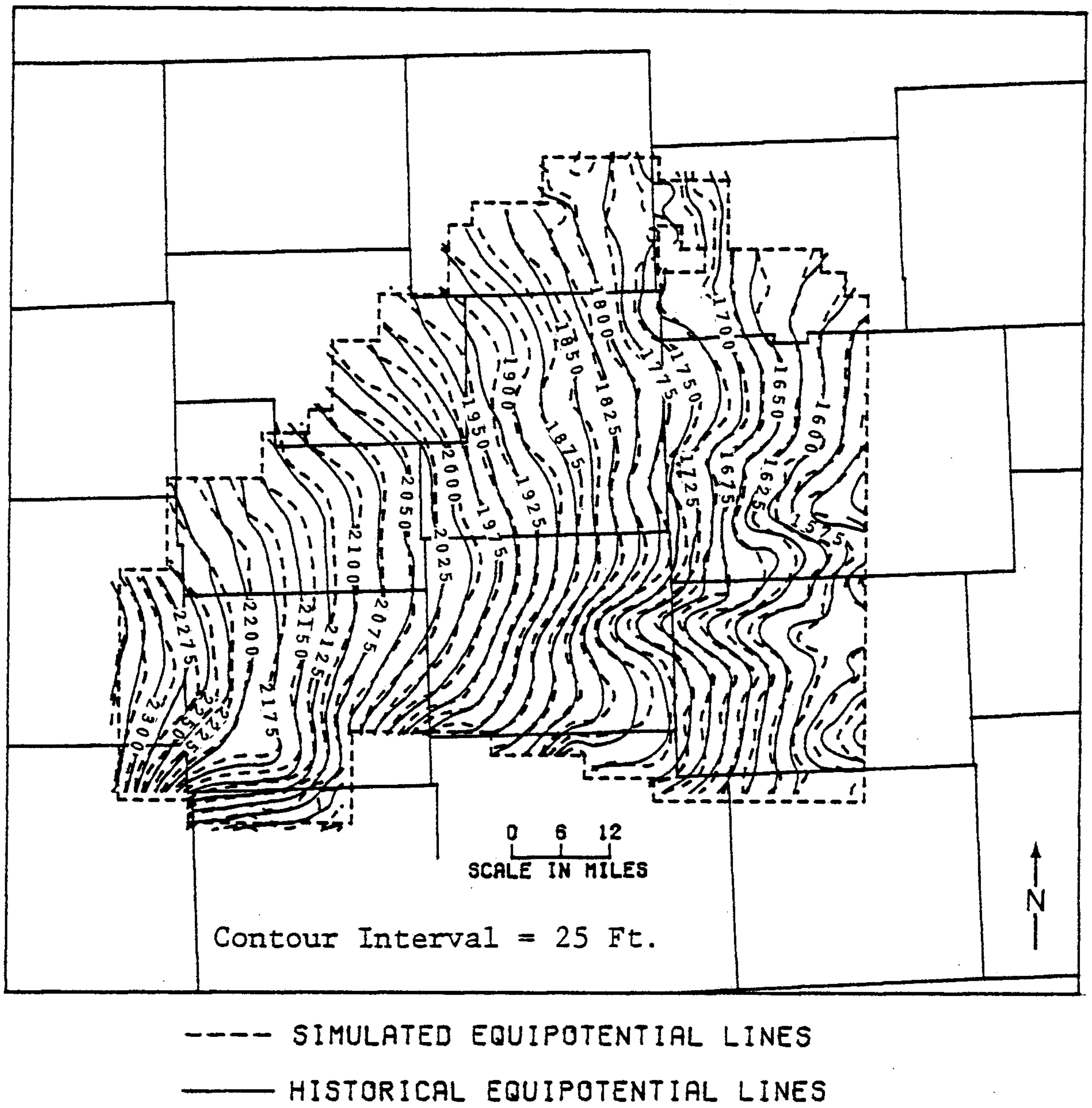

Figure 28. Simulated and altered input potentiometric surface -- 1975 (feet).

Table 7. Simulated Irrigation Withdrawals and Sum of Rates of Inflow and Outflow.

Pumping Period Ending January January	Volume of Irrigation Withdrawals (AF)	Sum of Rates* (cfs)
1955	125000 x .6	- 7.49
1960	445000 x .6	-13.92
1965	595000 x .6	- 9.33
1970	680000 x .6	-10.31
1975	1085000 x .6	-16.40

*Inflow Rate - Outflow Rate

Examination of Table 7 reveals that increases in the volume of irrigation withdrawals did not produce proportional increases in the sum of the rates of flow into or out of the model area. This implies that, throughout the development period, increases in natural inflow or decreases in natural outflow, or some combination of both, were occurring within the aquifer due to increased pumping stresses over time.

Table 8 shows a breakdown of fluxes for the simulation carried out with the model using the modified irrigation rates and a consumption correction factor of 0.6. Natural areal recharge remained constant throughout the simulation period and the rate of contribution from storage increased as irrigation withdrawals increased. The constant-head nodes underwent insignificant adjustments during the simulation. The discharging constant-gradient nodes showed a marked reduction in the net flux from the model due to pumping stresses. Figure 29 shows the relationships between incremental irrigation withdrawal, storage loss, and variable-flux boundary and river

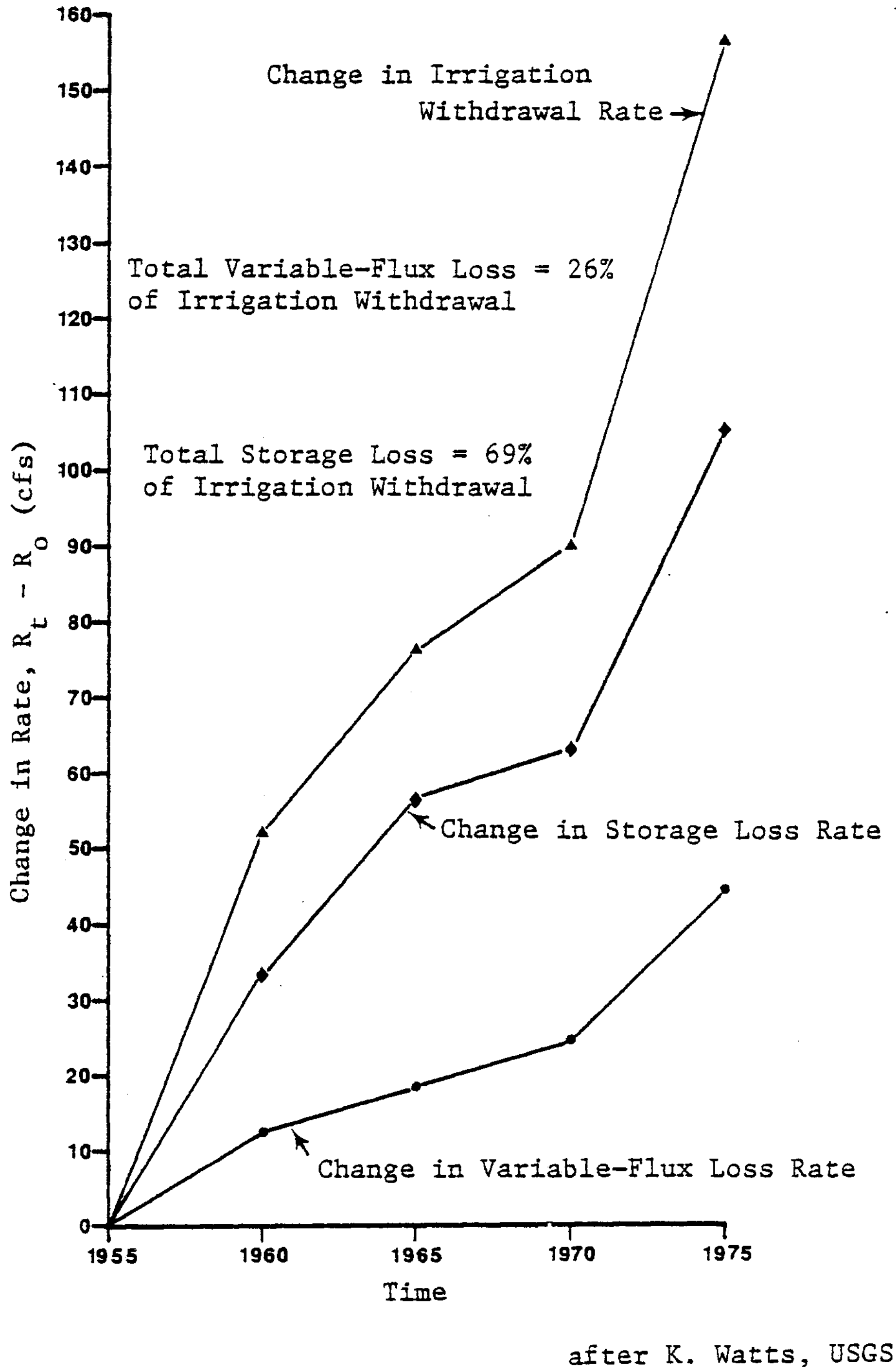

Figure 29. Incremental irrigation, storage loss, and boundary loss during the development period (cfs).

outflow. Assuming that boundary and river inflow remained essentially constant throughout the simulation, the change in variable-flux outflow is roughly equal to the change in net variable-flux outflow. From Figure 29, it is clear that storage losses were the primary source of irrigation water, comprising roughly 69% of total withdrawn groundwater. Surplus water from reduced net boundary and river outflow constituted only about 26% of total irrigation withdrawals. Thus, the tendency for the aquifer to become replenished by boundary and river contributions was dominated by storage depletion caused by irrigation withdrawals. However, for the small pumpage rates imposed on the aquifer, the transient effects implied by the dominant storage losses are negligible. Under conditions of larger imposed pumpage rates, these dominant storage contributions to irrigation withdrawals would presumably introduce significant transience to the flow system. The percentage of irrigation withdrawal obtained from storage would theoretically approach 100% for large withdrawal rates as the aquifer becomes depleted.

Table 8. Breakdown of Groundwater Fluxes for Transient Simulation (cfs)

Period Ending Jan.	Storage Losses	Natural Areal Recharge	Constant Gradient Flux In	Out	Irrigation Rate	Constant Head Flux In	Out	Sum of Rates
1955	7.28	224.53	70.16	-279.13	- 20.72	0.54	-10.14	- 7.49
1960	40.78	224.53	69.81	-266.96	- 72.52	0.54	-10.11	-13.92
1965	63.96	224.53	69.38	-260.72	- 96.97	0.55	-10.10	- 9.33
1970	70.71	224.53	68.69	-254.54	-110.23	0.55	-10.03	-10.31
1975	112.45	224.53	67.56	-234.21	-177.36	0.56	- 9.93	-16.40

Leakage from Permian and Cretaceous Units:

In addition to the adverse effects on baseflow, dewatering of the alluvial aquifer would also tend to induce further salt water intrusion from the Permian bedrock. Due to lack of sufficient data to adequately calibrate the salt-water leakage into the groundwater supply, this phase of the hydrology has been tacitly assumed to be incorporated with the natural recharge. A similar assumption holds for any groundwater exchange between the Cretaceous formations and the unconsolidated aquifer. Appendix A presents the best available information on the permeability of the Permian redbeds. One set of calculations based on this data indicate that up to 8% of the total natural areal recharge may come from saltwater leakage from the Permian bedrock.

Summary & Conclusions - Steady-State Calibration & Simulation Using USGS Model

After considerable scrutiny and modification of the data base, a calibrated two-dimensional numerical model of the region shown in Figure 9 was developed. This effort resulted in a model calibrated by trial-and-error for net natural areal recharge (precipitation and evapotranspiration, plus possible leakage from the Permian redbeds) and for a uniform value of hydraulic conductivity. **The average natural recharge rate amounted to 0.75 inches per year.** Hydraulic conductivity K was uniformly estimated to be equal to 85 ft/day. All internal and external boundaries were either of the no-flow or constant-head type. As a final step in calibration procedure, the constant-head boundary and river nodes were changed to variable-flux nodes by assuming constant-gradient conditions using Darcy's Law. Initial fluxes at these nodes were adjusted until a 16-year transient simulation produced a roughly steady-state head distribution. The head distribution resulting from this process was used to initialize transient calibrations for the consumptive-use correction factor α. The chief merit of the variable-flux scheme was that the boundary and river fluxes could respond to pumping stresses through variations in saturated thickness at the boundaries and rivers. Since the extent of irrigation development was not sufficient to produce significant changes in saturated thickness at the boundaries and rivers, constant-head boundaries may have served just as well. However, the variable-flux boundary and river calibration made it possible to better define a predictive model which would be capable of simulating changing stream and boundary conditions for large irrigation withdrawals expected during future development.

Simulation of historical irrigation development indicated that the irrigation stresses being imposed upon the system up to January of 1975 were not sufficient to cause more than a short term effect on the aquifer. A consumptive-use correction factor of 0.6 was used to simulate net irrigation withdrawals. Table 9 lists the average simulation errors and sum of squared simulation errors for the transient calibrations.

Table 9. Final Sum of Squared Simulation Errors and Error Statistics for Transient Calibrations

	$\Sigma\varepsilon^2$ (ft^2)	$\bar{\varepsilon}$ (ft)	Standard Deviation (ft)
1955	32,724	−0.60	7.01
1960	30,418	−0.38	6.75
1965	43,572	+0.50	8.08
1970	31,586	−0.58	6.88
1975	39,589	+1.39	7.76

It is clear from the results of this study that the Great Bend aquifer retains significant undeveloped capacity. If variable-flux boundary and river conditions are assumed to accurately simulate the loss of water out of the system, then the response of the model indicates that a significant portion of the potential irrigation development would simply divert water which would otherwise be lost from the aquifer to other aquifer systems. The effect of such diversions on external aquifer systems would certainly need to be assessed at some future time. Increased rates of irrigation withdrawals would tend to rely more heavily on storage losses as saturated thickness and, by inference, constant-gradient flux, decreases at the boundaries and rivers. At some particular point in time, these large storage losses would result in measurable system transience.

The final numerical model cannot be verified according to the existing available data due to the lack of significant transience in the system. Therefore, any attempt to forecast future aquifer response to increased irrigation activity should be performed with caution. Until a significant perturbation of the water table can be associated with a known distribution of irrigation pumpage, formal verification of the model parameters will not be possible.

The problem of water quality remains unaddressed in this study. Water of low quality exists in the Permian redbeds and in many of the unconsolidated units of the Great Bend aquifer. The extent to which groundwater development exacerbates the problem of salt-water intrusion into the alluvial aquifer should be considered in greater detail during future research efforts.

Calibration Using the Steepest-Descent Algorithm

The next part of the steady-state calibration focused on obtaining a distributed set of hydraulic conductivity values and on refining the precipitation recharge distribution using a steepest-descent optimization algorithm developed at Texas Tech University (Knowles, et al., 1972). The steepest-descent method is basically a variation of the nonlinear regression techniques frequently used to calibrate groundwater-flow models.

In addition to the steady-state calibration, several transient calibrations were performed in order to obtain a distributed set of specific yield estimates, as well as to determine the consumptive-use correction factor α. General properties of the steepest-descent algorithm are discussed in Appendix B. The calibration procedures and results for both the steady-state and transient calibations have been outlined in Appendix C.

REFERENCES

Bayne, C.K., 1956, Geology and ground-water resources of Reno County, Kansas: Kansas Geological Survey Bulletin 120, 250 p.

Bayne, C.K., 1960, Geology and ground-water resources of Harper County, Kansas: Kansas Geological Survey Bulletin 143, 184 p.

Bayne, C.K., Franks, P.C., and Ives, W., Jr., 1971, Geology and ground-water resources of Ellsworth County, central Kansas: Kansas Geological Survey Bulletin 201, 84 p.

Bayne, C.K. and Ward, J.R., 1974, Geology and hydrology of Rice County, central Kansas: Kansas Geological Survey Bulletin 206-3, 17 p.

Bear, J., 1979, Hydraulics of Groundwater: New York: McGraw-Hill, 567 p.

Blaney, H.F. and Hanson, E.G., 1965, Consumptive use and water requirements in New Mexico: New Mexico State Engineer, Santa Fe, Technical Report 32, 81 p.

Cobb, P.M., 1980, The distribution and mechanisms of salt water intrusion in the fresh water aquifer and in Rattlesnake Creek, Stafford County, Kansas: Unpublished M.S. thesis, The University of Kansas, 176 p.

Cooper, H.H., Bredehoeft, J.D., and Papadopulos, I.S., 1967, Response of a finite-diameter well to an instantaneous charge of water: Water Resources Research, v. 3, no. 3, 7 p.

Dixon, W.J. and Brown, M.B., 1979, BMDP-79, Biomedical computer programs, P-series: University of California Press, Berkeley, 880 p.

Fader, S.W. and Stullken, L.E., 1978, Geohydrology of the Great Bend Prairie, south-central Kansas: Kansas Geological Survey Irrigation Series 4, 19 p.

Fent, O.S., 1950, Geology and ground-water resources of Rice County, Kansas: Kansas Geological Survey Bulletin 85, 142 p.

Heimes, F.J. and Lucky, R.R., 1982, Estimating historical ground-water irrigation requirements in the high plains in parts of Colorado, Kansas, Nebraska, New Mexico, Oklahoma, South Dakota, Texas, and Wyoming: U.S. Geological Survey, Water Resources Investigations 82-40, 32 p.

Hvorslev, M.J., 1951, Time lag and soil permeability in groundwater observations: U.S. Corps of Engineers, Waterways Experimental Station Bulletin No. 36.

Keene, K.M. and Bayne, C.K., 1977, Ground water from Lower Cretaceous rocks in Kansas: Kansas Geological Survey Chemical Quality Series 5, 18 p.

Knowles, T.R., Claborn, B.J., and Wells, D.M., 1972, A computerized procedure to determine aquifer characteristics: Water Resources Center 72-5, Texas Tech University, Lubbock, 103 p.

Kume, J. and Spinazola, J.M., 1983, Geohydrology of sandstone aquifers in southwestern Kansas: Kansas Geological Survey Irrigation Series, in preparation.

Lane, C.W., 1960, Geology and ground-water resources of Kingman County, Kansas: Kansas Geological Survey Bulletin 144, 171 p.

Latta, B.F., 1948, Geology and ground-water resources of Kiowa County, Kansas: Kansas Geological Survey Bulletin 65, 151 p.

Latta, B.F., 1950, Geology and ground-water resources of Barton and Stafford counties, Kansas: Kanas Geological Survey Bulletin 88, 228 p.

Layton, D.W. and Berry, D.W., 1973, Geology and ground-water resources of Pratt County, south-central Kansas: Kansas Geological Survey Bulletin 205, 33 p.

Lobmeyer, D.H. and Weakly, E.C., 1979, Water in the Dakota Formation, Hodgeman and northern Ford counties, southwestern Kansas: Kansas Geological Survey Irrigation Series 5, 41 p.

McLaughlin, T.G., 1949, Geology and ground-water resources of Pawnee and Edwards counties, Kansas: Kansas Geological Survey Bulletin 80, 189 p.

McNellis, J.M., 1973, Geology and ground-water resources of Rush County, central Kansas: Kansas Geological Survey Bulletin 207, 45 p.

Sampson, R.J., 1978, SURFACE II Graphics System, Kansas Geological Survey, Lawrence, 240 p.

Sorenson, H.W., 1980, Parameter Estimation: New York: M. Dekker, 382 p.

Stullken, L.E., January 4, 1982, personal communication: Tape media transfer of irrigation data for Great Bend Prairie region.

Todd, D.K., 1980, Groundwater Hydrology, 2nd edition: New York, John Wiley and Sons, 535 p.

Trescott, P.C., Pinder, G.F., and Larson, S.P., 1976, Finite-difference in two dimensions with results of numerical experiments: Techniques of Water Resources Investigations of the U.S. Geological Survey, Book 7, Chapter C1, 116 p.

U.S. Geological Survey, 1975, Water resources data for Kansas water year 1975: U.S. Geological Survey Water Data Report KS-75-1, 405 p.

Waite, H.A., 1942, Geology and ground-water resources of Ford County, Kansas: Kansas Geological Survey Bulletin 43, 250 p.

Wilson, W.E. and Gerhart, J.M., 1980, Simulated effects of groundwater development on the potentiometric surface of the Floridian Aquifer, west-central Florida: U.S. Geological Survey, Open-File Report 79-1271, 119 p.

Zeller, D. (ed.), 1968, The stratigraphic succession in Kansas: Kansas Geological Survey Bulletin 189, 81 p.

APPENDIX A: Salt Water Leakage into the Great Bend Alluvial Aquifer

Prior to undertaking the previously discussed modeling effort, it was proposed that incorporation of leakage of salt water from the Permian units which underlie the Great Bend alluvial aquifer could be used to aid the calibration process. The quantity of leakage is believed to account for at least several percent of the total natural recharge into the aquifer. Fader and Stullken (1978) postulate that as much as 5,000 to 10,000 acre-feet per year of salt water leaks from the Cedar Hills Sandstone alone, assuming a hydraulic conductivity of 25 feet/day in the sandstone unit.

It was initially intended that data acquired during previous research of the leakage mechanism would be incorporated into the calibration procedure. However, sufficient data was not available during the calibration period to allow meaningful simulation of hydraulic interaction between the Permian and Cenozoic units. Nineteen well sites were available during the calibration period (see Table A-1), compared to the 36 sites which are presently established, but the majority of these wells were concentrated in Stafford County.

Estimates of hydraulic conductivity, vertical gradient, measured head, and fluid density were required at all sites for purposes of determining fluid motion between aquifers characterized by distinct quality constrasts. These estimates were available only at 6 of the original 19 sites, and were clustered in Stafford County. Only some of the required parameters were available at the 13 remaining sites. The incomplete parameter sets could not be used to uniquely define leakage properties at these sites.

Table A-1. Locations of KGS Well Sites in the Great Bend Prairie from which Useable Data was Available for this Study.

Site Number	Legal Description	County
1	12-23-12W NE/NE/NW	Stafford
2	36-23-12W NE/NW/NE	Stafford
3	36-23-13W SW/SW/SE	Stafford
4	36-23-14W SW/SE/SE	Stafford
5	6-23-12W NW/NW/NW	Stafford
6	6-25-13W NW/NW/NW	Stafford
7	36-24-13W SE/SE/SE	Stafford
8	11-25-12W NE/NE/NE	Stafford
9	31-24-10W SW/NW/SW	Reno
10	6-24-10W SW/SW/SE	Reno
11	6-22-10W NW/NW/SW	Reno
12	36-29-11W SW/SW/NE	Pratt
13	36-29-14W NE/NE/NE	Pratt
14	12-29-14W NW/NW/NE	Pratt
15	1-28-11W NE/NE/NE	Pratt
16	31-21-12W SW/SW/SW	Stafford
17	36-21-12W SW/SE/SE	Stafford
18	7-21-11W NW/NW/NW	Stafford
19	36-25-13W SW/SW/SE	Stafford

Most of the present sites still lack a full suite of parameters required to determine the direction and quantity of fluid movement between the bedrock and the lower-unconsolidated units. Until the observation well network is complete and a full suite of data is available at each well, only very sketchy hypotheses may be constructed concerning the distribution of hydraulic conductivity and the regional salt water flux. The remainder of this discussion will therefore be oriented towards presentation of the best currently-available data, and will include a modest attempt to estimate the volume of low-quality water which enters the unconfined alluvial aquifer system as recharge from underlying Permian units.

In the month of July, 1981, personnel from the Kansas Geological Survey conducted a series of "slug" tests in 19 tube wells which had been grouted into place in subcropping units of the Nippewalla Stage, Lower Permian Series. These units are believed to represent the Cedar Hills Sandstone, the Salt Plain Formation, and possibly the Harper Sandstone. Time-recovery data was collected at each of the 19 observation wells after static water levels were perturbed by the addition of a quantity of fresh water. Analysis of the data was performed using two methods. A semi-log-linear interpretation method developed by Hvorslev (1951) was used as a "first cut" in the field to estimate K. A transient type curve method (Cooper, Bredehoeft, and Papadopulos, 1967) was later applied to refine K and to estimate S_y. Several comments are in order. First, due to the method of well construction, the K measured in this study is probably representative of the horizontal component of K, K_h. Second, some wells seemed to take water at a higher rate than was expected on the basis of the low conductivity of the bedrock. Thus, some subjectivity entered into the choice of "good" and "bad" tests.

Table A-2 indicates the values of K_h obtained by the two methods indicated above. Formations which are believed to be screened are shown listed in the table. The table indicates a range of hydraulic conductivity of four orders of magnitude. This range compares favorably to ranges given by Bear (1979, p. 68) of 10^{-2} through 10^{-6} cm/sec for semipervious consolidated rocks and slightly less favorably with the range given by Todd (1980, p. 72) of 10^{-4} to 10^{-7} cm/sec. Although a spatial distribution of K_h is implied by the geographic distribution of sites, the sparseness of sites relative to the size of the area makes use of a single averaged value of hydraulic conductivity attractive. However, the relatively high value of K at sites 1, 5, and 10 requires some caution in taking this approach.

Table A-2. Compilation of "Slug" Tests Performed in the Permian Formations and Analyzed by Methods Due to Hvorslev and Cooper, and others (S values not shown).

Site Number	Formation	Hvorslev K_h (cm/sec)	Cooper K_h (cm/sec)	Comments
1	Salt Plain	5.2×10^{-3}	---	Seems too large (excess weathering?)
5	Cedar Hills	1.7×10^{-3}	---	Compare to 8×10^{-3} cm/sec = 25 ft/day
6	Undiff Perm(?)	9.6×10^{-6}	1.6×10^{-5}	
7	Cedar Hills/UP	7.0×10^{-5}	1.8×10^{-4}	See above note on Cedar Hills
8	Cedar Hills	---	1.24×10^{-4}	See above note on Cedar Hills
10	Salt Plain	3.4×10^{-4}	3.33×10^{-3}	
15	Salt Plain	4.2×10^{-6}	3.35×10^{-6}	
17	Salt Plain	3.1×10^{-6}	---	
18	Salt Plain	2.0×10^{-6}	---	
19	Cedar Hills	2.7×10^{-6}	---	See above note on Cedar Hills

In order to estimate the vertical component of flux, Darcy's Law was used. It was assumed that leakage from lower permian units into the alluvial aquifer was governed by steady-state conditions. The most complete suite of parameters for computing the Permian to Pleistocene fluid motion exists for well sites 1 through 11. These were installed in 1978 and 1979 and have been extensively sampled and measured (Cobb, 1980). Fluid head measurements were adjusted using density corrections calculated from chemical analyses from fluid in the wells. Gradients were computed by assuming that the vertical distance ΔL was measured from the center of the well screen to the top of the bedrock. The head in the bedrock well (h_1) was assumed to represent an average at the mid-point of the screen. The head in the well situated in the lower unconsoldiated aquifer (h_2) represented the average head value at the bedrock contact. The gradient was then defined as $(h_2 - h_1)/\Delta L$. A negative sign indicates upward movement of fluid. In the following table, well sites are listed for which K and $(h_2 - h_1)/\Delta L$ are approximately known. K_z was assumed to equal K_h as previously determined.

Table A-3. K_z, Vertical Hydraulic Gradient, and Calculated Vertical Velocity Flux for Selected Sites.

Site	K_z (ft/day)	$(h_2 - h_1)/\Delta L$	q (ft/yr)
1	14.70	-0.11	-590
5	4.93	-0.89	-1600
6	0.03	-0.47	-5.15
7	0.20	-0.01	-0.73
8	0.35	-0.07	-8.94
10	0.96	+0.01	+3.5

Two items are quite striking about Table A-3. First, if values for sites 1, 5, 6 and 8 are accurate and valid over large areas, there is considerably more salt water moving into the region than was expected. More attention should be given to this problem. The second fact of importance is that the bedrock also accepts a certain amount of water from the unconsolidated unit, as evidenced by the positive calculated flux at site 10. This raises the question, as yet unanswered, as to how much of the recharge water moving up from bedrock is actually a Permian contribution to recharge, and not merely a circulation of native unconsolidated aquifer water which dilutes some concentrated Permian salt water in transit. This awaits further investigation.

As stated earlier, the value of K measured in the slug tests may represent the horizontal hydraulic conductivity. In many geological deposits, especially shale and siltstone, it is not uncommon to find the horizontal component of K exceeding the vertical component by several orders of magnitude. If the K_h values in Table A-2 are reduced by two orders of magnitude to describe vertical conductivity K_z, then the computed fluxes fall into a more reasonable range than those calculated in Table A-3, ranging from a few feet to a few hundredths of a foot per year.

As a conclusion to this discussion, several hypothetical situations for leakage distribution have been outlined and some rough calculations can be made. It was initially assumed that all leakage occurs over a limited area extending from the Cedar Hills Sandstone over a region from the Barton County line to about Stafford, Kansas (see Fader and Stullken, 1978, Plate I). This includes about 45 square miles or 28,800 acres. It was also assumed that K_z = 4.93 ft/day over the entire leakage domain and that $(h_2 - h_1)/\Delta L$ was about -0.1, a reasonable value except possibly near gaining stream. Using these estimates, an annual contribution of about 14,000 acre-feet per year was calculated, a flux which is comparable to Fader and Stullken's value of about 10,000 acre-feet per year (Fader and Stullken, 1978). This amounts to a rate of 19.61 cfs. The total natural recharge calculated from the calibrated model for the study area was 224 cfs. Thus, leakage from a portion of the Cedar Hills may account for as much as 8% of the total natural recharge, while the value of Fader and Stullken is 6% of the total recharge. This conceptual model, using only that part of the Cedar Hills for which a high value of K_z has been documented, produced results compatible with published speculation.

A second possibility was explored by estimating generalized leakage over the Permian subcrop using an average gradient and a uniform K_z of low value. The approximate area of the subcrop was 1.8×10^6 acres. 2×10^{-6} cm/sec = 2.07 ft year was considered to be a reasonable average value for the majority of the subcropping units. Using a gradient of -0.1 feet, a volume of 3.7×10^5 acre-feet per year was computed, which was equivalent to a rate of 512 cfs. This last figure was about twice the total calibrated recharge rate and was obviously an overestimate of the recharge flux. The overestimate probably resulted from the fact that head gradients are probably not negative everywhere over the subcrop. A more detailed map of head gradient will have to be constructed as field work in the area continues. However, it is clear that a localized leakage domain posed by Fader and Stullken (1978) gives a more satisfactory leakage component than a generalized uniform leakage model.

APPENDIX B: The Texas Tech Steepest-Descent Algorithm (Knowles, *et al.*, 1972)

The steepest-descent optimization method is essentially a type of nonlinear regression technique which can be used to identify unknown parameters of the two-dimensional flow equation. Nonlinear regression is necessitated by the form of the flow equation given by equation (1), which cannot be explicitly solved for hydraulic head h in terms of the regression parameters hydraulic conductivity K, specific yield S_y, and net external recharge W.

Nonlinear regression is based on iterative solution of the normal equations

$$d_{r+1} = (Z_r^T \, w \, Z_r)^{-1} \, Z_r^T \, w(y_r - f)$$

where

d_{r+1} = the normalized parameter increment vector at iteration r+1

Z_r = the sensitivity matrix at iteration r

y_r = the vector of estimated dependent variables at iteration r

f = the vector of true dependent variables

w = the weighting matrix, usually chosen as the inverse of the parameter variance-covariance matrix

The steepest-descent method reduces to solution of the equations

$$d_{r+1} = Z_r^{-1}(y_r - f)$$

for an identity weighting matrix w and for no rotation of the search direction to account for differences in the sensitivities, a rotation generally performed using the Z_r^T matrix. Thus, the steepest-descent solution simply involves calculation of the sensitivites of the dependent variable with respect to all parameter estimates at iteration r and calculation of the error in the dependent variable at iteration r. The sensitivities are measures of the rate of change in the dependent variables with respect to changes in the parameters. Since the change in the simulated dependent variable is equivalent to the change in the simulation error for constant elements of f, the sensitivities can be viewed as the derivatives or slopes of the error surface in the parameter space with respect to the parameters. Thus, each row of Z may be viewed as a gradient vector for a given nodal error surface over the parameter space. The steepest-descent method is frequently referred to as the gradient-search method.

The Texas Tech model does not involve explicit solution of the normal equations, but instead relies on direct differentiation of the finite-difference equations to define the slopes of the error surface at each node with respect to all adjustable parameters. These slopes are then used to establish the direction of steepest-descent over the parameter domain, or the direction in which the greatest amount of error reduction can be attained with the least amount of change in the parameter estimates.

Figure B-1 illustrates the method used in the Texas model to approximately define the direction of steepest-descent over each nodal error function. For the two-dimensional KS_y parameter-space, the derivatives of the error function with respect to initial K and S_y estimates are represented by BA and BE. These derivatives, or error sensitivities, can be projected into the zero-error plane using simple trigonometric principles. The direction of steepest-descent can be determined by choosing the point along AE which represents the least total in change in dimensionless parameter units over the

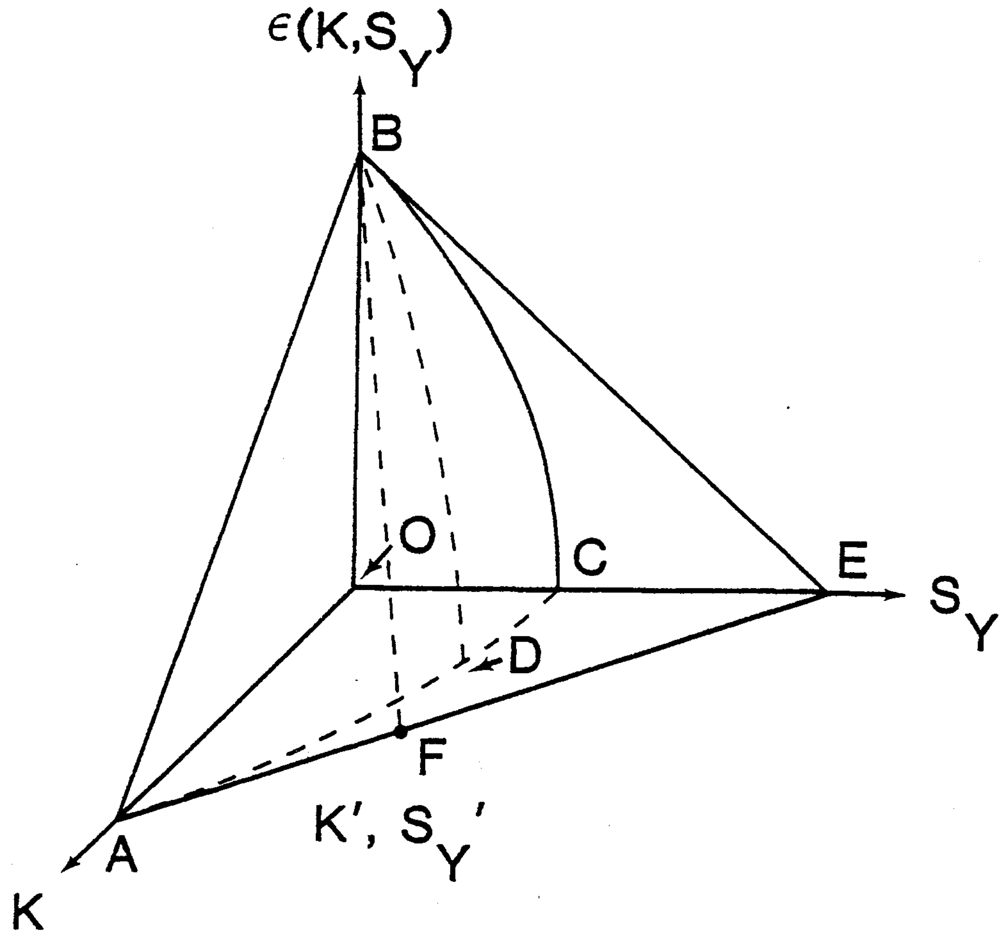

Figure B1. Schematic representation of the method used to define the steepest-descent search vector (after Knowles, et al., 1972).

KS_y space, indicated by (K', S_y'). Although the use of adjusted parameters K' and S_y' does not necessarily result in a zero-valued error during the subsequent re-simulation of head level, it does cause iterative convergence of the nodal error to a minimum value when the projection is repeatedly applied. Zero-valued simulation error will not occur in most instances even after a large number of iterations unless the input head distribution is error-free, which is unlikely to be the case. The projection would proceed in three dimensions if W were included as a parameter.

Error derivatives, or sensitivities, are determined by taking the derivative of simulated head with respect to adjustable parameters K, S_y, and W using a Crank-Nicolson finite-difference approximation of equation (1). It is assumed that the flow equation is continuously differentiable with respect to K, S_y, and W. It is also assumed that all three adjustable parameters K, S_y, and W are independent of each other, implying that net recharge W at any node is not affected by the value of K or S_y at that node during the adjustment procedure.

The resulting set of sensitivity equations, since they involve taking derivatives of quadratic unconfined head terms, are linear in head and can therefore be solved using the Gaussian elimination method. A separate system of equations

$$[A]\ [B] = [C] \qquad \text{(B1)}$$

is solved for each variable-head node, where [B] represents the vector of unknown error sensitivities at all nodes in the finite-difference grid with respect to parameter changes at the variable-head node. The system of equations can be greatly simplified by assuming that only the nearest 12 surrounding nodes are affected by parameter changes at each central, variable-head node. This may not be a valid assumption for high-conductivity situations, where changes in head at any node will tend to affect head at a large number of surrounding nodes. The system of equations is further reduced by considering only variable-head node sensitivities within the 12-node influence area, since, by definition, all constant-head nodes are insensitive to any changes in parameters and head levels at nearby active nodes. Sensitivities of constant- and zero-flux nodes can also be deleted from the B vector, since head at these nodes can be systematically related to head at adjacent interior active nodes. To illustrate this concept for zero-flux nodes, the boundary conditions

$$\frac{\partial h}{\partial x}\Big|_{\Omega} = 0$$

$$\frac{\partial h}{\partial y}\Big|_{\Omega} = 0$$

where Ω denotes the boundary, can be differentiated with respect to parameter ϕ

$$\frac{\partial}{\partial \phi}\left(\frac{\partial h}{\partial x}\right)\Big|_{\Omega} = 0$$

$$\frac{\partial}{\partial \phi}\left(\frac{\partial h}{\partial y}\right)\Big|_{\Omega} = 0$$

Assuming that derivatives of head h with respect to x, y, and ϕ are continuous, then

$$\frac{\partial}{\partial x}\left(\frac{\partial h}{\partial \phi}\right)\Big|_{\Omega} = 0$$

$$\frac{\partial}{\partial y}\left(\frac{\partial h}{\partial \phi}\right)_{\Omega} = 0$$

This implies that sensitivity of head at a no-flux boundary is constant with respect to space, and that sensitivities at nodes along no-flux boundaries are equal to sensitivities at adjacent nodes within the interior of the model. For the constant-flux case,

$$\frac{\partial h}{\partial x}\Big|_{\Omega} = c_1 \qquad , \qquad \frac{\partial}{\partial x}\left(\frac{\partial h}{\partial \phi}\right)\Big|_{\Omega} = 0$$

$$\frac{\partial h}{\partial y}\Big|_{\Omega} = c_2 \qquad , \qquad \frac{\partial}{\partial y}\left(\frac{\partial h}{\partial \phi}\right)\Big|_{\Omega} = 0$$

and the sensitivity of any constant-flux node is again equal to the sensitivity of the adjacent interior node.

Solution of equation B1 after each simulation is equivalent to simultaneous solution of equation B1 and equation (1). Mass-balance is maintained during the adjustment procedure during preceeding application of the simulation component of the model.

For the Great Bend study, it was necessary to assign certain constraints on the amount of parameter variation during each adjustment iteration in order to prevent divergence of nodal simulation error from the local minimum. These constraints also prevented excessive change in hydraulic conductivity K, to which simulated head is only slightly sensitive. In addition to imposed constraints on parameter-adjustment vectors, minimum and maximum parameter values were also assigned in an effort to maintain the approximately homogeneous conditions which had been observed throughout the alluvial aquifer. Whenever a constraint limited the value of any adjusted parameter, the remaining parameters were reduced by the same fraction. This procedure permitted the retention of the original steepest-descent search direction.

The parameter-adjustment scheme is illustrated in Figure B-2. All nodal errors are intially ranked from highest to lowest, and the parameter adjustment procedure is performed at each node in the order of decreasing simulation error. The error sensitivities at the central, maximum-error node and at all 12 surrounding nodes with respect to current parameter estimates at the central node are calculated using equation B1, and the direction of steepest-descent at the central node is approximated using the central-node sensitivities and the projection methods outlined previously. If any bounding constraints are violated, the parameter associated with the greatest magnitude of violation is adjusted, and the remaining parameters are adjusted according to the same proportion of reduction. After the final parameter search-vector lengths are specified, the sensitivities of error at all 13 nodes to central-node parameter changes are used to calculate error reductions at the 13 nodes, and the errors are reduced accordingly. Ranking of all nodal errors in the model area is repeated, excluding the errors at all central nodes for which new parameters have been defined, and the entire process is applied to the node at which the next largest error occurs. All nodes with errors of less than 0.5 feet were excluded from any type of parameter-adjustment procedure.

The Texas algorithm does not account for the possibility that several local minima in the squared-error distribution may occur within the feasible parameter region. To check for this possibility, it is necessary to perform a series of numerical experiments involving the assignment of different initial parameter guesses and comparison of final parameter estimates.

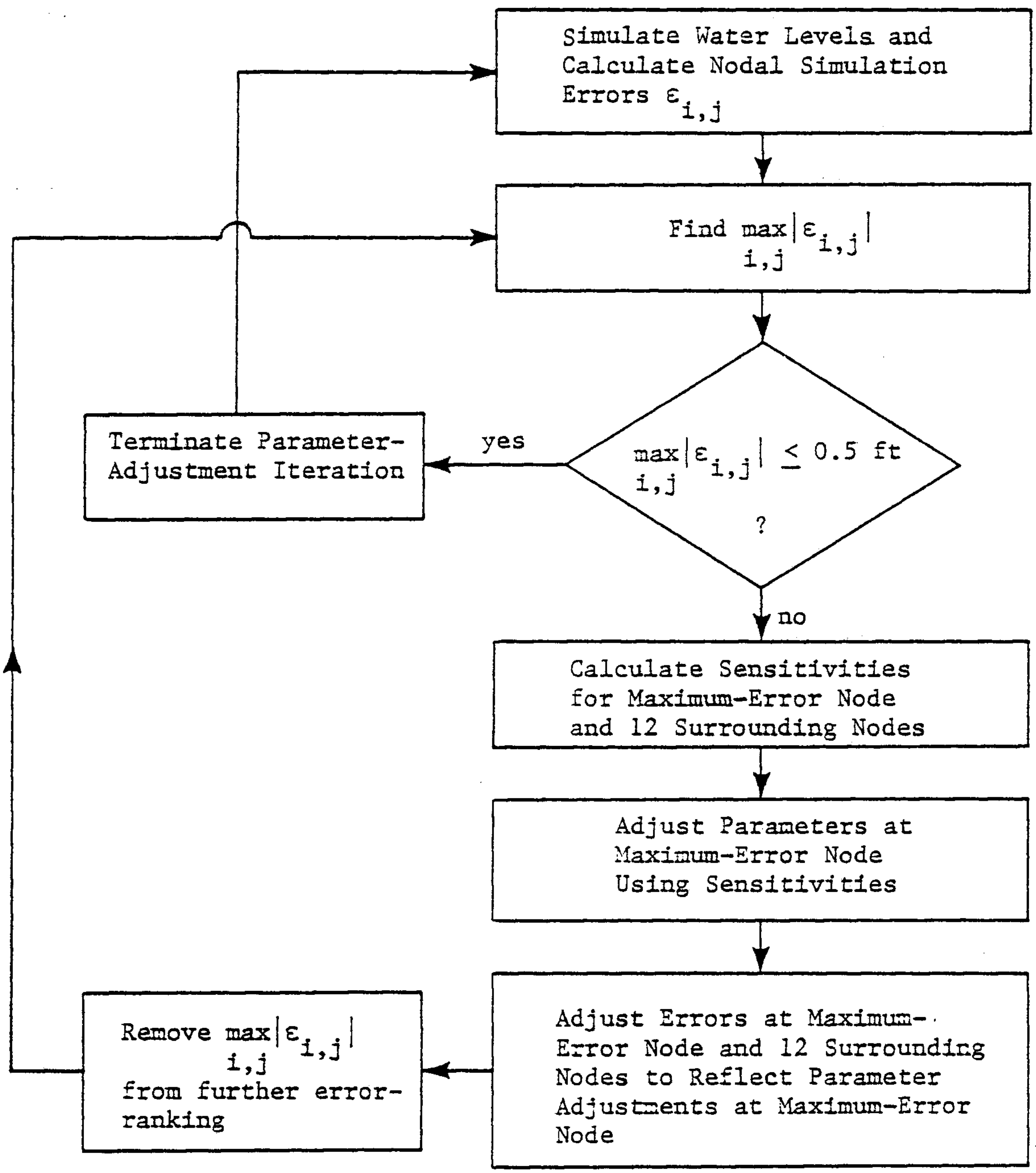

Figure B2. Flow chart of the steepest-descent algorithm.

APPENDIX C: Steepest-Descent Calibration Procedures and Results

Steady-State Calibration for Distributed Hydraulic Conductivity and Net Natural Recharge

A distributed set of hydraulic conductivity values and a more refined distribution of natural recharge were obtained using a computerized steepest-descent method which automatically minimized the sum of squared calibration error through simultaneous adjustment of K and R. This refining algorithm involved the repeated application of a sequence of operations which included solution of the governing finite-difference flow equations, evaluation of parameter performance on the basis of errors between the modified pre-development head and the simulated steady-state head, and adjustment of nodal parameters using sensitivity analysis. Modified pre-development head and bedrock distributions were used to initialize the simulation of head (see Figs. 10 and 11). As for the USGS steady-state calibration, constant-head conditions were initially used to describe aquifer behavior at permeable boundaries and rivers. Since all parameters obtained from the steepest-descent procedure were to be used to predict future water levels according to the USGS model, it was initially assumed that the USGS and Texas model simulated equivalent head values for given values of K and R. The equations used in the two models were, in fact, not identical due to differences in the manner in which conductivity and saturated thicknesses were averaged between adjacent nodes.

Initial Parameter Estimates:

Unlike the USGS steady-state calibration procedure, the steepest-descent calibration involved simultaneous adjustment of K and R through optimization of a two-dimensional parameter space rather than through separate adjustment of K and R. This required that bounding constraints of 60 and 100 ft/day be placed on K during each adjustment iteration such that simulation error would not be reduced at each node by excessive changes in K. Such excessive changes would be caused by decreased sensitivity of simulated head to spatially-variable hydraulic-conductivity for calibration involving heterogeneous aquifer conditions. This decreased sensitivity is, in fact, predicted by equation (1) for spatially-variable K.

Initial attempts to assign a zero-valued specific yield S_y to the Texas steady-state calibration resulted in divergence of the simulated head from the modified pre-develoment head distribution. Since convergence had previously been obtained during the USGS-model steady-state calibration run when the same input head distribution was used, it was originally believed that the choice of zero for specific yield resulted in an ill-conditioned head sensitivity matrix. However, this possibility was rejected after double-precision sensitivity solution failed to improve convergence characteristics of the steepest-descent procedure.

Figure C-1 shows the sum of squared simulation error for a steady-state calibration run initialized with zero-valued specific yields and K and R estimates from the previous USGS steady-state calibration. Most of the divergence occurred prior to any parameter adjustment at iteration 0, at which a sum of squared error in excess of 140,000 ft^2 was calculated. The problem of divergence therefore appeared to be related to the simulation component of the model rather than to the steepest-descent algorithm. The trend towards an

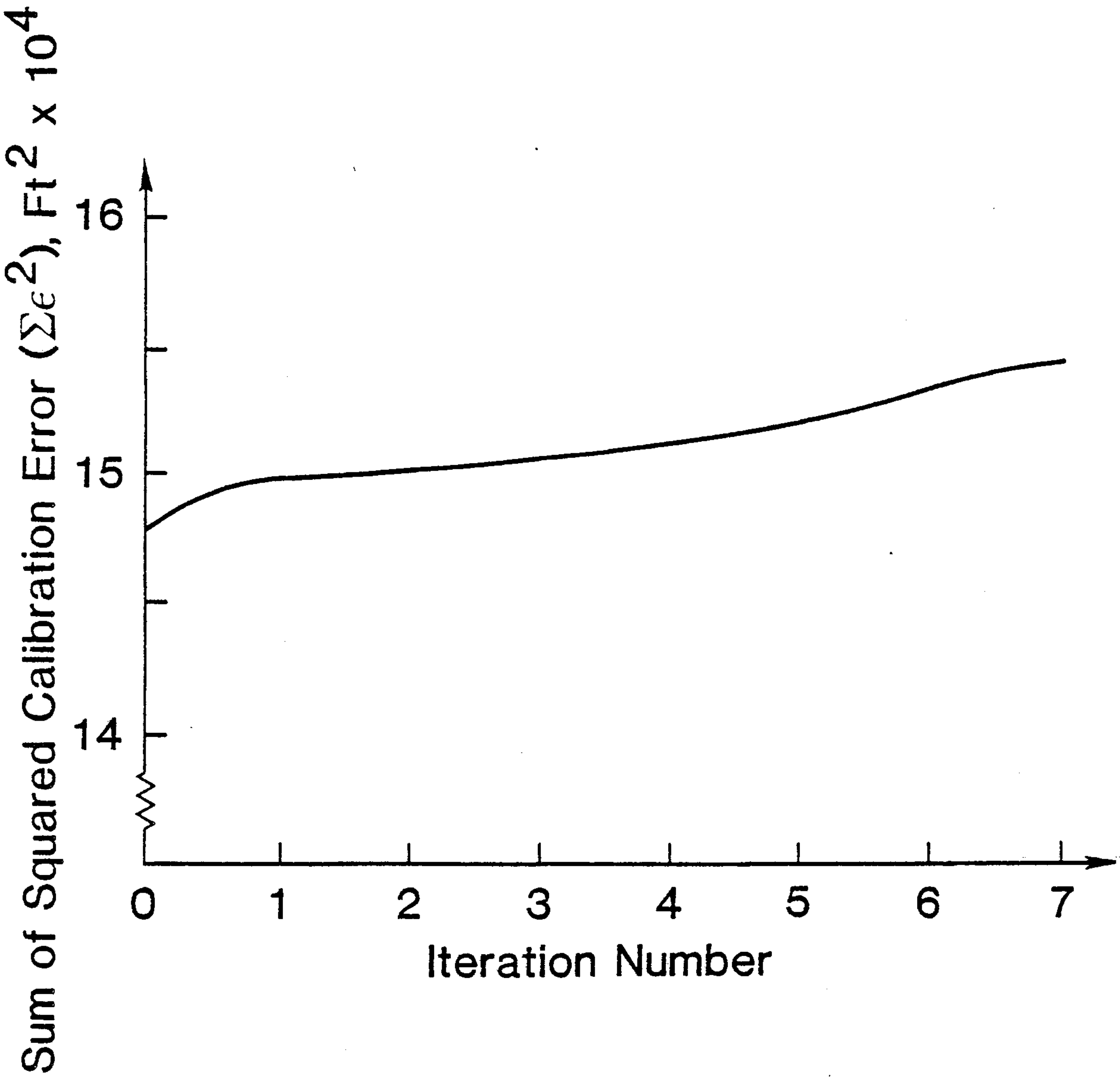

Figure C1. Sum of squared calibration errors vs iteration number for S_y = 0.0 using steepest-descent method.

increasing sum of squared error during subsequent adjustment iterations was actually quite weak, demonstrating that the parameter-adjustment technique did not significantly contribute to the diverging trend.

The mean simulation error obtained for the calibration attempt appeared to oscillate between positive and negative values, suggesting that the problem of overshooting was potentially responsible for the observed divergence. It was eventually recognized that the Gauss-Seidel iterative technique used to solve the flow equations during operation of the Texas model could not accommodate underrelaxation of the solution algorithm. Use of an underrelaxed iterative scheme would have effectively damped down the severe overshooting commonly associated with the large head changes that occur under forced steady-state conditions when S_y is chosen to be zero. The problem of overshooting was further reinforced by the nonlinear nature of the finite-difference flow equations. The requirement to input nonzero values of specific yield to the model raised some serious questions as to how these values of S_y would bias adjustments in conductivity and natural recharge estimates. If S_y had been allowed to vary simultaneously with K and R, the final head would probably not reflect steady-state conditions. It would have been possible to simulate after each adjustment iteration until steady-state conditions were attained, but this was considered unacceptable from a computational standpoint. The possibility of fixing S_y was considered, but this could have introduced bias into K and R. If S_y was underestimated, adjustments in K and R would have been excessive because simulated head would become more sensitive to these parameters. An attempt was made to use a generally-accepted value of 0.15 to fix S_y, but this apparently caused a large amount of adjustment in K and caused hydraulic conductivity to be set equal to its upper or lower constraints of 60 feet per day and 100 feet per day. The

S_y value of 0.15 was probably an underestimate of actual specific yield. Alternatively, when a larger specific yield of 0.20 was fixed, the system was able to absorb head errors before parameter adjustments were even performed, and K and R were scarcely changed. Attempts to increase the time increment in order to aid convergence to steady-state conditions were not successful.

It was considered infeasible to introduce underrelaxation to the iterative solution, since operation of the unmodified optimization model cost upwards of $40 per run on The University of Kansas Series 60 Honeywell computer system. It was eventually decided to use the unmodified version with nonzero values of S_y. S_y was initialized with a value of 0.15 and was allowed to vary simultaneously with K and R. The estimates of K and R from the previous USGS calibration were also used to initialize the model.

Maximum percentage changes in K, S_y, and R parameter values, or parameter search-vector lengths, were specified as 10%, 5%, and 10%, respectively. Choice of a relatively small specific yield search vector effectively prevented excessive changes in S_y during the calibration procedure and focused most of the adjustment on changes in K and R. Minimum and maximum permissible hydraulic conductivity was chosen to be 60 ft/day and 100 ft/day in an effort to retain the approximately-homogeneous characteristics of the alluvial aquifer. Minimum and maximum specific yield values were assumed to be 0.05 and 0.20, respectively. No bounding constraints were placed on natural areal recharge, since the actual recharge values are poorly-known and such limits would be ill-defined.

Independence of R with respect to K, which was implied during differentiation of the flow equation with respect to parameter values (see Appendix B), was assumed to be a valid approximation during steady-state calibration with the steepest-descent model. For the small values of R which were used to initialize the parameter identification algorithm, the assumption that R was only slightly influenced by K probably introduced a certain degree of error into the generated distribution of R.

Calibration Results:

After initializing the model with K and R values obtained from the previous USGS calibration and with a specific yield of 0.15, the steepest-descent algorithm was applied to the modified pre-development water table using 10 one-year iterations. Figure C-2 illustrates the change in the sum of squared calibration errors with respect to pre-development head for each iteration. The minimum sum of squared errors was attained at the seventh iteration, after which virtually no change in the sum was observed. This minimum sum of approximately 360 ft^2 was clearly an improvement over the final USGS sum of 21000 ft^2 obtained using the USGS model. However, it should be recognized that the sum of squared errors prior to any type of parameter adjustment was only 700 ft^2 (see Fig. C-2), compared to a sum of 21000 ft^2 obtained from the USGS model using the same K and R estimates. It was assumed that the use of a specific yield of 0.15, rather than an S_y value of 0.00 used for the USGS steady-state calibration, was primarily responsible for the discrepancy between the sum of squared error otained from the two models. The head distribution used to calculate the sum of 700 ft^2 was not in steady-state because of the use of a non-zero value of S_y, while the head used to calculate the 21000 ft^2 sum corresponded to steady-state conditions for which a specific yield of 0.00 had been assigned.

It was assumed that the value of 360 ft^2 for the final sum of squared error represented the minimum of the global sum of the squared error function over the K-S_y-R parameter space, since the steepest-descent procedure reduces

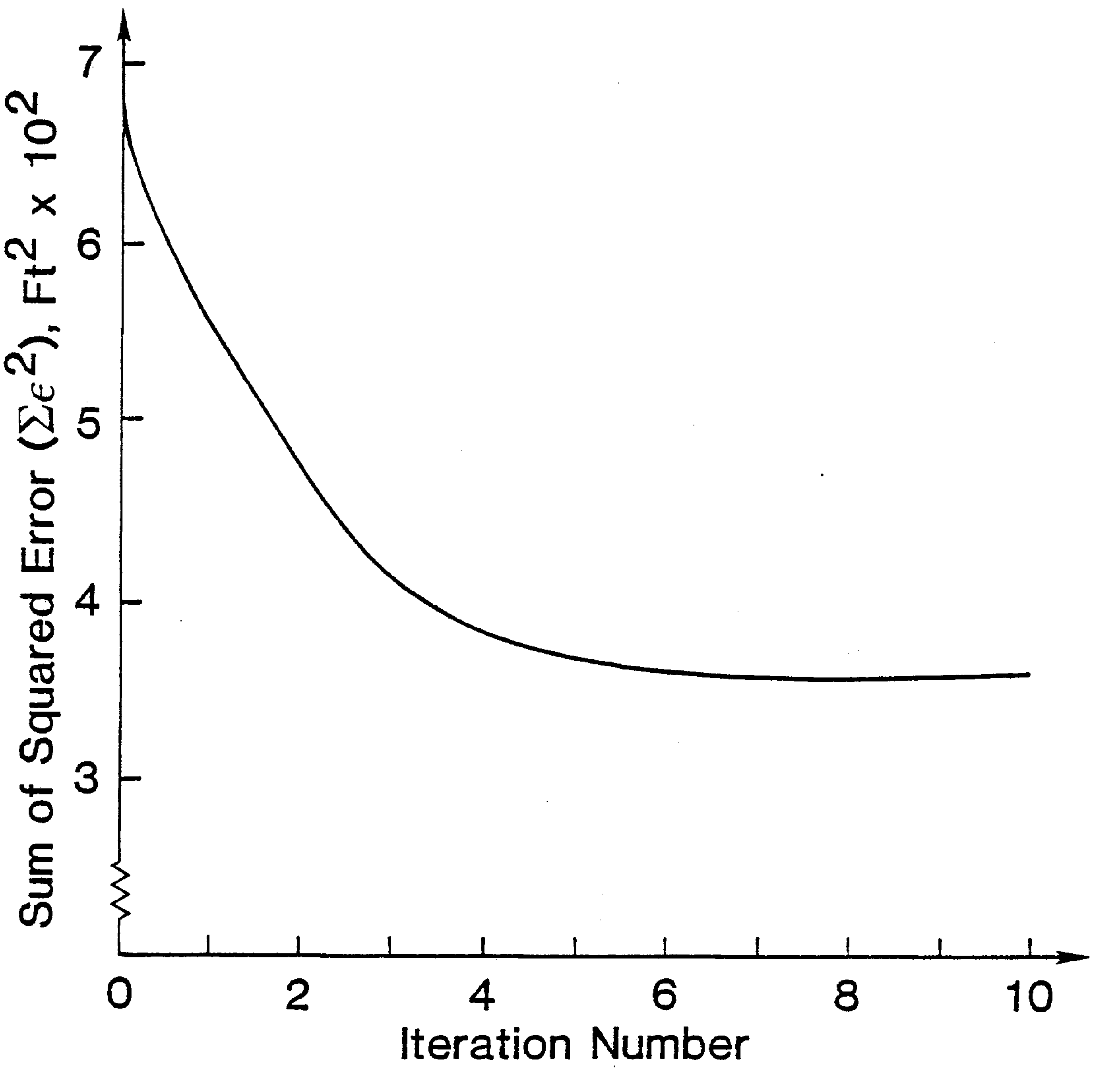

Figure C2. Sum of squared calibration errors vs iteration number for steepest-descent steady-state calibration.

to a nonlinear, least-squares optimization problem (Sorenson, 1980). Due to the inclusion of parameter constraints on K and S_y, this minimum may not actually be a global minimum, but may be viewed as a global minimum with respect to the defined feasible region in the parameter space.

The possibility that another, smaller minimum sum of squared error may have existed within the assigned feasible region was tested by initializing K at 65 feet per day and S_y at 0.10. Although the steepest-descent procedure required an almost doubled number of iterations to converge, the final sum of squares stabilized at 360 ft^2, implying that the final parameter set occurred at a global minimum within the defined feasible region.

The possibility that the final, simulated head distribution did not conform to true steady-state conditions was next considered. When the final values of simulated head and adjusted K, S_y, and R parameters were input back into the simulation component of the Texas model, the head distribution converged to a slightly different head distribution after 3 one-year time steps. Figure C-3 shows the change in the sum of squared simulation errors over time, where simulation error was defined relative to the 'steady-state' head obtained using non-zero specific yield values during the previous calibration. This new head distribution was at steady-state to within 0.01 feet.

Figure C-4 illustrates the frequency distribution of calibration errors for the regenerated steady-state head distribution, relative to the modified pre-development water table. Calibration of the model using the steepest-descent method resulted in a reduction of the average simulation error from 0.5 to 0.2 feet and a reduction of the standard deviation from 5.5 feet to 2.8 feet, as compared to the statistics of the USGS constant-head calibration. Simulation errors for the steepest-descent steady-state calibration roughly

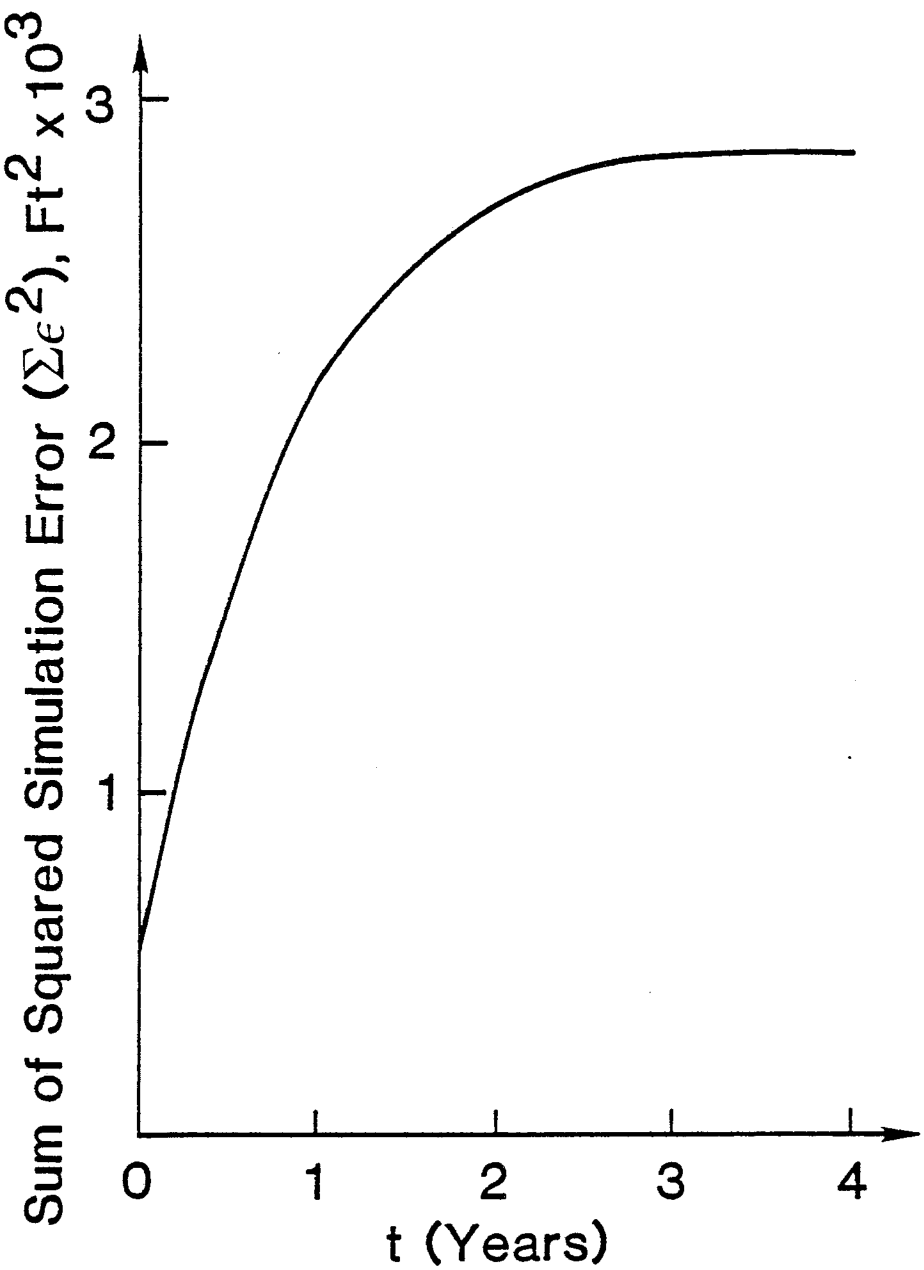

Figure C3. Sum of squared simulation errors vs time for steady-state convergence.

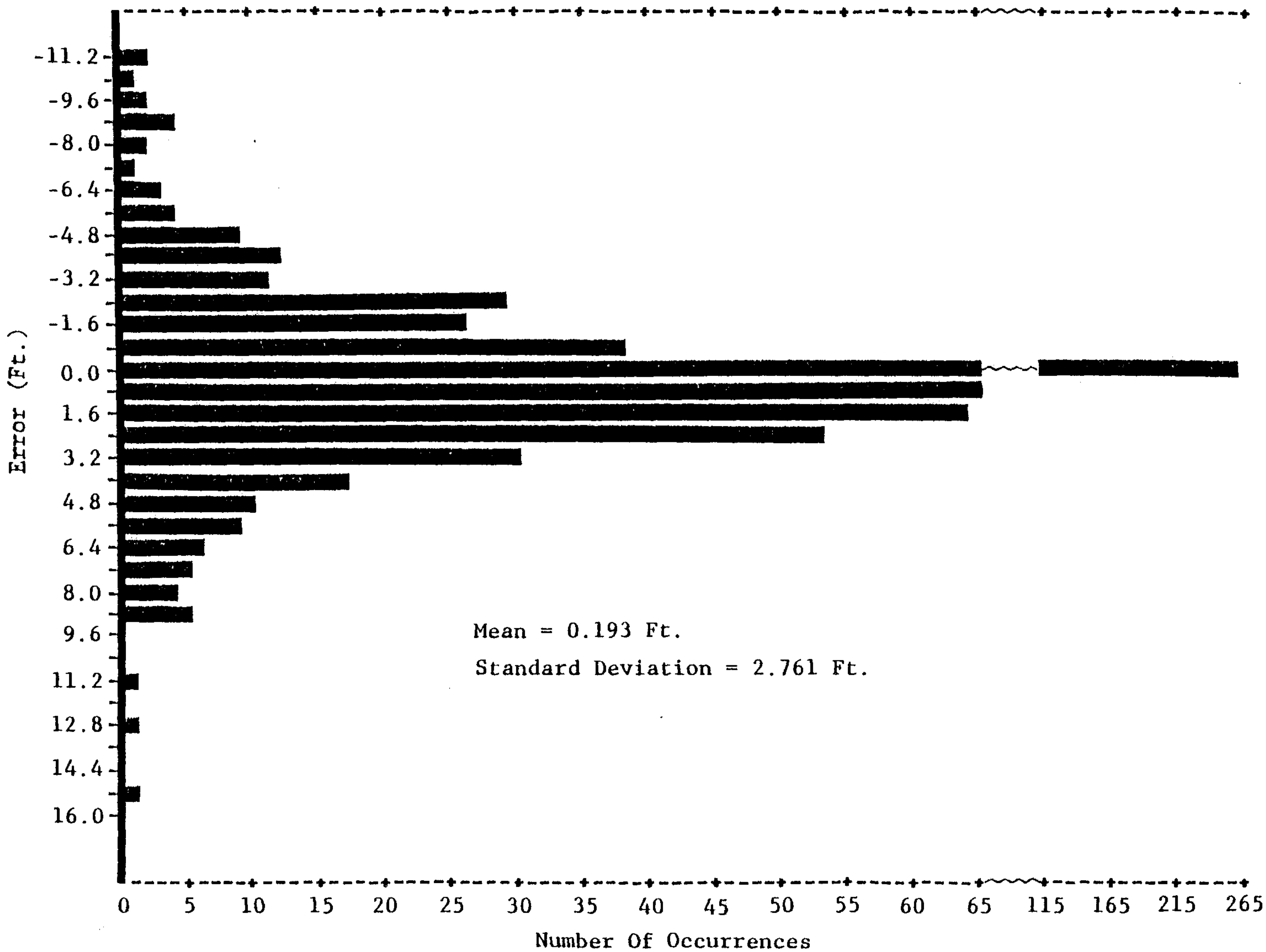

Figure C4. Frequency histogram of steepest-descent steady-state calibration errors.

ranged from -14.0 feet to 12.0 feet, compared to a range of -10.0 to 20.0 feet for the previous USGS calibration. The spatial distribution of error is shown in Figure C-5. Like the USGS distribution of error, most of the larger errors occurred in the southeastern and southwestern regions of the grid, presumably due to the severe reduction of large gradients in these areas during the grid coarsening procedure.

The final sum of squared error relative to pre-development head was reduced to 5100 ft^2, which amounted to a roughly 4-fold reduction in the sum of 21,000 ft^2 obtained from the USGS calibration. Further error reduction was prevented by bounding constraints on K of 60 and 100 feet per day and probably by the requirement for non-zero specific yields. The symmetry of the histogram with respect to zero drawdown implied that errors were randomly distributed about zero and could possibly be attributed to measurement error and to the random errors introduced by the head-averaging procedure used to coarsen the grid.

Note that the initial sum of squared error of 700 ft^2 obtained prior to any parameter adjustments was much smaller than the final sum of 5100 ft^2 obtained after adjustments were performed. However, the simulated head used to calculate the former sum was not in steady-state due to specification of nonzero specific yields, while the head used to calculate the latter sum described steady-state conditions. In an effort to prove that the sum of 700 ft^2 corresponded to transient conditions, a 25-year simulation was performed in the absence of aquifer stress to obtain steady-state convergence using a specific yield of 0.15 and the USGS K and R parameter sets which resulted in the initial squared error of 700 ft^2. Steady-state conditions were attained after 20 one-year time steps using an error closure of 0.01 feet. The sum of squared simulation error relative to the modified pre-development head

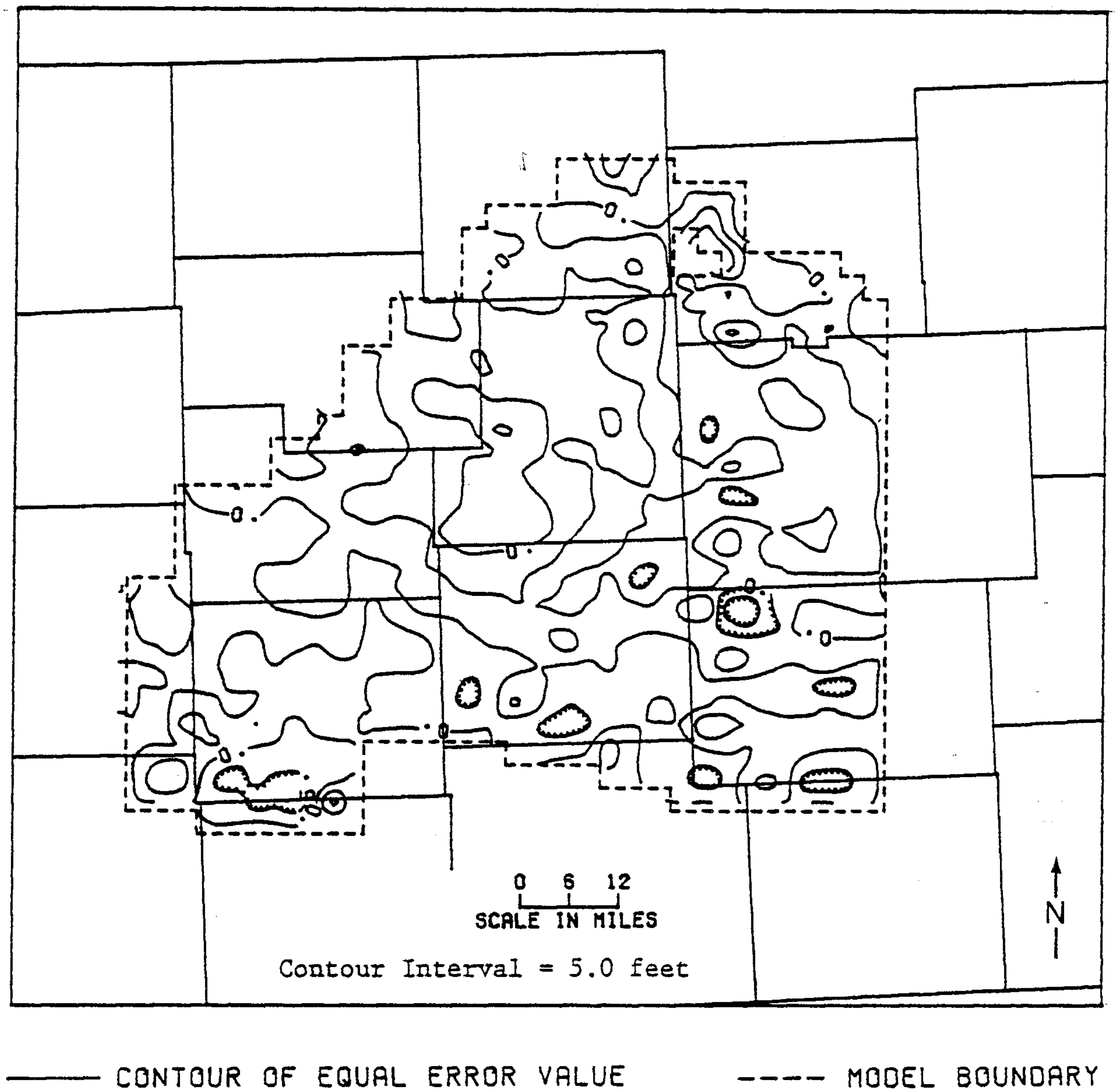

Figure C5. Spatial distribution of steepest-descent steady-state calibration errors (feet).

increased to 31,000 ft^2. The fact that this sum was not equal to the sum of 21,000 ft^2 obtained from the USGS steady-state model with equivalent K and R parameters and constant head river and boundary conditions was attributed to differences in the averaging procedures used to define average internodal aquifer properties.

Given that the steady-state squared error sum of 31,000 ft^2 obtained using undefined parameter sets was much larger than the steady-state sum of 5100 ft^2 obtained using the steepest-descent model, it is clear that the parameter-adjustment algorithm was effective in obtaining an improved steady-state distribution, despite the requirement to use nonzero specific yield estimates.

When the final steady-state head and the refined parameter distributions obtained from the steepest-descent model were input to the USGS finite-difference model, the head which was regenerated diverged from the input head distribution. Assuming that deviations were equal to the difference between the steady-state head produced by the optimization algorithm and the USGS regenerated head, a sum of squared deviations in excess of 100,000 ft^2 was calculated.

It was believed that such excessive divergence of head could be primarily attributed to the differences in averaging methods for T and saturated thickness which were used by the two models. While the USGS model defines internodal transmissivity as the harmonic mean of adjacent nodal transmissivities, weighted for distance, the Texas model defines average internodal hydraulic conductivity using an arithmetic average of K at adjacent nodes. Furthermore, saturated thickness at any given node was averaged spatially and temporally in the Texas mode, but was defined as the saturated thickness during the preceding iteration at the node in the USGS model.

Figure C-6 depicts the adjusted hydraulic conductivity distribution for the steady-state calibration performed using the Texas model. There was an overall tendency for K to decrease from the initial estimate of 85 feet per day. Areas within the hatchured contours represent regions of the aquifer with hydraulic conductivities of between 60 and 70 feet per day. The smoothing operation which was required to produce a continuous mapping tended to reduce larger conductivities of up to 100 feet per day which occurred along the principal stream valleys, where the desposits are younger and less compacted. This distribution was later averaged with K distributions obtained during transient calibration, and then smoothed over space to reflect more realistic field conditions. Matrix Listing #1 in Appendix E contains the adjusted conductivity estimates used to perform the mapping. The adjusted natural recharge was also smoothed for mapping purposes and is shown in Figure C-7, while final recharge estimates are documented in Matrix Listing #2, Appendix E.

Figure C-8 illustrates the steady-state water table obtained from the parameter-adjustment procedure. Comparison with the superimposed modified pre-development water table shows that the regional properties of the steady-state flow regime were reproduced accurately during the steepest-descent calibration.

Transient Calibrations

Transient calibrations were performed for the 1955, 1960, and 1965 water tables. The 1970 and 1975 head distributions were retained for purposes of indirectly validating the calibrated model through use of the consumptive-use correction factor α which was previously described in the section concerning trial-and-error calibration with the USGS model.

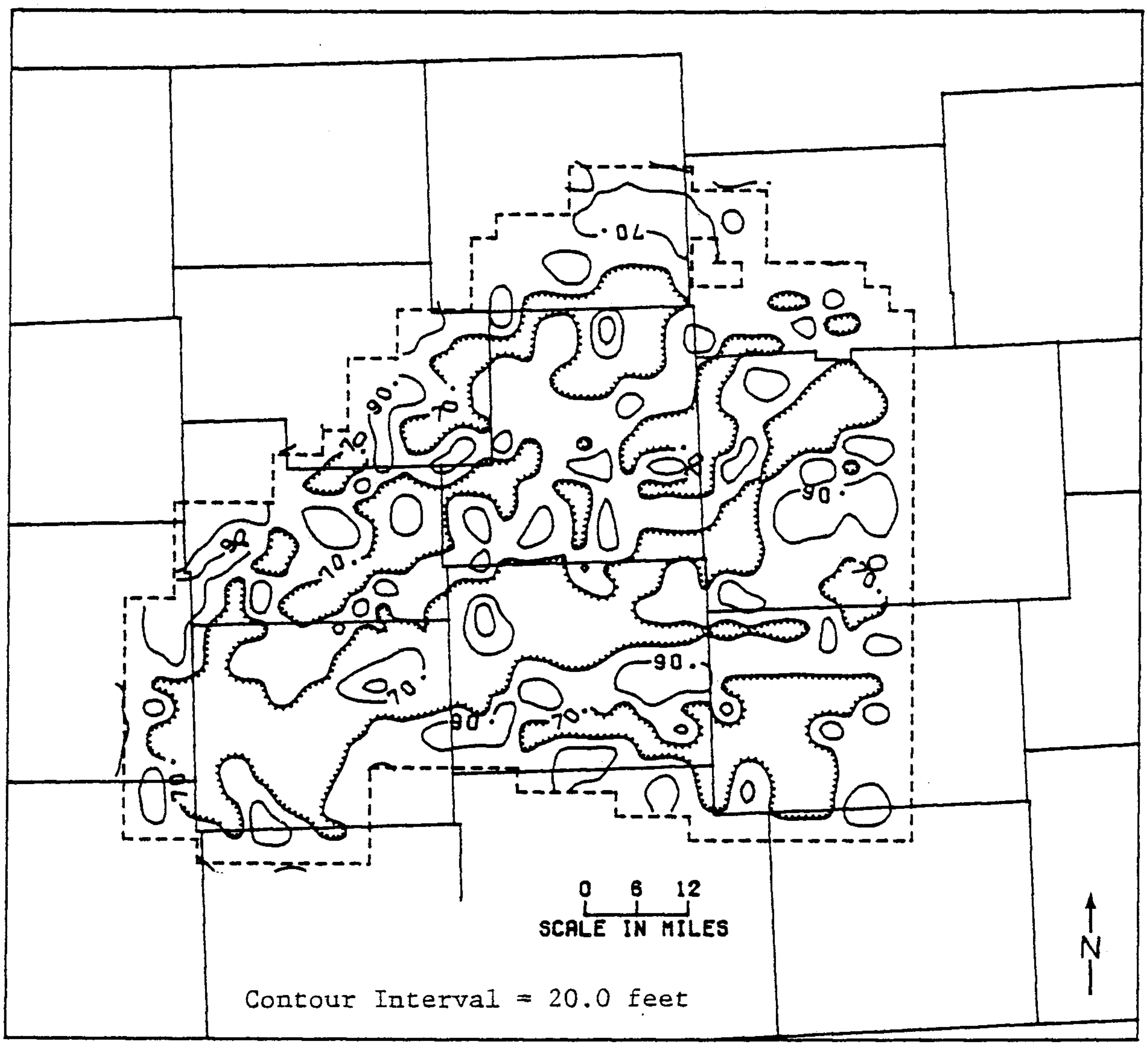

——— CONTOUR OF EQUAL CONDUCTIVITY ---- MODEL BOUNDARY

Figure C6. Distributed hydraulic conductivity estimates from steepest-descent steady-state calibration (feet/day).

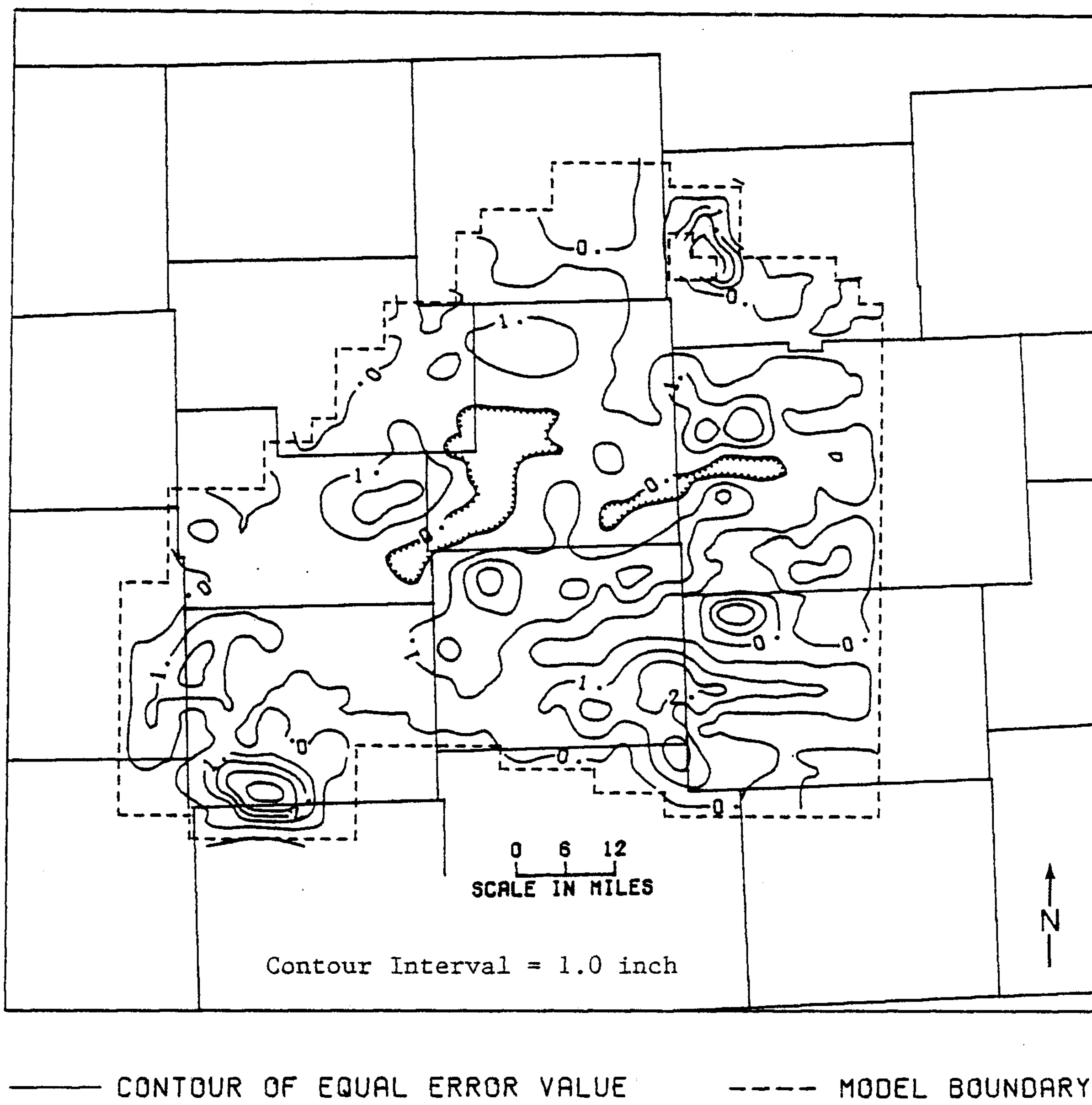

Figure C7. Distributed natural recharge estimated from steepest-desent steady-state calibration (inches/year).

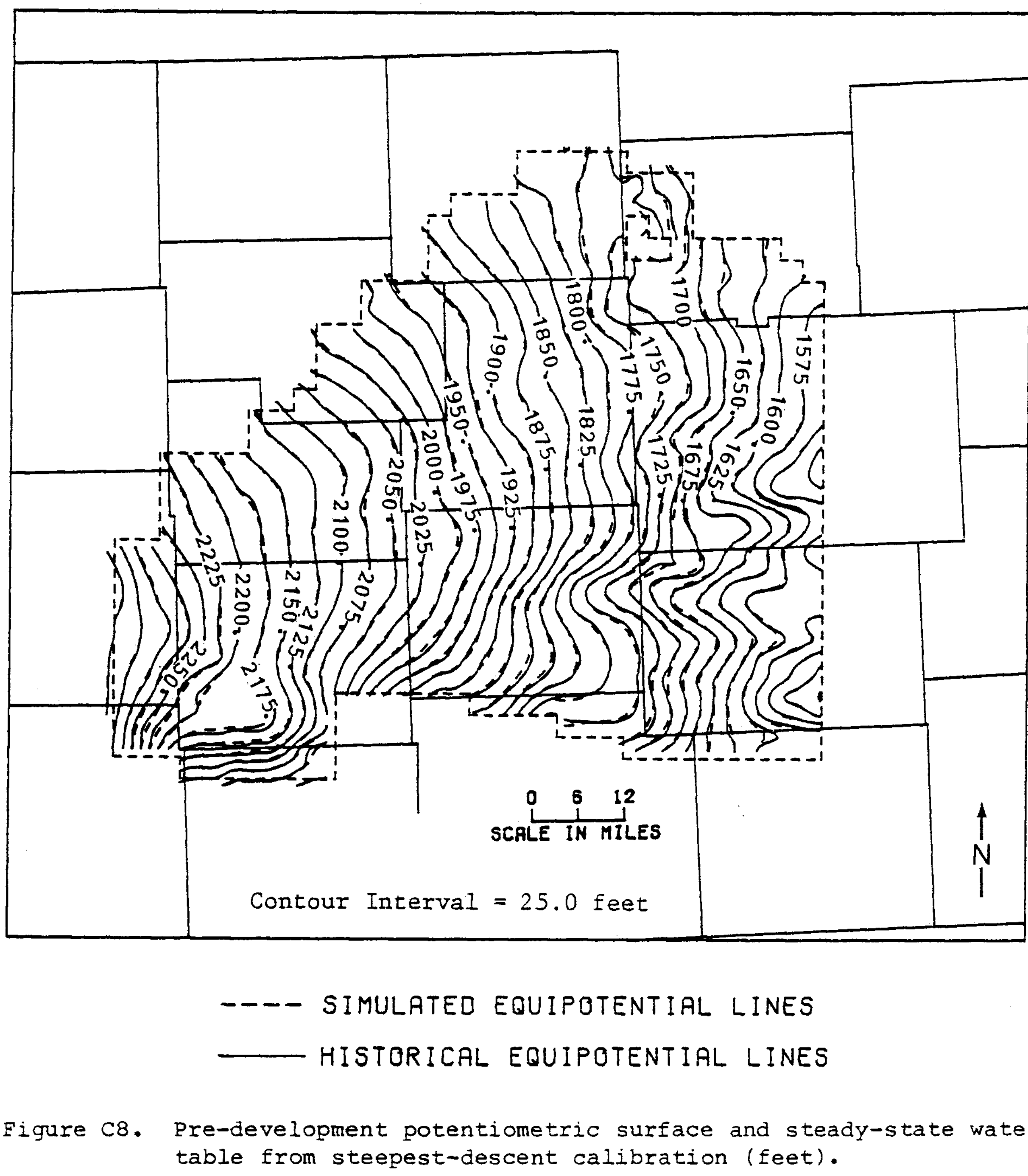

Figure C8. Pre-development potentiometric surface and steady-state water table from steepest-descent calibration (feet).

Initial values of K, S_y, and W, where W represents the sum of natural recharge and irrigation withdrawals, as well as maximum search-vector lengths and limiting parameter or variable bounds, were held constant for all transient calibration runs. The use of equivalent parameter-adjustment indices effectively ensured that the K, S_y, and R parameter sets obtained during the steepest-descent calibration procedure would be similar in nature, and would describe approximately time-invariant system characteristics. Modified 1955, 1960, and 1965 historical water tables discussed in the main report were used to perform the transient calibrations, which involved variation in K, S_y, and net recharge W.

Calibration Errors:

Figures C-9 to C-11 show the sum of squared error versus interation number for calibration against the 1955, 1960, and 1965 head data. In all cases, the sum of squared calibration error decreased with iteration number, indicating that the steepest-descent algorithm was effective in reducing discrepancies between the modified historical head and the simulated transient head distributions.

The final sum of squared error for the three calibrations was consistently between 400 and 500 ft^2. Examination of model output showed that K and S_y upper or lower limits were reached sometime during the sixth adjustment iteration. Due to the fact that adjustments in total net recharge W were terminated as soon as constraints on K or S_y were encountered, no further variation in the sum of squared calibration error was observed after the sixth iteration.

The distribution of calibration error over the study area for the three calibrations is shown in Figures C-12 to C-14. Many of the larger errors

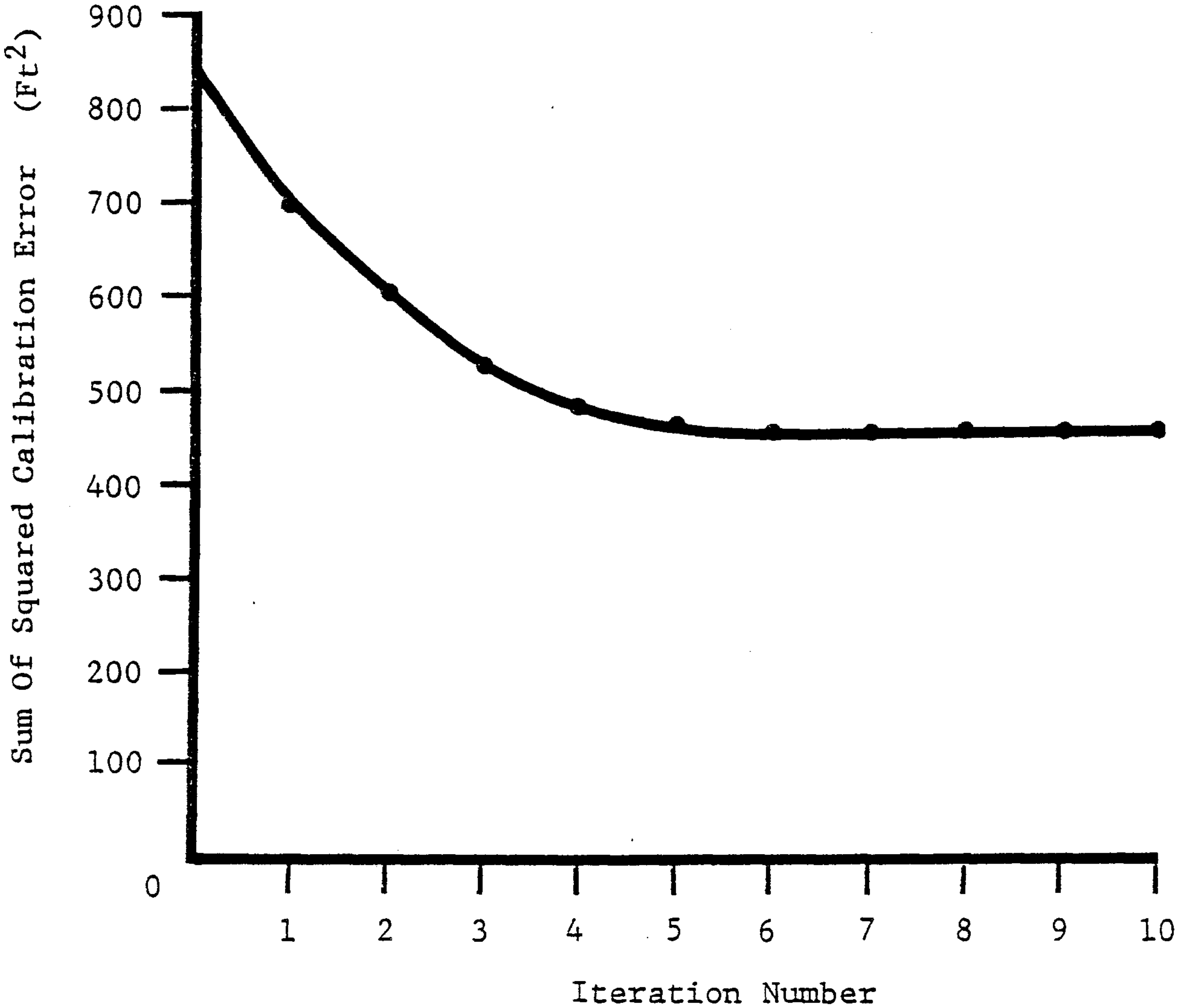

Figure C9. Sum of squared calibration errors vs. iteration number -- 1955.

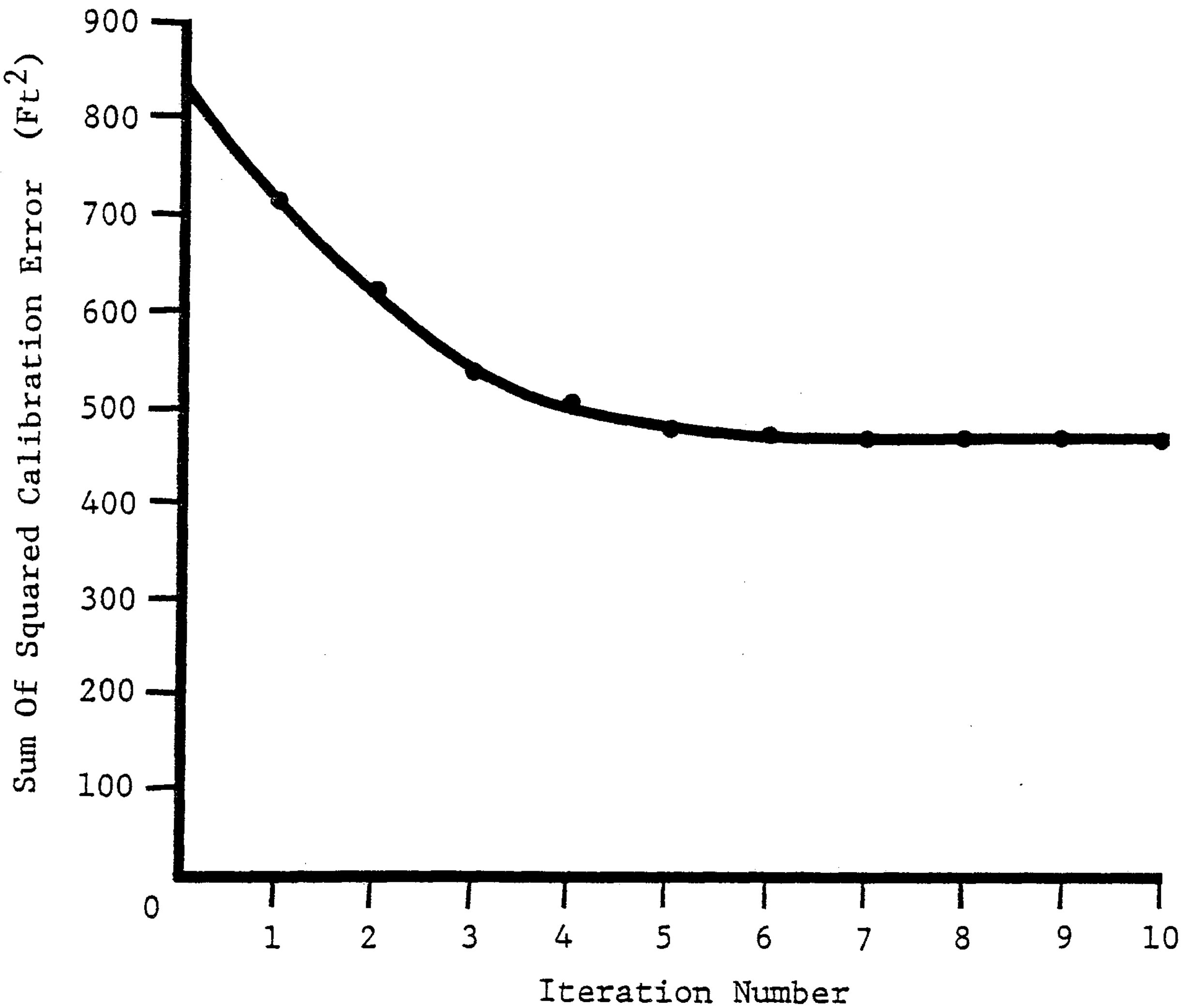

Figure C10. Sum of squared calibration errors vs. iteration number -- 1960.

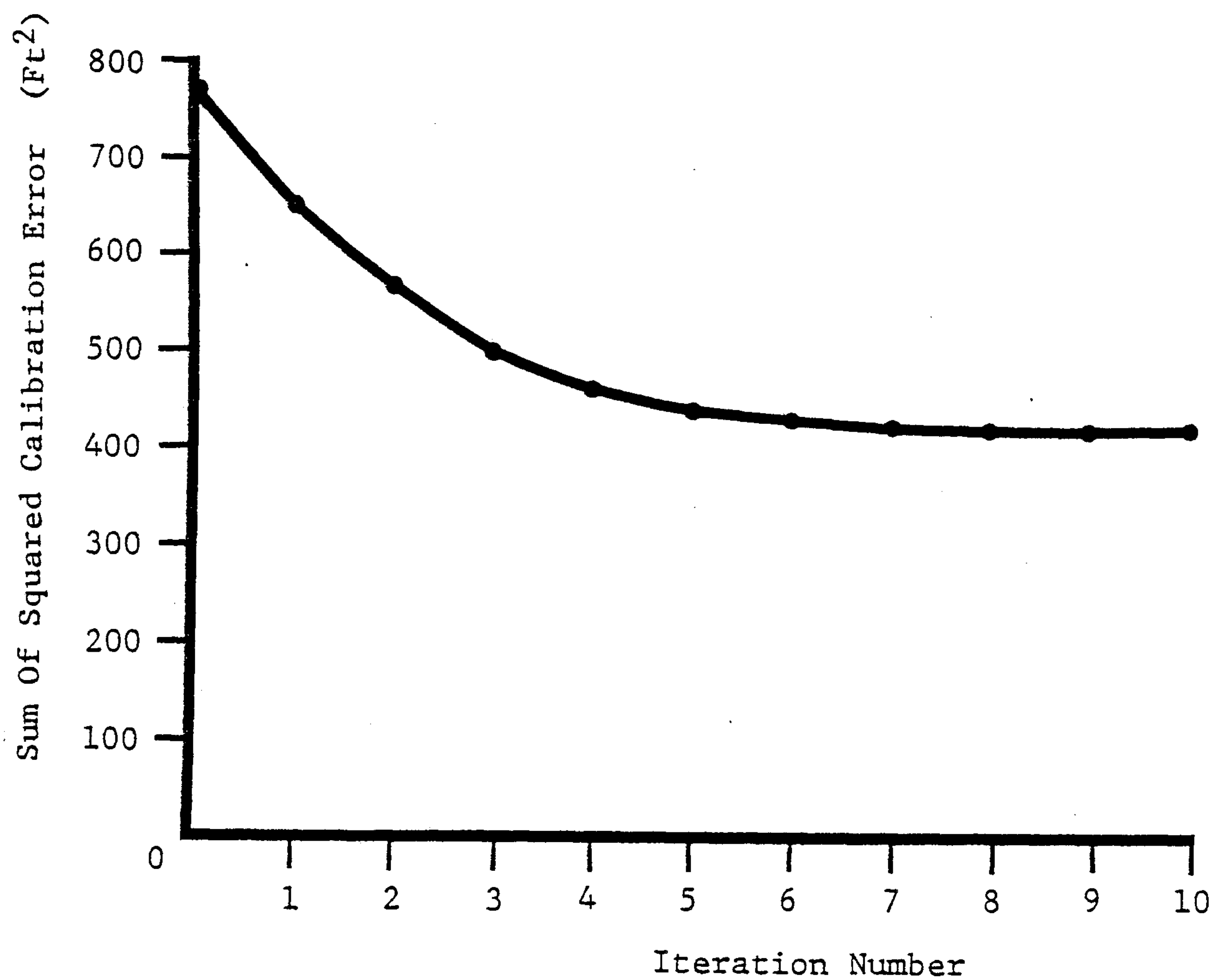

Figure C11. Sum of squared calibration errors vs. iteration number -- 1965.

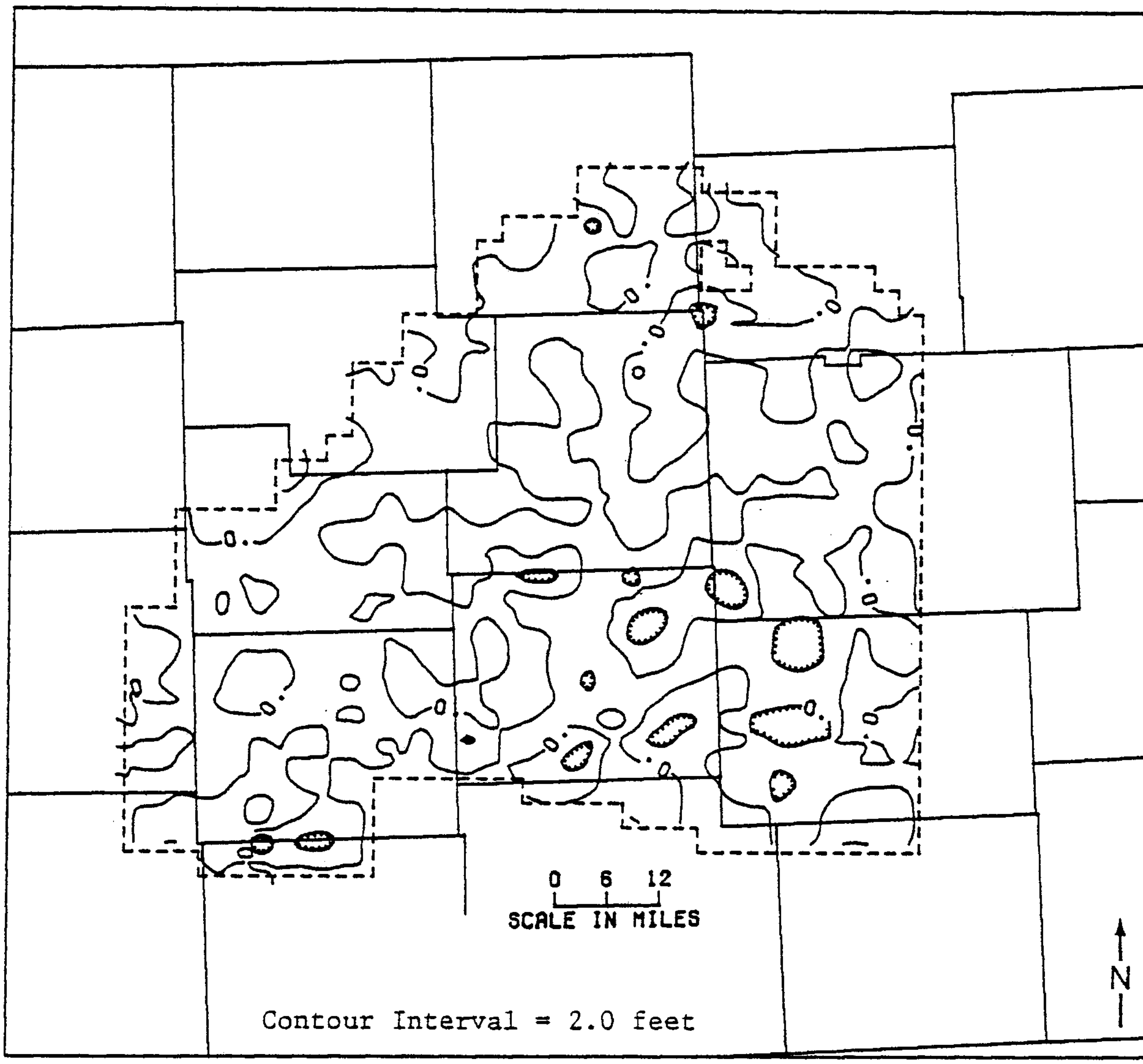

—— CONTOUR OF EQUAL ERROR VALUE ---- MODEL BOUNDARY

⊥⊥⊥⊥ Contour value less than or equal to zero

Figure C12. Spatial distribution of 1955 steepest-descent calibration error (feet).

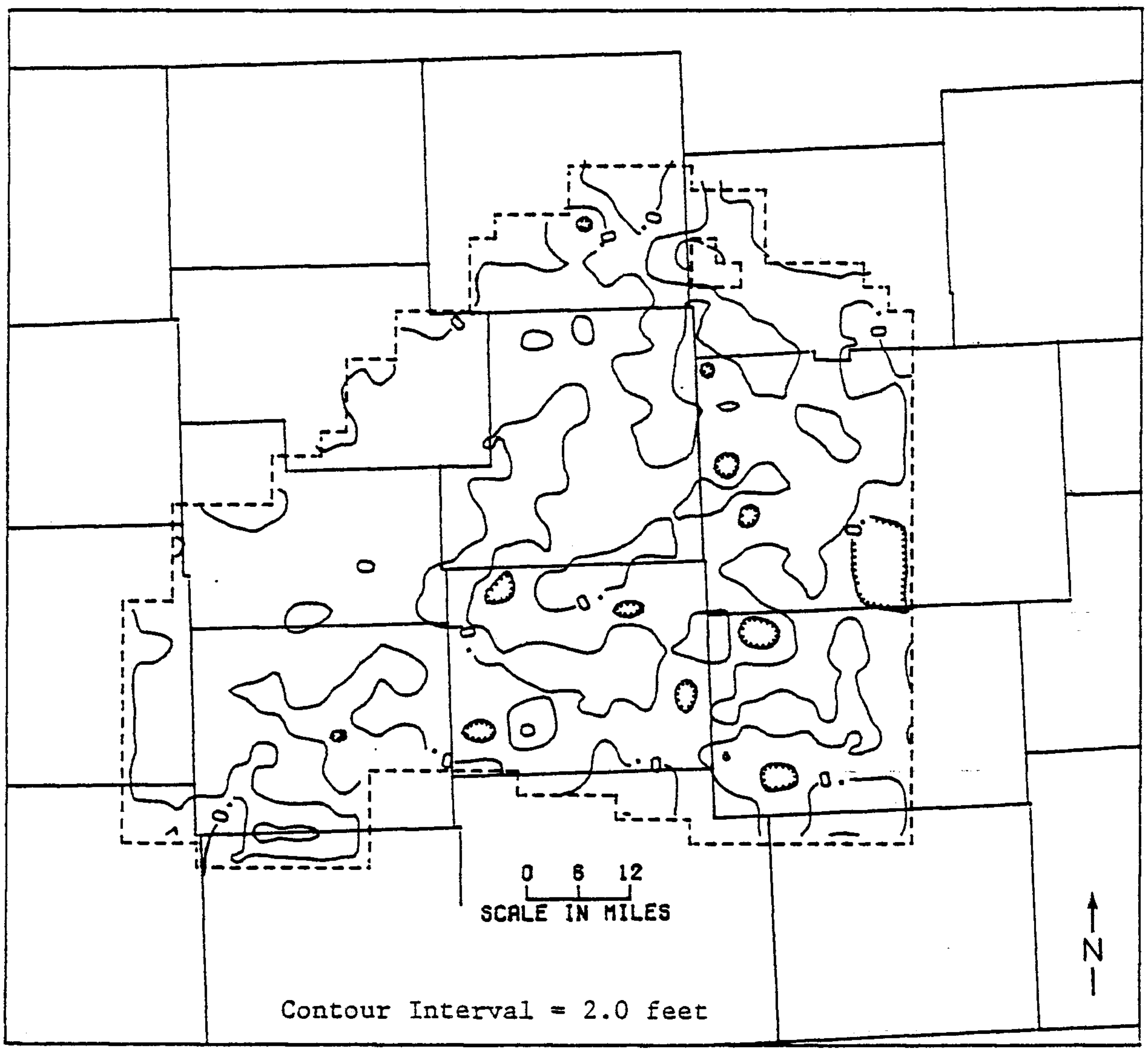

CONTOUR OF EQUAL ERROR VALUE ---- MODEL BOUNDARY

Contour value less than or equal to zero

Figure C13. Spatial distribution of 1960 steepest-descent calibration error (feet).

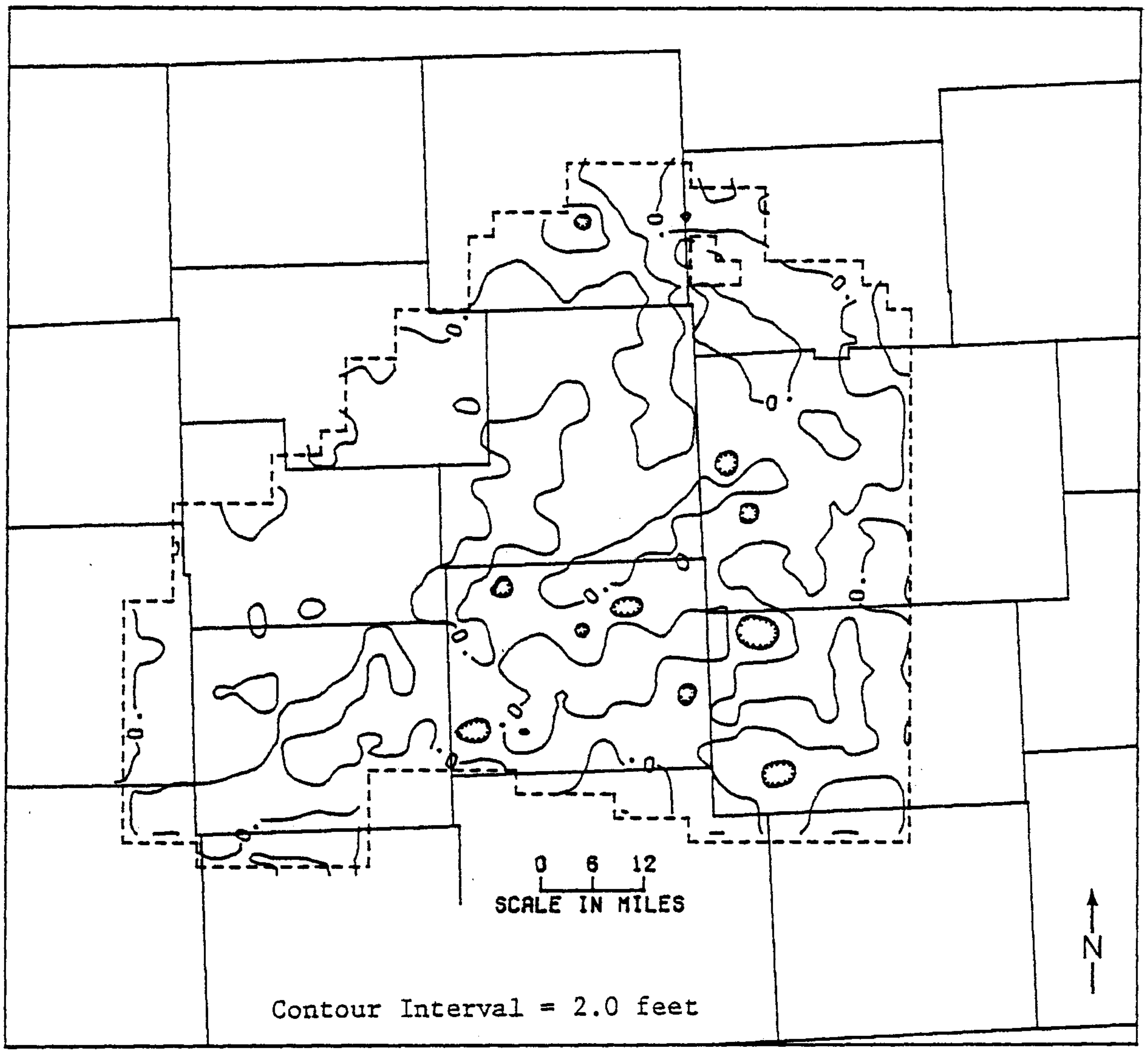

——— CONTOUR OF EQUAL ERROR VALUE ---- MODEL BOUNDARY

Contour value less than or equal to zero

Figure C14. Spatial distribution of 1965 steepest-descent calibration error (feet).

occurred in the vicinity of the assigned river nodes, suggesting that improper placement of rivers within the study area may have adversely affected the calibration procedure. The assigned river nodes, which were treated as constant-head nodes of infinite storage for each stationary calibration procedure, may actually have been misplaced in areas of finite storage. In addition, errors due to the limitations of using a coarse grid to simulate steep, local hydraulic gradients to the southeast and southwest appeared to persist.

Calibration for Hydraulic Conductivity:

An initial, uniform hydraulic conductivity of 85 ft/day was assigned to each calibration. This value represented the optimal conductivity obtained during the USGS trial-and-error steady-state calibration. Conductivity was allowed to vary by 10% during each adjustment iteration, and was constrained to be greater than 60 ft/day and less than 100 ft/day. Since it was assumed that conductivity is a time-invariant aquifer parameter, the three final K parameter sets obtained from the 1955, 1960, and 1965 head data sets were averaged with the K distribution shown in Figure C-6, then smoothed with respect to space by averaging the K value at each node with non-zero conductivity at eight surrounding nodes. Figure C-15 shows the final, smoothed conductivity distribution later used to simulate aquifer response. These values are shown in Matrix Listing #3, Appendix E.

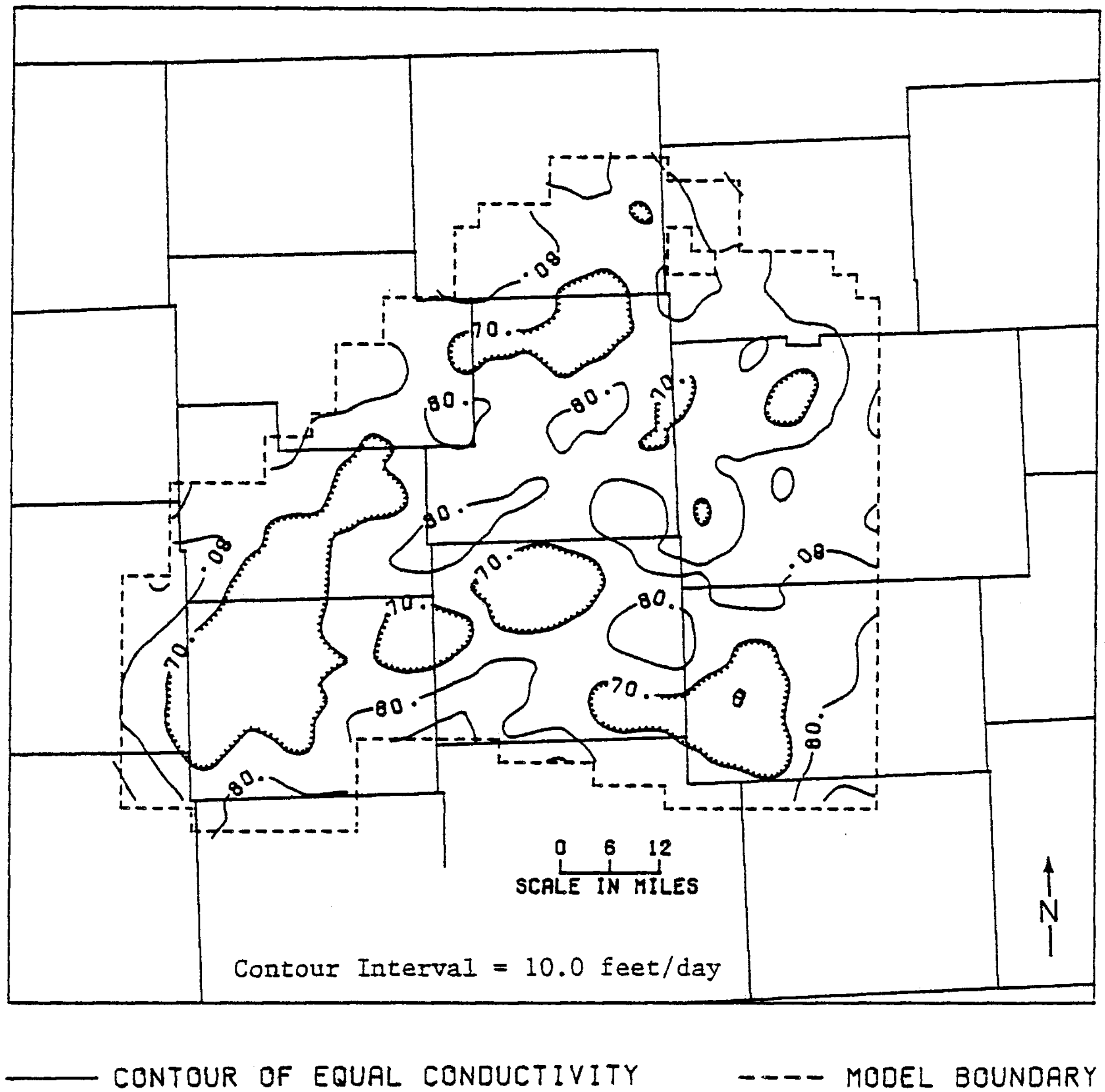

Figure C15. Time- and space-averaged hydraulic conductivity estimates from transient calibrations (feet/day).

Calibration for Specific Yield:

As mentioned previously, development of the alluvial aquifer has not appeared to have introduced significant transient effects into the Great Bend aquifer flow regime. Thus, any specific yield values determined during the course of calibration against the 1955, 1960, and 1965 water tables were potentially meaningless in the context of the governing steady-state conditions.

This meaninglessness is related to the fact that, in the limiting case of steady-state conditions, head levels are completely insensitive to actual values of S_y assigned to the aquifer. This is reflected by the fact that, for a situation in which no change in head occurs in the aquifer, the definition of specific yield as a ratio of withdrawal volume to aquifer-dewatered volume becomes undefined because aquifer-dewatered volume is zero. Thus, any set of S_y values could be used to describe the system, since the error of the S_y estimate is theoretically infinite. Thus, steady-state water levels cannot be used to identify unique sets of specific yield estimates. The indeterminate nature of S_y for steady-state conditions, when $\partial h/\partial t = 0$, is predicted by equation (1).

For the nearly steady-state conditions which appear to have prevailed during the development period, it is clear that a very large standard error of estimate would be associated with each S_y parameter obtained from the steepest-descent model. The great insensitivity of the slightly-perturbed transient head data to S_y must therefore be kept in mind if the values of specific yield published in this report are to be used to predict aquifer response under the more pronounced transient conditions expected in future years.

All calibrations were initialized with a uniform specific yield of 0.15, which was assumed to be a representative value for the unconfined, unconsolidated Great Bend alluvial aquifer. Figure C-16 shows the averaged, smoothed specific yield distribution obtained from the three transient calibrations. Nodal values of average specific yield are given in Matrix Listing #4, Appendix E.

Calibration for W:

Due to the uncertainty associated with rates of groundwater withdrawal Q and natural recharge R, both sets of parameters were collectively adjusted through adjustment of total net recharge W. The R matrix from the USGS steady-state calibration was used to initialize the natural recharge variable, while modifications of reported pumpage rates were used to initialize Q. The total recharge-discharge parameter W was allowed to vary by 10% during each adjustment iteration, with no specified limits on the possible values of W, since such limits are not known with any certainty.

Unmodified reported pumpages Q were distributed over all interior nodes and then added to the corresponding nodal natural recharge rates. Resolution of adjusted W into R and Q was performed after the final W parameter set was obtained by assigning all positive W values to R and all negative W values to Q. R distributions from all calibrations were averaged for later use during the verification stage (see Fig. C-17). Averaged precipitation values at each node are given in Matrix Listing #5, Appendix E. The adjusted pumpages obtained after decomposition of W are listed in Appendix E.

Differences between input pumpage Q and pumpage obtained after decomposition of W were used to define a relation between the irrigation

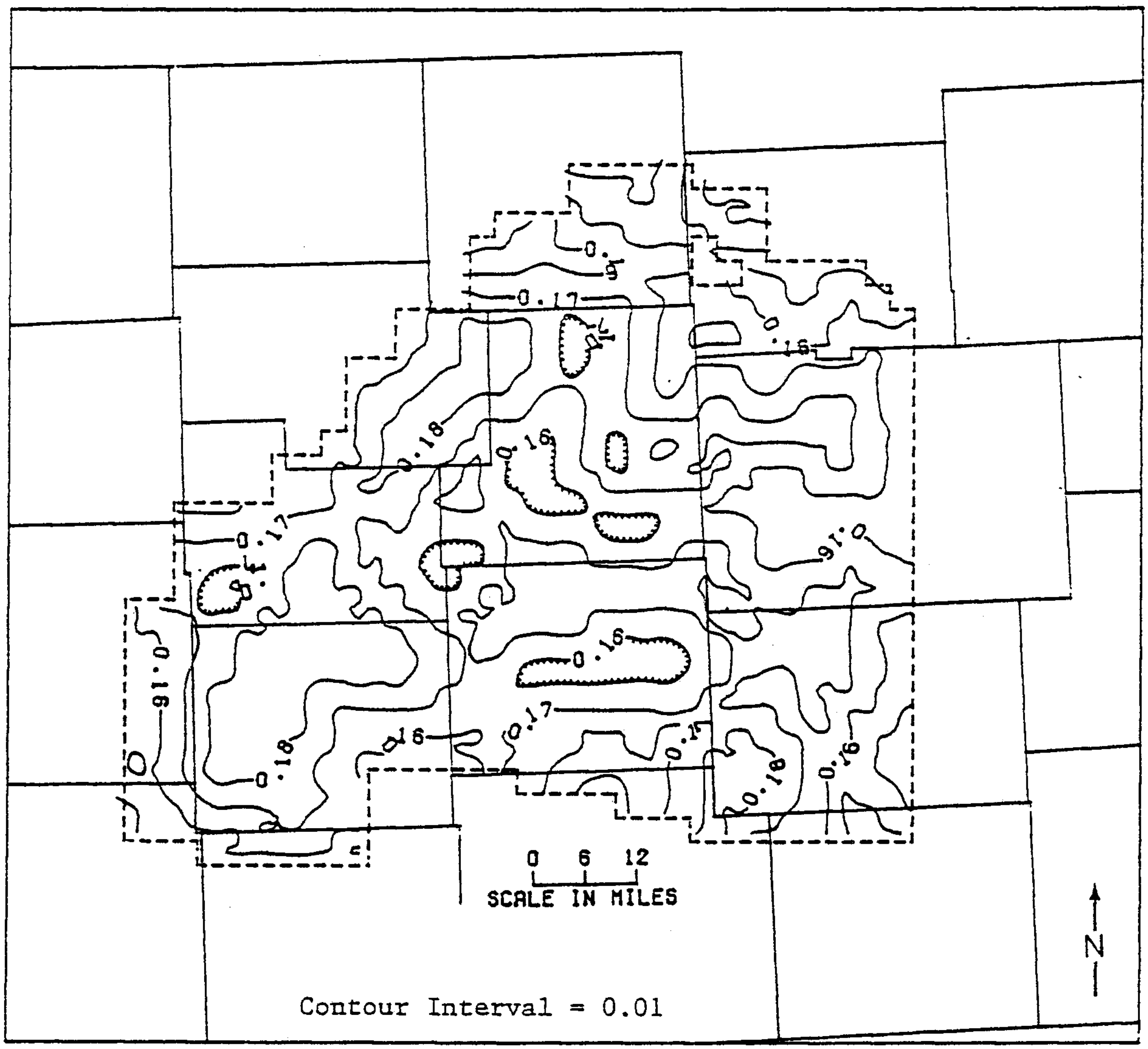

—— CONTOUR OF SPECIFIC YIELD ---- MODEL BOUNDARY

Figure C16. Time- and space-averaged specific yield estimates from transient calibrations.

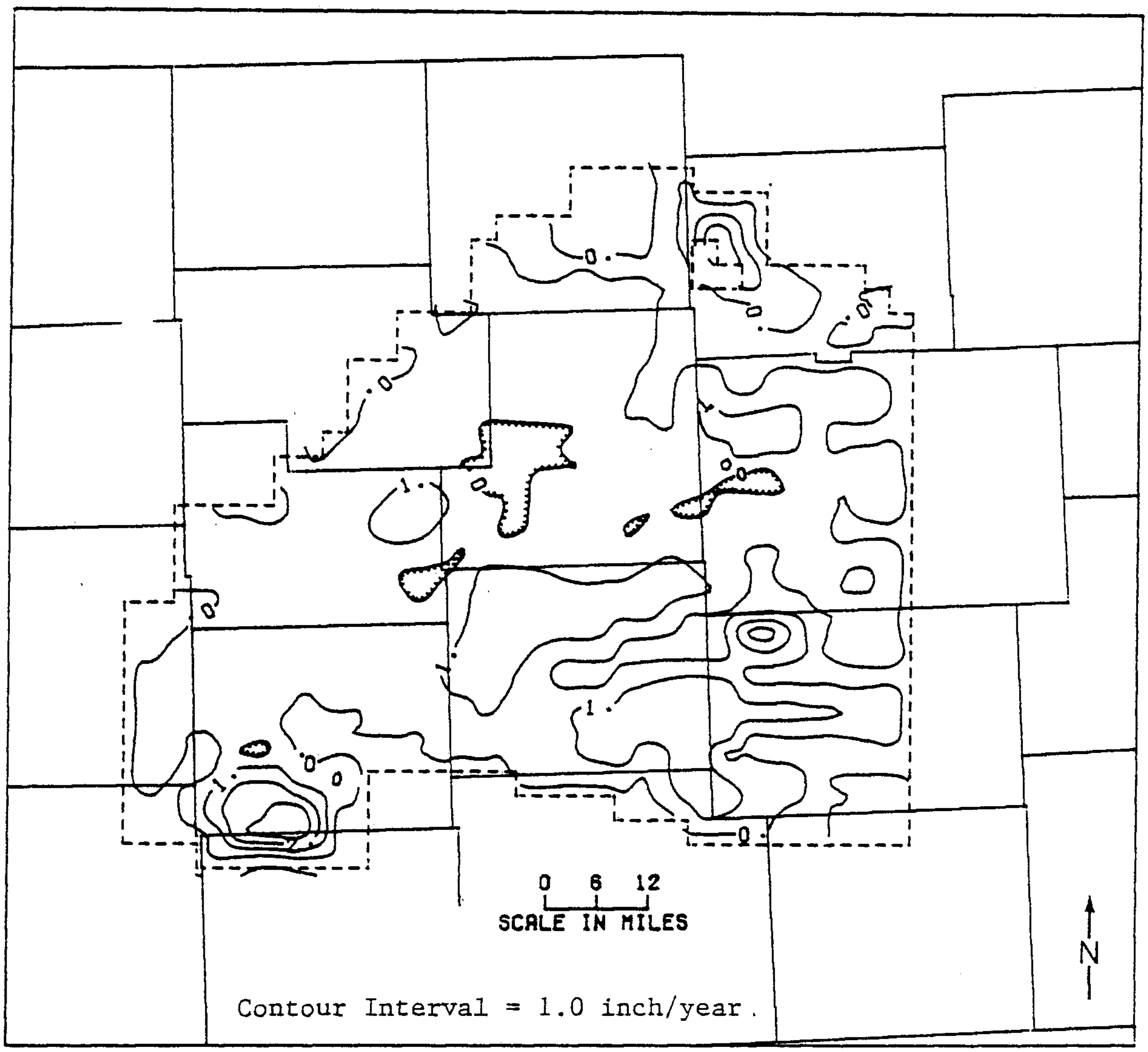

——— CONTOUR OF EQUAL RECHARGE ---- MODEL BOUNDARY

Figure C17. Time- and space-averaged natural recharge estimates from transient calibrations (inches/year).

consumptive-use correction factor α and reported pumpages. α was defined to be the ratio of the adjusted pumpage rate to the pumpage rate assumed prior to adjustment, and represented a correction factor for the withdrawn groundwater which was effectively removed from the aquifer through evaportanspiration. A strong linear relation between α and reported Q was observed when calibration was performed against the 1955, 1960, and 1965 head data (see Fig. C-18). The correlation coefficient for the α vs. annual pumpage relation was calculated to be 0.99. The standard error of estimate for α was determined to be about 0.01. Of course, it should be noted that the regression was performed only on the basis of 3 data sets. Despite this drawback, and for lack of any better information, the regression line was assumed to represent a reasonable relationship between α and reported pumpage rates. It was assumed that the value of α did not assymptotically approach a value of 1.0 within the range of pumping rates observed during the development period. The direct relation between α and the reported pumpage rate is somewhat physically-based, since it predicts that increases in irrigation applications would cause greater consumptive use due to evaporation from accumulating irrigation pondage. No attempt was made to relate changes in α with respect to time to temporal variations in climatic conditions or cropping patterns. Extension of the line to zero reported pumpage is, of course, physically meaningless. α values for the 1970 and 1975 reported pumpage rates were read from the line and were later used as input to a 25-year validation run. It was believed that prediction of α values constituted a reasonable verification methodology for conditions of negligible drawdown.

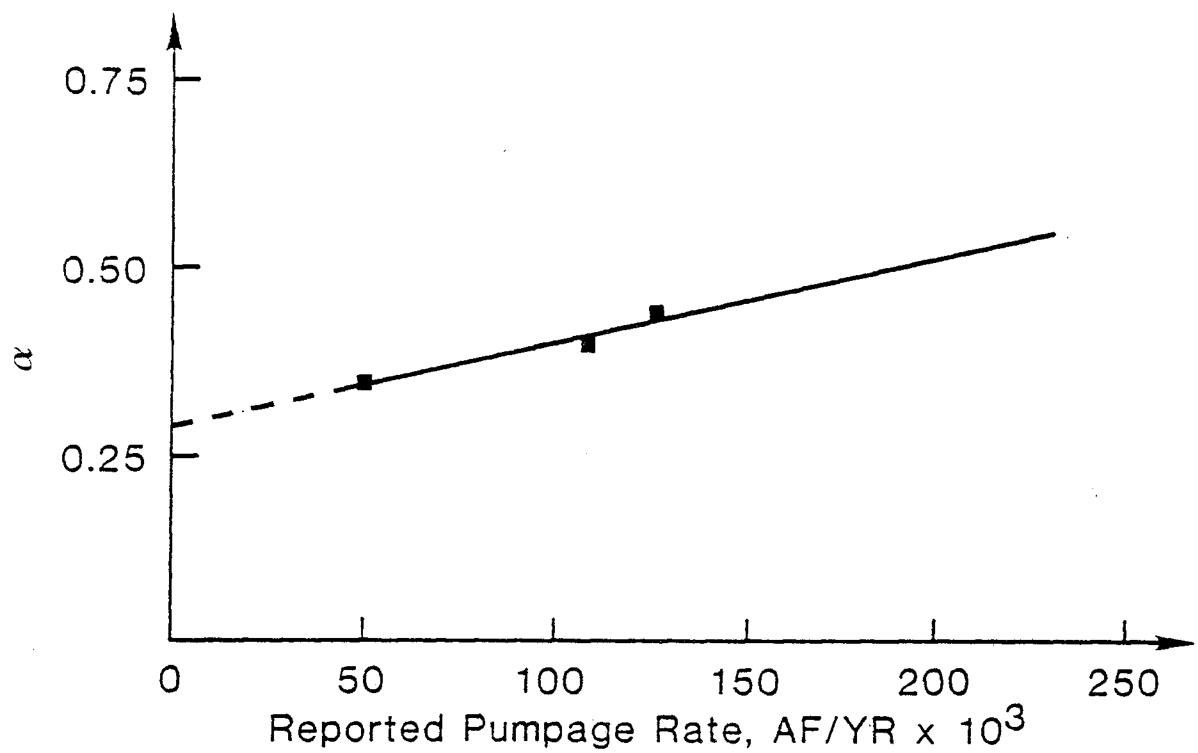

Figure C18. α vs. reported pumping rate.

Model Validation

Under the steady-state conditions which appear to prevail over the Great Bend alluvial aquifer, formal model validation could not be performed. Validation essentially involves testing the model under conditions which differ from the conditions used to calibrate the model. Although well withdrawal rates appear to have been increasing with respect to time (see Table 5), these rates still represented negligible stresses on the aquifer flow regime. Thus, formal model verification will need to be performed at some later date, when pumping stresses begin to have a measurable effect on hydraulic head.

The averaged K and R distributions illustrated in Figures C-6 and C-7, as well as an averaged version of the calibrated specific yield distributions obtained from transient calibrations, were used to simulate flow over a 25-year period extending from 1950 to 1975 using five-year pumping periods. The consumptive-use correction factor α was implicitly incorporated into the calibrated Q sets for the 1950 to 1965 simulation period, with α values of 0.50 and 0.60 predicted from Figure C-18 for the 1965-1970 and 1970-1975 pumping periods. The original, reported set of pumpages was assigned to Q for these periods and was explicitly adjusted for consumptive use by the projected α values during the simulation. Head was initialized at the head obtained from the steady-state optimization calibration after it was regenerated to remove transient perturbations introduced by the use of non-zero specific yields (see Fig. C-8). A time-step of one year was used during the simulation procedure.

The constant-gradient, variable-flux algorithm outlined in previous sections was initialized by performing nodal mass-balances at the boundaries and rivers using the generated steady-state head shown in Figure C-8.

Updating of boundary and river fluxes was performed every year, but due to the roughly steady-state conditions which prevailed during the development period, little change in these fluxes was actually observed during the 25-year simulation.

Figure C-19 shows the sum of squared simulation error over the 25-year validation period. The results of several numerical experiments indicated that these squared error sums were insensitive to whether smoothed versions of the parameter sets or unsmoothed parameter distributions were used.

The spatial distributions of simulation errors for each 5-year pumping period are illustrated in Figures C-20 to C-24. Very large simulation errors tended to occur near the boundaries, where constant-head conditions were assigned for each stationary calibration procedure. These errors were probably caused by misplacement of constant-head, infinite-storage nodes in areas which are characterized by finite storage.

The fact that simulation errors were so much larger than previous calibration errors leads to the conclusion that the generated steady-state head levels used to initialize the simulation and the transient head levels could not be related through time in any meaningful way. Calibration errors could be made arbitrarily small for each set of transient head data because the calibration procedure did not involve relating head levels through time. However, when calibration results were used to simulate head over time, the time-dependency of each simulated head distribution upon the preceding simulated head distribution, especially between 1950 and 1955 when the initial conditions heavily influenced the simulation, produced large errors between simulated and adjusted transient head levels. The sum of squared error was even larger when observed transient head levels were used to define simulation

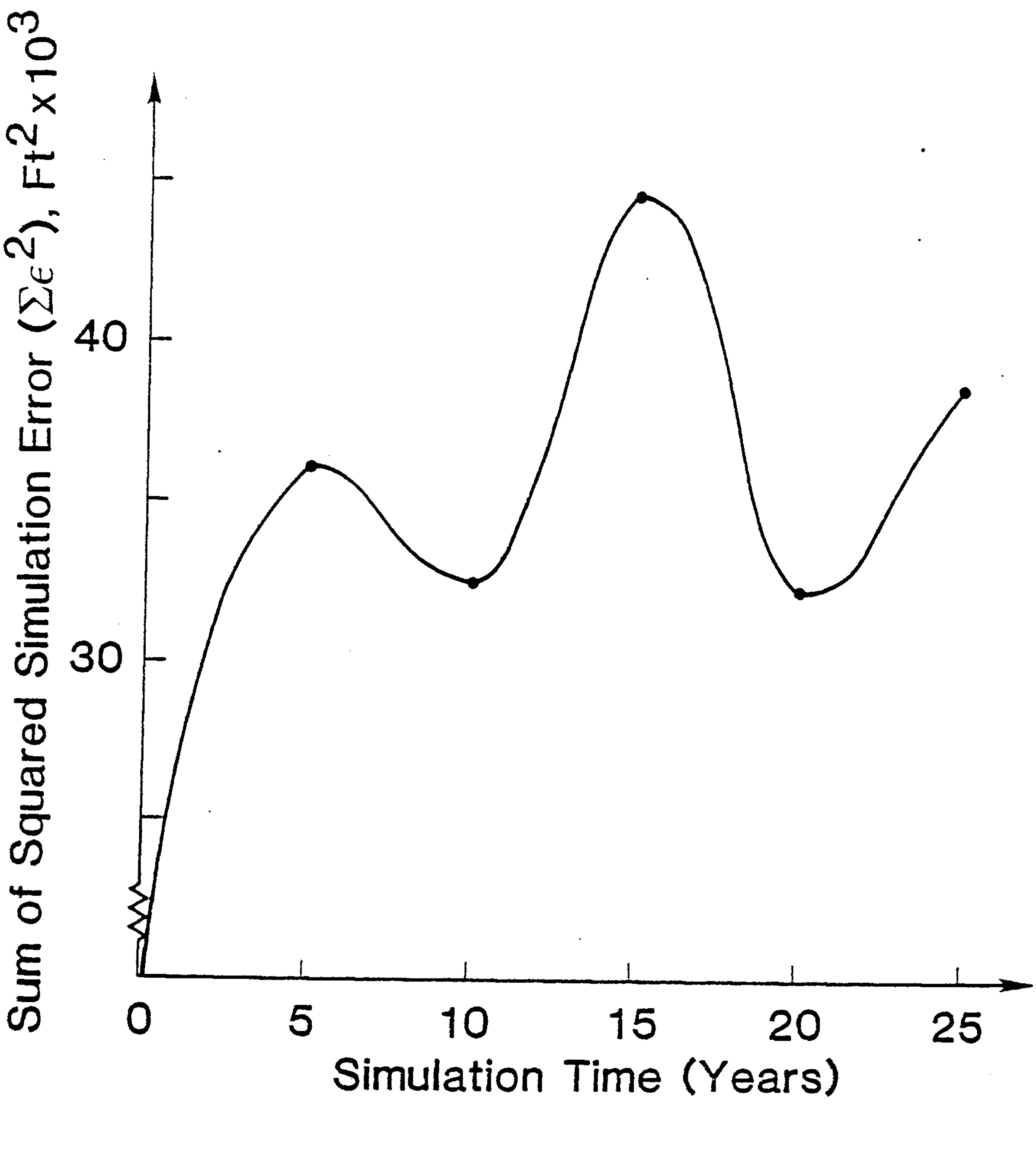

Figure C19. Sum of squared simulation errors vs. development time.

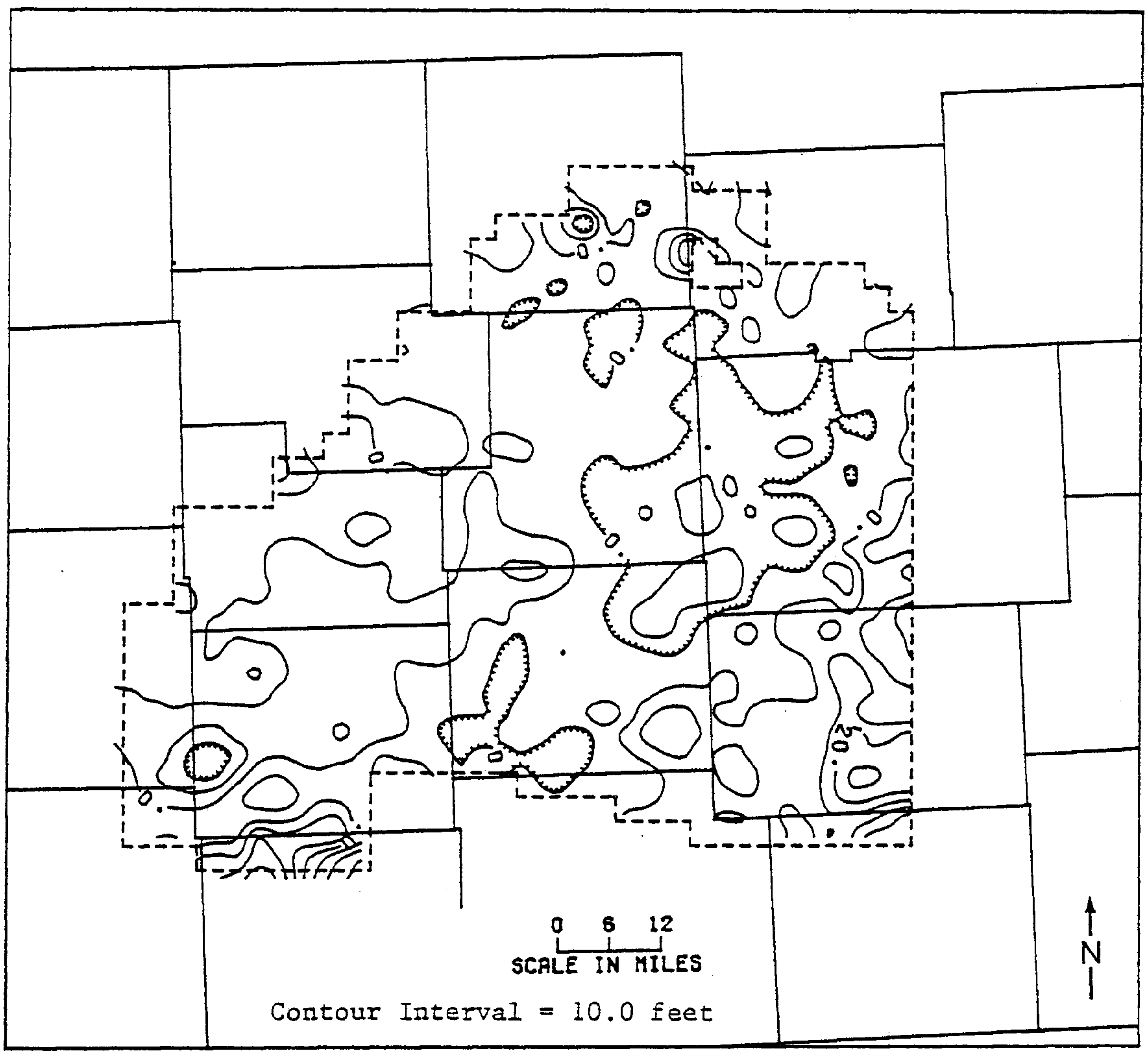

—— CONTOUR OF EQUAL ERROR VALUE ---- MODEL BOUNDARY

Figure C20. Spatial distribution of 1955 simulation errors (feet).

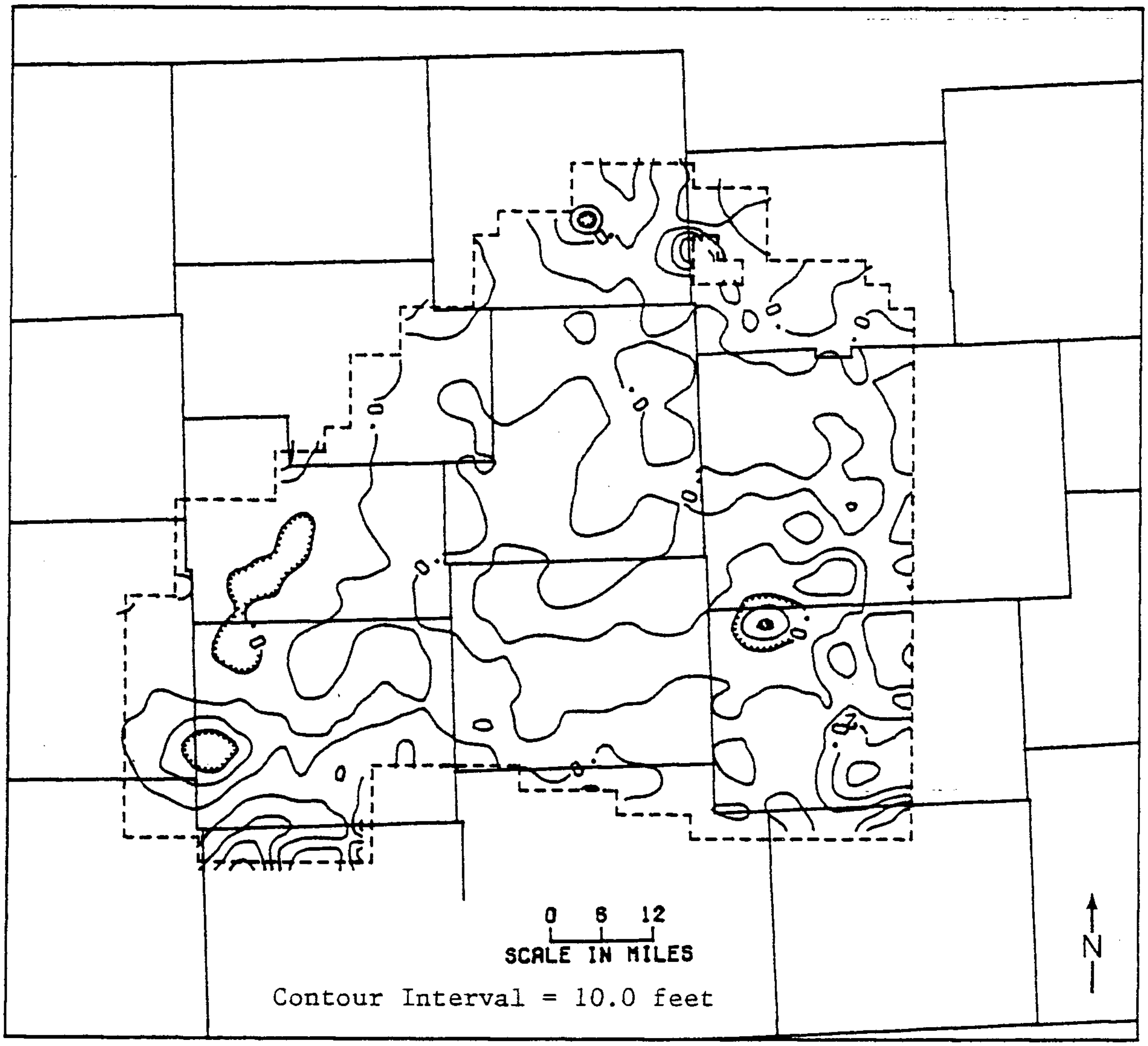

—— CONTOUR OF EQUAL ERROR VALUE ---- MODEL BOUNDARY

Figure C21. Spatial distribution of 1960 simulation errors (feet).

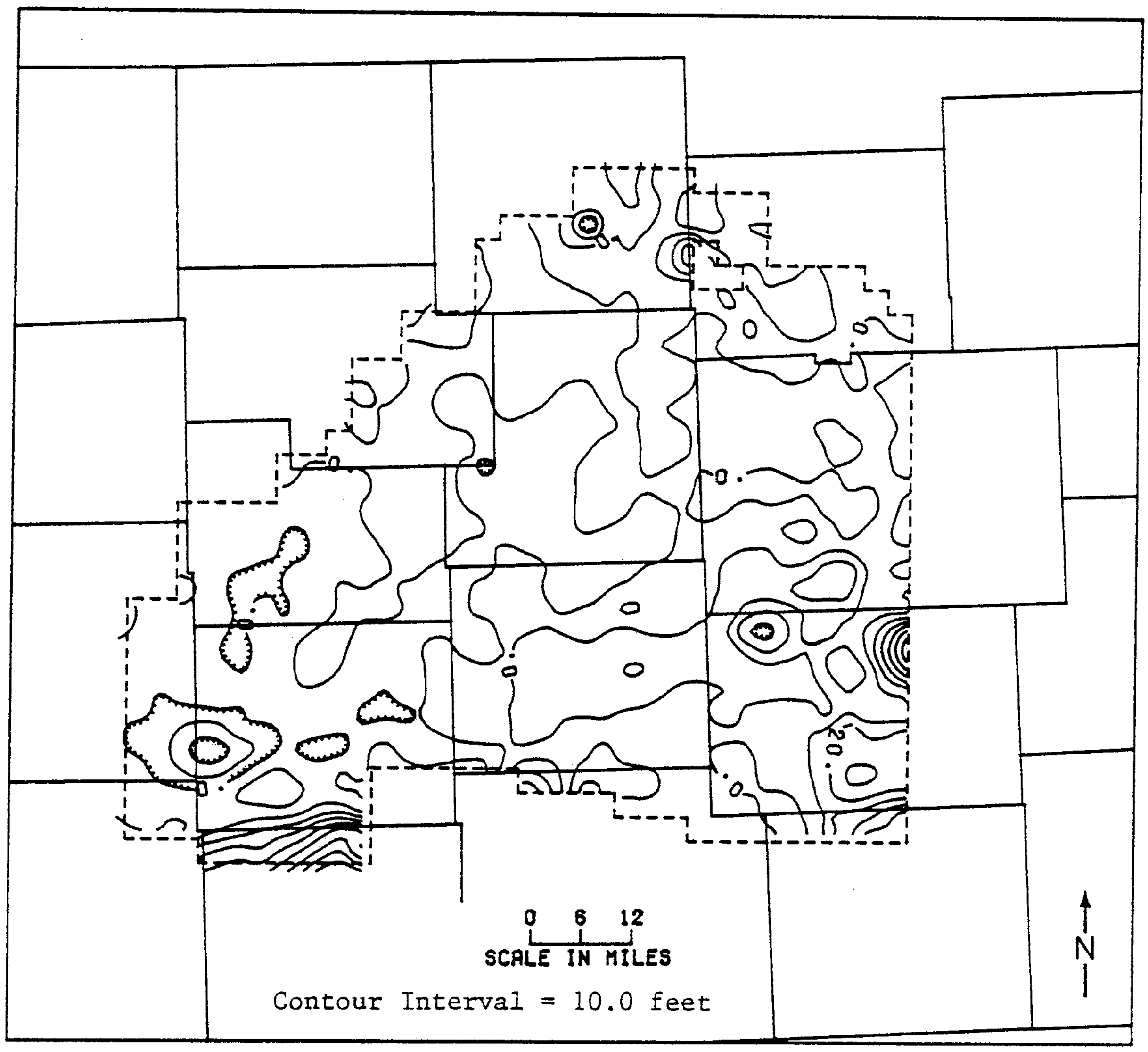

——— CONTOUR OF EQUAL ERROR VALUE ---- MODEL BOUNDARY

Figure C22. Spatial distribution of 1965 simulation errors (feet).

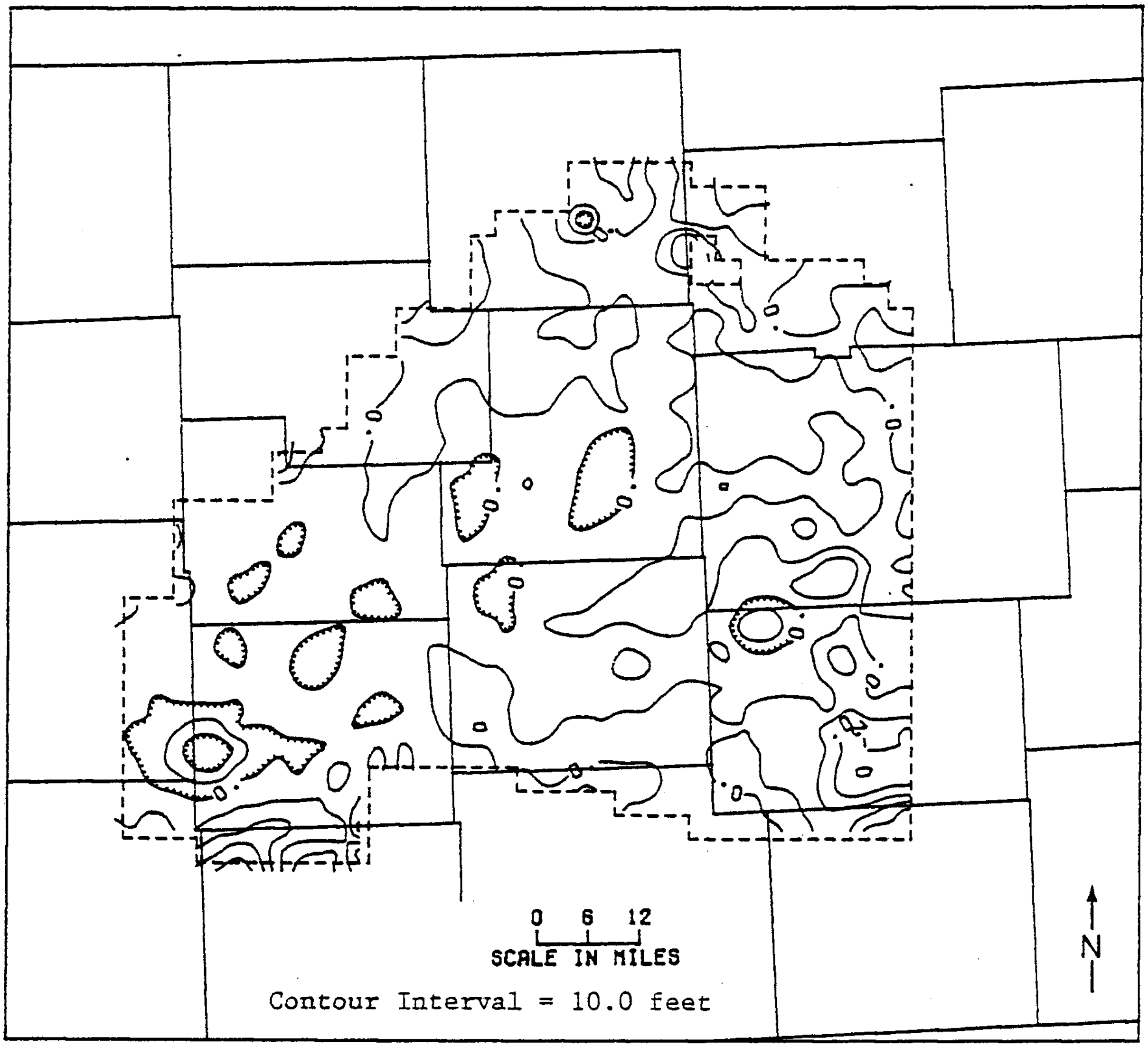

CONTOUR OF EQUAL ERROR VALUE ---- MODEL BOUNDARY

Figure C23. Spatial distribution of 1970 simulation errors (feet).

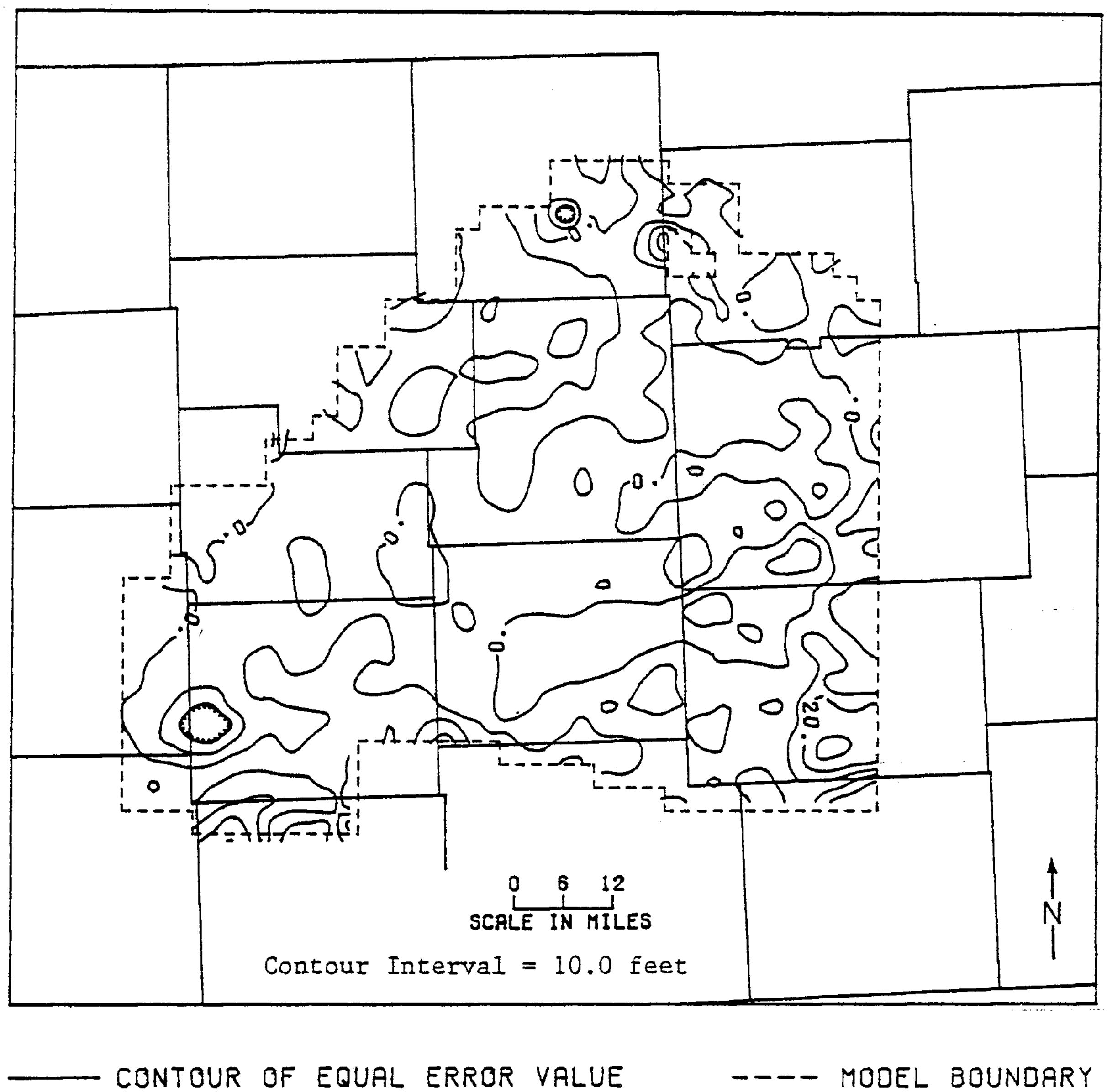

Figure C24. Spatial distribution of 1975 simulation errors (feet).

error. It was clear that large errors of estimate for S_y were primarily responsible for the distortion of time-dependency between steady-state and transient head distributions.

For situations in which transient head data is accurately known, the use of projected consumptive-use correction factors represents a practical verification procedure in the absence of measureable system transience. From a management point of view, the absence of significant drawdown in the aquifer flow regime is an indication that groundwater supplies in the Great Bend alluvial aquifer are not in immediate danger of becoming depleted.

Summary of Steepest-Descent Calibrations

The steepest-descent optimization algorithm used to refine the parameters obtained from the USGS steady-state calibration reduced the sum of squared error from 21000 ft^2 to 5100 ft^2. Further reduction was probably prevented by the requirement to input non-zero values of specific yield, which tended to introduce transient perturbations in the initial head obtained from the Texas model. The feasibility of modifying the algorithm to perform underrelaxation will be given further consideration during the future applications of the optimization model. It is likely that other nonlinear regression models which have been specifically designed for steady-state calibration will instead be used during future calibration efforts involving steady-state head data.

The steepest-descent algorithm, which is based on the assumption of transient conditions, did not present any problems related to model operation during transient calibration, when non-zero specific yield estimates were required for simulation of transient effects. However, under the steady-state conditions which appeared to prevail during the development period, the specific yield distribution was not sensitive to the head levels observed during this time, and was not considered to be a reliable reflection of aquifer storage properties. A 25-year simulation performed for validation purposes was not considered entirely successful. Use of refined parameter distributions for K, S_Y, R, and α did not offer any improvement in the sum of squared simulation errors obtained during the validation stage when compared to the validation results obtained from the USGS model using unrefined parameter sets. Large validation errors were primarily associated with poor S_Y estimates obtained from historical water tables that were not influenced by significant transient effects.